Journal of the OPTICAL SOCIETY of AMERICA

VOLUME 38
No. 9

SEPTEMBER
1948

Size, Shape, and Contrast in Detection of Targets by Daylight Vision. II. Frequency of Seeing and the Quantum Theory of Cone Vision . . . . EDWARD S. LAMAR, SELIG HECHT, CHARLES D. HENDLEY, AND SIMON SHLAER 741

Visual Acuity as Measured with Various Orientations of a Parallel-Line Test Object . . . . G. C. HIGGINS AND K. STULTZ 756

Multi-Prism Spectrographs with Glass Optics by Carl Zeiss, Jena . . . . . G. HANSEN 759

Formation of Optical Images by X-Rays . . . . . PAUL KIRKPATRICK AND A. V. BAEZ 766

Transmission of Powder Films in the Infra-Red . . . . . R. L. HENRY 775

Quantometer, a Direct Reading Instrument for Spectrochemical Analysis . . . . . M. F. HASLER, R. W. LINDHURST, AND J. W. KEMP 789

Wide Range Analysis for Zinc Using Spectrographic Line Widths . . . . . E. JOHN EASTMOND AND BERNICE E. WILLIAMS 800

Report on Colorimetry and Artificial Daylight 803

Temperature Coefficient of the Refractive Index of Water . . . . . J. B. HAWKES AND R. W. ASTHEIMER 804

Optical Properties of Ni, Co, Fe, Mn, and Cd . . . . . F. BUECHE 806

Symposium on Luminescence 810

Fluorescence of Uranium Trioxide Hydrates . . . . . DWAYNE T. VIER, MELVIN L. SCHULTZ, AND JACOB BIGELEISEN 811

Letters to the Editor:

On the Inadequacy of the Measurement of Emission Characteristics of Fluorescent Substances without Spectral Resolution . . . . . Z. BODÓ 815

Standard Response Functions for Protanopic and Deuteranopic Vision . . . . . YVES LE GRAND 815

Example of Metamerism: Extreme Example of Color Change with Varying Illuminant . . . . . F. C. DEXTER AND E. I. STEARNS 816

Temperature Dependence of the Emission Bands of Zinc Oxide Phosphors . . . . F. H. NICOLL 817

Infra-Red Stimulability of $CaSiO_3$:Pb and $CaSiO_3$:(Pb+Mn) . . . . . JAMES H. SHULMAN, ROBERT J. GINTHER, AND LYLE W. EVANS 817

Published monthly
at Prince and Lemon Sts., Lancaster, Pa.
by the
AMERICAN INSTITUTE OF PHYSICS
Incorporated
57 East 55 Street, New York 22, New York
FOR AND UNDER THE EDITORIAL SUPERVISION OF THE
OPTICAL SOCIETY OF AMERICA

THE OPTICAL SOCIETY OF AMERICA

Officers of the Society

RUDOLF KINGSLAKE, *President*
Eastman Kodak Company
Rochester, New York

WILLIAM F. MEGGERS, *Vice President*
National Bureau of Standards
Washington 25, D. C.

ARTHUR C. HARDY, *Secretary*
Massachusetts Institute of Technology
Cambridge 39, Massachusetts

W. W. GRAEPER, *Treasurer*
Bausch & Lomb Optical Company
Rochester 2, New York

The Board of Directors consists of the above officers; the Editor of the Journal; the Past President; and five directors-at-large.

G. R. HARRISON, *Editor and Past President*
Massachusetts Institute of Technology
Cambridge 39, Massachusetts

Directors-at-Large

FRANK BENFORD
General Electric Company
Schenectady, New York

F. M. BISHOP
Eastman Kodak Company
Rochester 4, New York

WALLACE R. BRODE
Ohio State University
Columbus 10, Ohio

A. H. BENNETT
American Optical Company
Buffalo 11, New York

E. H. LAND
Polaroid Corporation
Cambridge, Massachusetts

Local Sections

STANLEY S. BALLARD, *Secretary for the Local Sections*

Rochester Section

JOHN H. MCLEOD, *President*
HARRY D. POLSTER, *Vice President*
JAMES R. BENFORD, *Secretary*
LUVILLE T. STEADMAN, *Treasurer*

Detroit Section

DAVID L. FRY, *Chairman*
KARL W. BEYER, *Vice Chairman*
DANIEL L. HARMON, *Secretary*
W. R. O'NEILL, *Treasurer*

Niagara Frontier Section

GALEN PORTER, *President*
LELAND E. HAVENS, *Secretary*
CLAIR M. BIRDSALL, *Treasurer*

Ohio Valley Section

M. E. MERCHANT, *Chairman*
J. F. WOODRUFF, *Chairman-elect*
C. S. MILLS, *Secretary-Treasurer*

Patrons

AMERICAN OPTICAL COMPANY — BAUSCH & LOMB OPTICAL COMPANY
EASTMAN KODAK COMPANY

Corporation Members

ALLIED CHEMICAL AND DYE CORPORATION, NATIONAL ANILINE DIVISION, Buffalo, New York
AMERICAN CYSTOSCOPE MAKERS, INC., New York, New York
AMERICAN OPTICAL COMPANY, Southbridge, Massachusetts
ARGUS, INCORPORATED, Ann Arbor, Michigan
BAUSCH & LOMB OPTICAL COMPANY, Rochester, New York
BELL & HOWELL COMPANY, Chicago, Illinois
BELL TELEPHONE LABORATORIES, INC., New York, New York
CENTURY LIGHTING, INC., New York, New York
CORNING GLASS WORKS, Corning, New York
R. R. DONNELLEY & SONS COMPANY, Chicago, Illinois
E. I. DUPONT DE NEMOURS & COMPANY, INC., Chemical Department, Experimental Station, Wilmington, Delaware
EASTMAN KODAK COMPANY, Rochester, New York
EDMUND SALVAGE COMPANY, Oaklyn-Audubon, New Jersey
FAIRCHILD AVIATION CORPORATION, Jamaica, New York
FARRAND OPTICAL COMPANY, INC., New York, New York
FISH-SCHURMAN CORPORATION, New York, New York
GAERTNER SCIENTIFIC CORPORATION, Chicago, Illinois
W. & L. E. GURLEY, Troy, New York
INTERCHEMICAL CORPORATION, New York, New York
KEUFFEL & ESSER COMPANY, Hoboken, New Jersey
KOLLSMAN INSTRUMENT DIVISION OF SQUARE D COMPANY, Elmhurst, New York
NATIONAL CARBON COMPANY, Cleveland, Ohio
NATIONAL TECHNICAL LABORATORIES, South Pasadena, California
PERKIN-ELMER CORPORATION, Glenbrook, Connecticut
POLAROID CORPORATION, Cambridge, Massachusetts
PORTMAN MACHINE TOOL COMPANY, New Rochelle, New York
SIMPSON OPTICAL MANUFACTURING COMPANY, Chicago, Illinois
SOCONY-VACUUM LABORATORIES, Paulsboro, New Jersey
ARTHUR H. THOMAS COMPANY, Philadelphia, Pennsylvania
UNIVIS LENS COMPANY, Dayton, Ohio
ZENITH OPTICAL COMPANY, Huntington, West Virginia

THE OPTICAL SOCIETY OF AMERICA was organized in 1916 "*to increase and diffuse the knowledge of optics in all its branches, pure and applied, to promote the mutual interests of investigators of optical problems, of designers, manufacturers and users of optical instruments and apparatus of all kinds and to encourage cooperation among them.*" It aims to serve the interests of all who are engaged in any branch of optics from fundamental research to the manufacture of optical goods.

MEMBERSHIP

Regular Members: "Any person who has contributed materially to the advancement of optics is eligible for regular membership."

Associate Members: "Any person who is interested in optics is eligible for associate membership."

Corporate Members: "Any corporation desirous of encouraging the work of the Society is eligible for corporation membership."

Patrons: The payment, within any one year, of $1000 or more toward the expenses of the Society by any corporation or individual entitles such corporation or individual to the rank of patron.

The Society cordially invites to membership all who are interested in any branch of optics, either in research, in instruction, in optical or illuminating engineering, in the manufacture and distribution of optical goods of all kinds, or in physiological and medical optics.

ANNUAL DUES

Regular members, $8.50; Associate members, $6.00; Corporate members, $50.00. These dues include subscription to the Society's official journal, the *Journal of the Optical Society of America.*

CHANGES OF ADDRESS

All changes of address of members of the Optical Society of America should be communicated to the Secretary, Professor Arthur C. Hardy, Massachusetts Institute of Technology, Cambridge 39, Massachusetts.

Journal of the
OPTICAL SOCIETY
of AMERICA

VOLUME 38, NUMBER 9 SEPTEMBER, 1948

Size, Shape, and Contrast in Detection of Targets by Daylight Vision. II. Frequency of Seeing and the Quantum Theory of Cone Vision*

EDWARD S. LAMAR,** SELIG HECHT,*** CHARLES D. HENDLEY,† AND SIMON SHLAER††
Laboratory of Biophysics, Columbia University, New York, New York
(Received February 24, 1948)

Frequency-of-seeing curves have been obtained for targets having various image perimeters at background brightnesses of 2950 and 17.5 foot-lamberts, respectively. A description of the data has been obtained on the basis of the assumption that the absorption of a light quantum by a foveal cone is a random event which is subject to the laws of chance. On this basis the data indicate that the detection of a target takes place across the image boundary; that in order to detect the target, at least one of the cones along the boundary must absorb at least 4 quanta, and that this critical number of quanta is the same for each of the two background brightnesses investigated. At the higher brightnesses, this critical number of quanta absorbed from the target is about equal to the random fluctuation to be expected in the number absorbed from the background during the critical time of one exposure.

I. FREQUENCY OF SEEING

THE measurements reported in the first of this series of two papers[1] deal with the contrast required for detecting rectangular targets of various sizes and symmetries against a large background of uniform brightness. Two background brightnesses were studied: one of 2950 foot-lamberts, and one of 17.5 foot-lamberts. The target was brighter than the background and it was presented in one of eight radial positions around a central reference point. The observer was required to report merely the position of the target, not its shape or its orientation.

If I is the brightness of the background, and ΔI is the brightness added by the target, then the purpose of the measurements was to determine the value of the threshold contrast $(\Delta I/I)_t$ at which the observer reports the position of the target correctly five times out of eight presentations. To secure this value of $(\Delta I/I)_t$ we exposed the target at a series of four to six values of the contrast $\Delta I/I$ so selected that the frequency of seeing the target correctly varied from once or twice out of eight presentations to the maximum of eight times out of eight. By plotting the frequency of correct answers against $\log(\Delta I/I)$, as determined directly from the setting of an optical

* This work was done under a contract, recommended by the Committee on Medical Research, between the Office of Scientific Research and Development and Columbia University.
** Member of the Operations Evaluation Group, Navy Department, Washington, D. C.
*** Died, September 18, 1947.
† Now at the University of Utah Medical School, Salt Lake City, Utah.
†† Now at the Los Alamos Scientific Laboratory of the University of California, Los Alamos, New Mexico.
[1] E. S. Lamar, S. Hecht, S. Shlaer, and C. D. Hendley, "Size, shape, and contrast in detection of targets by daylight vision. I. Data and analytical description," J. Opt. Soc. Am. **37**, 531 (1947).

wedge, and drawing a smooth curve through the measurements one could ascertain with adequate precision the threshold contrast $(\Delta I/I)_t$ for seeing the target correctly five times out of eight. All the foveal data in the first paper were secured in this way.

Because of previous work on the visibility of light at the threshold of vision[2] the precise shape of such frequency-of-seeing curves has acquired a real meaning in terms of retinal events and the quantum nature of light. We have therefore deemed it desirable to examine these new data from this point of view, even though the measurements were not designed for this particular purpose.

In making the original measurements, each contrast for each target was presented for only one set of eight exposures, the position of the target for any given exposure being any one of the eight possible radial positions. This was adequate for the purpose of finding the threshold contrast $(\Delta I/I)_t$ graphically. However, eight presentations per point are not enough to establish the *form* of the frequency-of-seeing curve with the precision required for our present purposes. It is therefore necessary to combine the results of several observers with several targets. Before doing this, we must decide which sets of measurements can legitimately be combined, and what procedure should be used to combine them. This is one of the objects of the next section.

II. USEFUL FLUX AND THE RETINAL IMAGE

The original measurements[1] were made with a series of rectangular targets which varied in area between 0.5 and 800 square minutes visual angle and differed in ratio of length to width between 2 and 200. We found it possible to unify all the data by assuming that the eye makes its judgment of contrast across the boundary of the target image rather than over its whole area.

It turned out that in the contrast recognition of a target the physiologically useful flux may be considered as coming from a strip extending 1 or 1.5 minutes from the edges of the target. Let L and W be the length and width of the target, and let w be the width of the useful ribbon inside the target perimeter. Then the useful area A_1 is

$$A_1 = 2w(L+W-2w) \tag{1}$$

if W is greater than $2w$ and

$$A_1 = LW \tag{1a}$$

if W is less than $2w$, and the useful flux is $(\Delta I/I)_t A_1$. The measurements then show that this useful flux bears a simple relationship to the target perimeter R, within experimental error, for all areas and targets larger than a few minutes of arc. For those targets shorter than a few minutes of arc, the useful flux is essentially constant. With these exceptions, the entire set of data may be described, within experimental error, by the one equation

$$(\Delta I/I)_t A_1 = cR^k \tag{2}$$

in which c is a constant and k is an exponent whose value lies between $\frac{3}{8}$ and $\frac{3}{4}$. This was the basic unification presented in Figs. 12 and 13 of the first paper of this series.

In a later section, the first paper of this series went on to consider the physical interpretation of the useful flux. Because of diffraction and chromatic and spherical aberration in the optical system of the eye, rectangular targets of small area do not produce sharp images on the retina which correspond to the shape and area of the targets. Instead they produce fuzzy disks several minutes in diameter. For targets whose dimensions are less than a few minutes the size of the image disk on the retina is essentially constant and only its brightness varies with size of the targets. However, even larger targets do not form sharp retinal images. Their edges are always fuzzy over a distance about equal to the strip width w.

The fact that for large targets the image perimeter is essentially equal to the target perimeter, and for small targets the image perimeter is essentially constant, suggests that in Eq. (2) it may be the image perimeter rather than the target perimeter which should be employed. This, also, was stated in the first paper of this series. Estimates of the image perimeter have been made and the data replotted. This new unification of the data is as good as the old one for the larger targets and includes the smaller

[2] S. Hecht, S. Shlaer, and M. H. Pirenne, "Energy, quanta, and vision," J. Gen. Physiol. **25**, 819 (1942).

targets instead of leaving them as exceptions. The exponent k for this new formulation lies between $\frac{3}{4}$ and $\frac{4}{5}$.

The useful flux has a definite interpretation in terms of the retinal illumination produced by the target. Calling E the retinal illumination produced by the background and ΔE the retinal illumination added by the image of the target we found that

$$(\Delta E/E)_t = c(\Delta I/I)_t(A_1/A_2) \qquad (3)$$

where c is a constant, A_1 is the area of useful flux from the target and A_2 equals the retinal image perimeter R times w, the width of the ribbon of useful flux just inside the target edge, which is also about the width of the fuzzy edge of the image. In other words $A_2 = Rw$. Substituting the value of $(\Delta I/I)_t A_1$ from Eq. (2) into Eq. (3) and rewriting Rw for A_2 we get

$$(\Delta E/E)_t = cR^k/Rw \qquad (4)$$

from which it follows that

$$(\Delta E/E)_t = (c/w)R^{k-1}. \qquad (4a)$$

As the size of the target increases, A_1 approaches A_2 and $(\Delta E/E)_t$ approaches $(\Delta I/I)_t$. Hence the constant c is equal to unity and

$$(\Delta E/E)_t = (\Delta I/I)_t(A_1/A_2). \qquad (5)$$

$(\Delta E/E)_t$ has been computed using Eq. (5) for each of the various targets at each of the two target background brightnesses. The results together with the image perimeters are plotted in Fig. 1. In order to make these computations the image perimeter was estimated in accordance with the following scheme for obtaining the approximate image dimensions. If the length of the target is less than twice the strip width w, the perimeter of the image is taken as $2\pi w$. If the target length is greater than $2w$ but its width less, the image length is taken as L, the target length and the image width is taken as $2w$. If the target width is greater than $2w$, the image dimensions are taken to be the same as the target dimensions.

Equation (5) is an approximation to $(\Delta E/E)_t$ which follows in logical steps from the empirical results of the first paper of this series. Within the precision of those measurements it is satisfactory and is adequate for our present purposes.

The above formulation of the data from the first paper of this series answers the question as to which sets of measurements may be properly combined to obtain frequency-of-seeing curves. Those images which have the same perimeters have also the same values of $(\Delta E/E)_t$. It appears, therefore, that the perimeter of the image is the significant variable so that the data from those targets which produce about the same image perimeters should be grouped together.

We shall have occasion to refer again several times to the relationship between the peripheral dimensions of the target image and its retinal contrast. The fact that the retinal contrast varies inversely as the $\frac{1}{4}$ or $\frac{1}{5}$ power of the image perimeter will serve as one of the criteria for the validity of several proposed explanations for the measurements.

III. PROBABILITY OF SEEING

From the considerations just brought out it seems clear that for any given background brightness and value of the retinal contrast $\Delta E/E$, the chances of seeing the target depends essentially on the length of the perimeter of the target image on the retina. For the large targets, the retinal image perimeter, in angular measure, is equal to the target perimeter itself. For small targets, because of diffraction, the two are not equal. We have computed the retinal image perimeters of all our targets and have divided them into six groups, each group having approximately the same image perimeter. We thus have two sets of six groups, one set for each of the two background brightnesses used.

In order to understand the procedure for combining the results of many experimental runs to

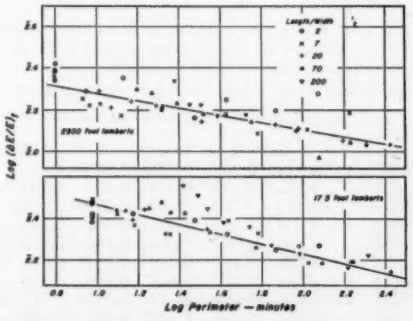

FIG. 1. Relationship between the logs of retinal threshold contrast $(\Delta E/E)_t$ and image perimeter R.

obtain one frequency-of-seeing curve it is to be remembered that for any given target the retinal contrast $\Delta E/E$ is proportional to the target contrast $\Delta I/I$. Hence frequency-of-seeing curves with $\log(\Delta I/I)$ as abscissa have the same shape as frequency-of-seeing curves with $\log(\Delta E/E)$ as abscissa. The only difference is that the second curve is shifted along the abscissa by an amount equal to the logarithm of the constant of proportionality. If, therefore, we are interested only in curves' shape, it is immaterial whether we use $\log(\Delta E/E)$ or $\log(\Delta I/I)$ as abscissa. For reasons of convenience we shall use $\log(\Delta I/I)$.

Consider first a single run as it is used to determine the threshold contrast $(\Delta I/I)_t$. This quantity represents five correct answers out of eight presentations and is based on some 30 to 40 judgments by the observer. Hence with fair accuracy it can be considered as the threshold value characteristic of the observer at the time of the experimental run.

We know from experience that the observer can and does change from time to time and therefore $(\Delta I/I)_t$ will differ from time to time even for the same target. Furthermore, targets producing the same image perimeters and hence the same values of $(\Delta E/E)_t$ may differ in ratio of length to width and hence have different values of $(\Delta I/I)_t$. But our observations show that the frequency of seeing correctly, as a function of $\log(\Delta I/I)$ always has the same general shape, for all targets giving about the same image perimeters, even though the location on the $\log(\Delta I/I)$ axis may shift, from target to target and from time to time. Therefore, if many experimental runs are to be combined to determine the precise shape of the frequency-of-seeing curve, correction must be made for any changes in the threshold $(\Delta I/I)_t$ from run to run and from target to target. The simplest procedure is to shift the curves along the $\log(\Delta I/I)$ axis so that the various values of $\log(\Delta I/I)_t$ coincide. This can be accomplished most easily by using as abscissa not $\log(\Delta I/I)$ directly but $\log(\Delta I/I) - \log(\Delta I/I)_t$. This puts the value of $\log(\Delta I/I)_t$ for each of them as equal to zero, and the points from the various runs may then be plotted on one graph. The corresponding values of $\log(\Delta E/E)_t$ are averaged and will be discussed in due course.

After the individual runs of a selected series have been combined and plotted together, the single points must be averaged in some way so as to yield a frequency-of-seeing curve which is relatively free from individual point fluctuations. It may be said at once that no significant differences show up whether the points are averaged in groups vertically or horizontally. However, we averaged the group points along the ordinates for theoretical reasons. Fluctuations along the abscissas can be caused only by changes in the threshold $(\Delta I/I)_t$ during the course of a run. A single experimental run lasts at most fifteen minutes, and it seems improbable that the sensitivity of the retina, which determines $(\Delta I/I)_t$ would change significantly during so short a time. On the other hand, the ordinates, representing the number of correct answers out of eight exposures, should be subject to considerable variation even during a single run. In the first place, guessing is allowed and even encouraged when the observer is doubtful. In the second place, as we shall see later, chance plays a large part in the frequency of seeing because it

TABLE I. Relationship between probability of seeing and contrast for images of various perimeters with a target background brightness of 2950 foot-lamberts.

$\log(\Delta I/I) - \log(\Delta I/I)_t$	Probability of seeing—Image perimeter in minutes 6.3	12.5	19	31	115	168
−0.291	0.143	0.107	0.190	0.096		0.500
−0.218	0.184	0.134	0.036	0.026	0.184	0.000
−0.146	0.282	0.181	0.199	0.211	0.233	0.232
−0.073	0.300	0.327	0.358	0.362	0.374	0.312
0.000	0.540	0.550	0.553	0.584	0.578	0.552
0.073	0.750	0.764	0.733	0.741	0.781	0.845
0.146	0.883	0.875	0.865	0.919	0.890	0.895
0.218	0.956	0.960	0.977	0.975	0.985	0.985
0.291	0.987	1.000	1.000	0.971	1.000	0.980
0.364	1.000	1.000	1.000	1.000		

TABLE II. Relationship between probability of seeing and contrast for images of various perimeters with a target background brightness of 17.5 foot-lamberts.

$\log(\Delta I/I) - \log(\Delta I/I)_t$	Probability of seeing—Image perimeters in minutes 9.4	13.5	20.4	32	98	169
−0.364	0.000	0.000				0.000
−0.291	0.000	0.071	0.000			0.083
−0.218	0.198	0.097	0.017	0.047	0.120	0.130
−0.146	0.234	0.241	0.224	0.143	0.180	0.222
−0.073	0.431	0.468	0.373	0.420	0.313	0.355
0.000	0.572	0.589	0.518	0.517	0.563	0.555
0.073	0.714	0.689	0.745	0.781	0.810	0.714
0.146	0.875	0.832	0.917	0.940	0.880	0.913
0.218	0.937	0.960	1.000	0.968	1.000	0.953
0.291	1.000	0.965	0.960	1.000	0.955	1.000
0.364	1.000	1.000				

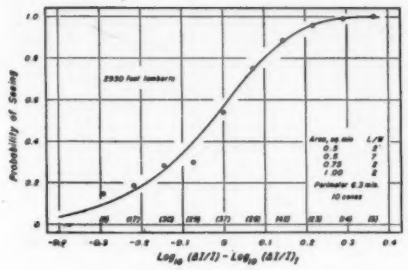

FIG. 2.

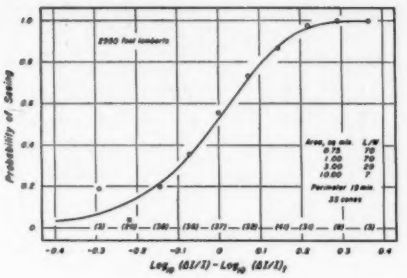

FIG. 4.

depends on the absorption of a small number of light quanta. Because of these reasons we averaged the points vertically, grouping all the points which fell within a band corresponding to a width of three millimeters on the wedge in the optical device used to alter the value of the contrast $\Delta I/I$. This band is equivalent to 0.073 log unit on the abscissas.

Having secured in this way a set of average measurements recording the number of correct answers out of eight exposures against $\log(\Delta I/I) - \log(\Delta I/I)_t$ we must next convert these values to probabilities of seeing. The argument is straightforward. Let N_s be the number of times out of eight exposures that the target was actually seen by the observer. Then $8-N_s$ is the number of exposures that were not seen. Since there are 8 positions and the observers were encouraged to guess, then $\frac{1}{8}$ of the number not really seen, $8-N_s$, were reported correctly purely by chance. Hence the number of correctly reported answers, N_c, out of eight exposures is

$$N_c = N_s + (1/8)(8-N_s), \tag{6}$$

which yields

$$N_s = (8/7)(N_c-1) \tag{7}$$

when solved for N_s the number actually seen. Since there are 8 exposures the probability P of seeing the target in any one exposure is $N_s/8$ which gives

$$P = N_s/8 = (N_c-1)/7 \tag{8}$$

merely by dividing Eq. (7) by eight.

IV. PROBABILITY OF SEEING AND PERIMETER

Using Eq. (8) we converted all the averaged frequency-of-seeing curves into probability-of-seeing curves, and these now form the basic data for the present paper. These data are given in Tables I and II for the two background brightnesses of 2950 foot-lamberts and 17.5 foot-lamberts.

For purposes of theoretical examination the data are also presented graphically as the points in Figs. 2–7 for the 2950 foot-lambert background, and in Figs. 8–12 and 13 for the 17.5 foot-lambert background. The abscissas are $\log(\Delta I/I) - \log(\Delta I/I)_t$ and the ordinates are the probability of seeing the target in a single exposure. Each figure contains a statement of the areas and asymmetries of the targets grouped together for it. There is also given the computed

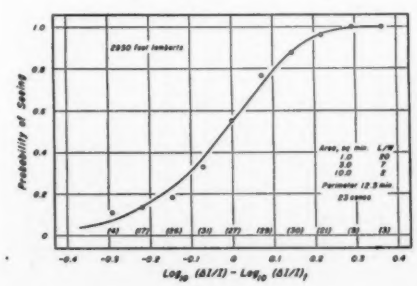
2950 foot lamberts
Probability of Seeing
Area, sq min L/W
1.0 70
3.0 7
10.0 1
Perimeter 12.3 min.
23 cones
(4) (17) (26) (21) (27) (19) (30) (21) (9) (3)
-0.4 -0.3 -0.2 -0.1 0 0.1 0.2 0.3 0.4
Log10 (ΔI/I) - Log10 (ΔI/I)t

FIG. 3.

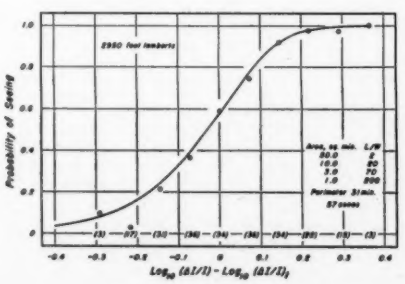

FIG. 5.

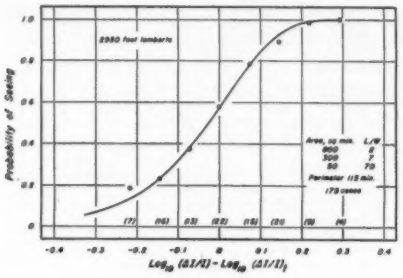

FIG. 6.

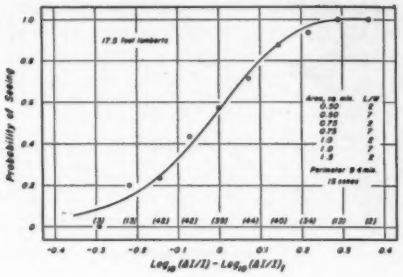

FIG. 8.

average perimeter of the image on the retina of the group of targets, as well as the number of retinal cones included along this perimeter. These are obviously approximate values; the former is computed from the diffraction images already discussed while the latter is computed from the measurements of Osterberg (1935) and will be discussed later more in detail. These values must be considered as approximate and are of interest not for their precise numerical magnitude, but more for their order of magnitude. The number in parenthesis under each averaged point is the number of individual runs which were combined to produce it. The solid line in each case is a theoretical curve whose meaning and derivation will be discussed later.

The data thus far presented show two significant properties. The first is that as the perimeter of the retinal image increases, the average retinal threshold contrast $(\Delta E/E)_t$ decreases. A plot of the two as given in Fig. 1 for the two different background brightnesses shows that the average retinal threshold contrast $(\Delta E/E)_t$ varies inversely as a fractional power of the computed retinal image perimeter. For the 2950 foot-lambert background the fractional power is about $\frac{1}{5}$ while for the 17.5 foot-lambert background it is more nearly $\frac{1}{4}$. These relations were presented earlier in Section II, and will serve as a criterion for the validity of the theoretical explanation to be considered.

The other properties of the data, shown in the last two groups of figures is that as the perimeter of the retinal image of the target increases the slope of the frequency-of-seeing curve also increases. The increase is not large but is gradual and steady. Between 20 and 90 percent probabilities of seeing, the smallest perimeter data, for the high and low background brightnesses cover 0.35 and 0.34 log unit respectively along the abscissa, whereas the longest perimeter data cover 0.29 and 0.29 log units. The average difference is about 19 percent of the lower figure.

V. MEANING OF A SINGLE EXPOSURE

Before proceeding to the theoretical meaning of the data we must examine the question of what happens during a single exposure of three seconds. This was the duration of each exposure to the target, and was originally chosen for practical reasons. The observer takes a certain time for a

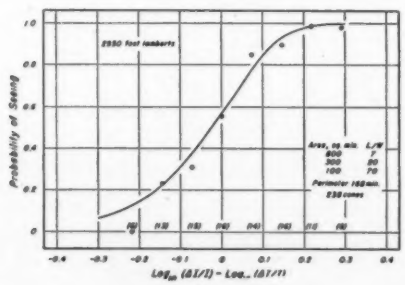

FIG. 7.

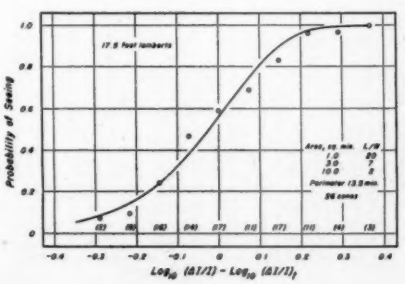

FIG. 9.

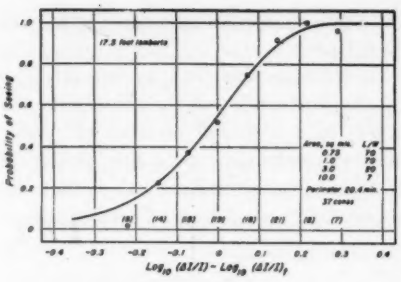

FIG. 10.

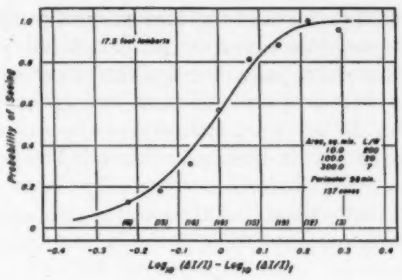

FIG. 12.

"look" at the target. If he sees the target then he reports its position. But if he does not see it on a first look, does he have an opportunity for another look before the exposure is over? Surely if he can have more than one look during the exposure then the chance of his seeing the target is greater than if he has the opportunity of only one look at it.

How long is a "look"? Some light on this question is supplied by the work of Graham and Kemp[3] who measured $(\Delta I/I)_t$ as a function of the time of exposure to light. They found that for any given background brightness the product of $(\Delta I/I)_t$ and the time of exposure was constant below a fairly definite critical exposure time τ. Beyond this critical time, $(\Delta I/I)_t$ was constant. This is in line with the photo-chemical conception of cone stimulation because on such a theory, if the time of exposure is short, it is the total light flux which is important, whereas if the exposure is sufficiently long to allow the reaction to go to equilibrium, it is the rate at which light flux strikes the retina which determines visual response.[4,5]

From Graham and Kemp's data it follows that if the eye remains turned in a given direction and the time of exposure exceeds the critical value, no increase in chance of seeing can be expected through further increase in exposure time. The critical time of exposure obtained by Graham and Kemp depends somewhat upon the background brightness. For the two brightnesses 2950 and 17.5 foot-lamberts it is estimated from the data of Graham and Kemp to be about 0.024 and 0.046 seconds, respectively, due allowance having been made for pupil size. This is so much less than three seconds that a "look" for our purposes can be defined as a fixation of duration greater than the critical time τ.

The question which arises in the interpretation of the frequency-of-seeing curves is whether or not more than one fixation was employed by the observer, i.e. did he look; look away long enough

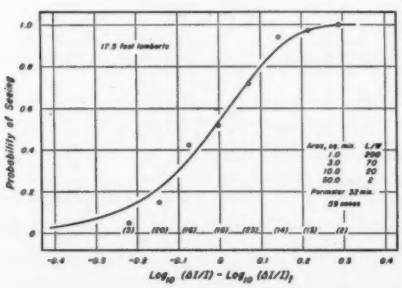

FIG. 11.

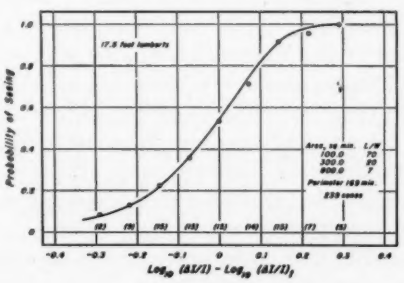

FIG. 13.

[3] C. H. Graham and E. H. Kemp, "Brightness discrimination as a function of the duration of the increment in intensity," J. Gen. Physiol. **21**, 635 (1938).

[4] S. Hecht, "Rods, cones, and the chemical basis of vision," Physiol. Rev. **17**, 239 (1937).

[5] H. K. Hartline, "The discharge of nerve impulses from the single visual sense cell," Cold Spring Harbor Symposia on Quantitative Biology **3**, 245 (1935).

to establish chemical equilibrium with the background and look again; or did he look only once. From working with the various observers, it seems clear that some of them maintained fixation on the reference spot during the entire exposure so that in these cases there is little question but that the frequency-of-seeing curves refer to a single "look." Although the accuracy of comparison was not high, there was no significant difference in curve shape among the various observers. It seems safe to suppose, therefore, that three seconds exposure time, while ample for a single look does not permit effective use of more than one look. We have assumed this to be true for convenience, and the theoretical treatment to follow rests on this assumption. Nothing basic would be changed if we assumed that during a three-second exposure the observer could take a second look if he failed to see the target on the first look. The treatment would be essentially the same, but somewhat more complicated. And since we do not wish to build a complex theoretical structure on these data, we will stick to the one-look-one-exposure assumption.

VI. PROBABILITY THEORY AND POISSON'S LAW

We propose to explain the measurements in terms of the quantum nature of light and the mosaic structure of the retina. According to the quantum theory, light is emitted and absorbed as discrete quanta of given energy content. These quanta are absorbed by the receptor elements in the retina and this absorption constitutes the initial event in the visual process. In the present measurements the retinal receptors are the central foveal cones which to a large extent are individually connected with single ganglion fibers of the optic nerve. Since each quantum absorption by a foveal cone must be considered as an independent and random event, the total behavior may be considered from the point of view of probability theory.

Consider a situation in which a certain "trial" is made, as for example, the tossing of a coin, the rolling of a die, or the incidence of a quantum of light on the retina. Let the probability of success in the trial be p, for the tossing of a head, the rolling of a given number or the absorption of the light quantum by a cone, and let the probability of failure be q. Since the trial must either succeed or fail, $p+q=1$.

Let us suppose now that we are interested in finding the probability of a given number of successes out of a specified number of trials. The binomial theorem says that the probability of exactly n successes out of m trials is the nth term in the expansion of $(p+q)^m$. To illustrate

$$(p+q)^m = q^m + mq^{m-1}p + m(m-1)q^{m-2}p^2/2! + \cdots. \quad (9)$$

The zeroth term, q^m, is the probability of complete failure in m trials; the first term $mq^{m-1}p$ is the probability of exactly one success, and the second term $m(m-1)q^{m-2}p^2/2!$ is the probability of exactly two successes, and so on for the entire m terms of the expansion.

Poisson showed that if p is small compared to unity, each term in the binomial expansion can be approximated quite accurately by a simpler expression in terms of the expected number of successes ϵ defined as the product of p, the probability of success per trial and m, the total number of trials, i.e.

$$\epsilon = mp. \quad (10)$$

In terms of the expected number of successes ϵ, the probability p_n of exactly n successes in m trials is given by Poisson as

$$p_n = \epsilon^n e^{-\epsilon}/n! \quad (11)$$

where e is the base of the natural logarithms. The probability P_n of at least n successes out of m trials is given by

$$P_n = \sum_n^m (\epsilon^n e^{-\epsilon}/n!). \quad (12)$$

For finite values of ϵ, if p is small, m must be large so that

$$P_n = \sum_n^\infty (\epsilon^n e^{-\epsilon}/n!). \quad (13)$$

Both p_n and P_n have been computed for various values of ϵ and of n and can be found in published tables.[6]

Equation (13), for our present purposes represents the probability that n or more quanta will be absorbed by the retina when it is given an ex-

[6] T. C. Fry, *Probability and Its Engineering Uses* (D. Van Nostrand Company, Inc., New York, 1928).

posure to light of such intensity that *on the average* ϵ quanta are absorbed by the retina from it.

VII. FOVEAL CONE VISION AND PROBABILITY

How can these ideas be applied to our measurements relating the threshold contrast $(\Delta E/E)_t$ to the frequency of seeing? Instead of answering this question directly we propose to record the steps we ourselves took in finding the answer. The problem consists in looking for a set of assumed characteristics of cone vision which will describe all the properties of the experimental observations. The account of this search will be presented as a series of three cases, and will include the failures as well as the success, since each failure represents a step toward a successful description.

The basic assumption common to all cases is that the incidence of a light quantum on the retina and its subsequent absorption by a cone is not a definitely predictable event but is subject to statistical fluctuations, that is, it is governed by chance. Indeed it is this very lack of exact knowledge which makes possible a description of cone vision which fits the experimental results.

When a light quantum is incident on the foveà, either it is absorbed by a cone or it is not absorbed. The probability p that a light quantum is absorbed by a cone depends upon the concentration of the photosensitive substance, probably iodopsin, in the cone. This concentration in turn depends upon the background brightness through its influence on the stationary state concentration of the photosensitive substance.[4] For any given background brightness the concentration of sensitive material is constant, and therefore the probability of absorption p is a constant. In addition to the quanta from the background, we are interested in those which are supplied by the ΔI field in a definite time, which according to Graham and Kemp[3] is probably less than 0.1 second.

Case I

As a first trial let us assume that in order to see a target, at least n quanta must be absorbed by the cones of the fovea covered by the image of the target regardless of the shape or size of the target. These n quanta come from the light ΔI added by the target area A. The expected or average number of absorbed light quanta is ϵ, and is proportional to the number of quanta incident in unit time, that is to the total light flux $\Delta I \times A$ or ΔE times the area of the image.

The assumption that at least n quanta must be absorbed within the image area regardless of shape or size leads to two experimental consequences. The first is that for any probability P_n of seeing the target, the product of $\Delta I/I$ and the target area A must be constant or that the product of $\Delta E/E$ and the image area must be constant. This means that for any given value of P_n the contrast $\Delta I/I$ must be inversely proportional to the target area A or equivalently that $\Delta E/E$ must be inversely proportional to the image area. The second consequence is that, since the minimum number of quanta n is the same for all varieties of target, the frequency-of-seeing curves should be the same for all targets. This follows from Eq. (13), since if n is the same for all targets, the probability of seeing, P_n is a function of ϵ only.

Neither of these experimental consequences is true. In the first paper of this series we found that the product of threshold contrast $(\Delta I/I)_t$ and the target area A is constant only for the very smallest targets, those whose dimensions both are less than 2 or 3 minutes visual angle. The product of $(\Delta E/E)_t$ and the image area is not constant even for these. The larger the area, the larger is the product of $(\Delta I/I)_t$ and A. Moreover, instead of the contrast threshold $(\Delta E/E)_t$ being inversely proportional to the image area, we find that it is inversely proportional to a fractional power of the perimeter of the image.

The second consequence is that the frequency-of-seeing curves should all be alike. The curves in Figs. 2 to 7 and 8 to 13 show clearly that they are not identical. Instead, the curves become steeper with increasing perimeter of image and cannot be superimposed one on the other.

We must therefore conclude that the assumption underlying Case I is not valid for the cones in the fovea.

This is not unexpected. In the central fovea each cone is individually connected with a ganglion cell, and probably has a private fiber in the optic nerve. It is therefore unlikely that the absorption of light quanta by such separate cones would add up as simply as if they were all ab-

sorbed by the same cone. Addition of this kind would be expected in the rods of the periphery where hundreds of rods appear to be connected with a single ganglion fiber, and a simple inverse relation between contrast and area does obtain for relatively large areas with rod vision.

Case II

The concept of physiologically useful flux which we discussed in Section II rests on the idea that it is only those cones in a narrow strip adjacent to the boundary of the retinal image which determine the recognition of the target. For our second case, therefore, let us assume that only those light quanta which are absorbed within this narrow strip are effective in rendering the target visible, and that the constant minimum number of quanta n must be absorbed in this boundary strip to result in target recognition. Under these circumstances the expected average number of absorbed quanta ϵ is proportional to the light flux within this narrow strip, which in turn is directly proportional to the product of $\Delta E/E$ and the image perimeter R.

The assumption in this case also leads to two experimental consequences. First, since the region of useful flux must absorb n or more quanta, then for a given probability P_n of seeing the target, the contrast $\Delta E/E$ should be inversely proportional to the image perimeter. And second, since there must always be absorbed n or more quanta within this perimeter area, the frequency of seeing curves for all targets should have the same shape as in Case I.

Our measurements demonstrate that neither of these consequences is realized. Section II, as well as Fig. 1 shows that $\Delta E/E$ does not vary inversely as the perimeter. And of course as in Case I the frequency-of-seeing curves are not identical for the different target sizes. Therefore, the assumption cannot be true that n or more quanta must be absorbed by the cones along the perimeter of the image to render the target visible in the fovea.

Case III

The basic assumption has been that in order for a target to become visible, a certain number of quanta n must be absorbed in some manner and in some location by the cones. In Case I we assumed further that these n or more quanta may be absorbed anywhere within the area of the image on the retina. This turned out to be untenable. In Case II we restricted the absorption of these n or more quanta to the narrow strip just inside the image boundary. This also turned out to be untenable. For Case III let us assume that the area within which n or more quanta must be absorbed is further restricted to one or more sections of the narrow strip just inside the image boundary. What this means is that the presence of a target will be recognized if one or more small segments of the perimeter each absorbs n or more light quanta. This may seem too much of a restriction until it is recalled that during the measurements, only the presence and position of the target was required and not its shape or size. Thus the recognition of only a small segment of it is necessary for an adequate determination of its presence.

In order to test the assumptions of Case III, we must first consider the form which will be taken by the function describing the probability of seeing the target under these conditions. The probability that at least n light quanta will be absorbed in a given section of the boundary is P_n. The probability that less than n quanta will be absorbed in the given section is $1-P_n$. If there are k sections around the image perimeter, then the probability that less than n quanta will be absorbed in each of the k sections is $(1-P_n)^k$. Therefore, the probability P that at least n quanta will be absorbed in at least one of the k sections is

$$P=1-(1-P_n)^k \qquad (14)$$

which, according to our original assumption of Case III is the probability of seeing the target.

If Eq. (14) is a satisfactory description of cone vision in the fovea then it must be possible to find a value of n which is the same for all sections of the image perimeter. It must be possible also to find a unit section such that if the number k of sections around a given image perimeter is substituted in Eq. (14), the resulting frequency-of-seeing curve will have the same shape as the experimental one for the given image. This must be true for all sizes and symmetries of the targets.

Let us consider these consequences in order.

The first problem is to find the minimum number of quanta n required for seeing the target, and the size of the unit section of the perimeter within which the number of quanta must be absorbed. We can do this best from the measurements in Fig. 2 recording the frequency of seeing the smallest targets, because the number k of these unit sections is sure to be least in the smallest target.

Our procedure in this respect was entirely empirical. An arbitrary trial value of n was selected and P_n computed as a function of the expected average number of quanta ϵ by means of the Poisson law as expressed in Eq. (13). Then for each value of P_n obtained in this way, we computed P from Eq. (14) using a series of values for k. The computed values were then plotted as a family of curves, one curve for each value of k, with the probability of seeing P as ordinate, and $\log_{10}\epsilon$ as abscissa using the same scales as in Fig. 2. Figure 2 was then placed over this family of curves, and by transmitted light, its experimental points were compared in turn with each curve in the family until the value of k was found whose curve best fitted the points. The entire procedure was then repeated with other values of n and the best value of k found in each case, until we could choose a pair of values of n and k whose curve gave the best fit for the points in Fig. 2.

While tedious, this is not a difficult method, and the choice of a pair of values for n and k is fairly straightforward. For the points in Fig. 2 the best pair of values turned out to be $n=4$ and $k=10$. The curve for these values is the one drawn in Fig. 2 and it is apparent that it is an adequate description of the measurements.

VIII. NUMBER OF CONES AND FREQUENCY OF SEEING

Before testing the other experimental consequences of Case III, it is worth examining the magnitudes of the values for n and k found for the data in Fig. 2. Our assumption is that at least one unit segment of the image perimeter must absorb n or more quanta to render the target visible. The value of n turns out to be 4, which is not only the same order of magnitude but almost the same numerical value as the 5 or 6 light quanta found necessary for the rod threshold by Hecht, Shlaer and Pirenne.[2] Apparently this seems to be the number of light quanta which must be *absorbed* by a unit in order to release impulses in the associated nerve fiber resulting in vision regardless of the state of adaptation of the retina. We shall discuss this later.

The value of k also turns out to have a simple meaning. The frequency-of-seeing data in Fig. 2 are for the smallest targets at high brightness. The geometrical images of these targets on the retina are all smaller than the diffraction pattern of a point source as produced by the 2-millimeter artifical pupil, and the targets may therefore be thought of as point targets. Computations presented in the first paper of this series[1] show that the central disk of this diffraction pattern is 2 minutes visual angle. Its perimeter is therefore 6.3 minutes. Since k, the number of visually significant sections in this perimeter, is 10, each section is 0.63 minutes long. No great leap of the imagination is required to identify this distance with the diameter of a foveal cone. Østerberg[7] gives 0.55 minutes as the distance between cone centers in the densest region of the central fovea; for the slightest off-center cones the distances become larger quite rapidly. Since, however, our observations were made with the most central region of the fovea, 0.55 minutes is probably a correct value to use. It therefore seems strongly probable that the length of a visually independent section of the image perimeter is really the diameter of a single cone. The difference between 0.55 minutes, the measured cone diameter, and 0.63 minutes, the computed diameter of a visually independent segment merely says that the critical cones do not lie with their centers on the periphery of the diffraction disk, but that they lie just within this perimeter, and are thus part way up the curve of brightness gradient of the disk.

The length of the unit section of the periphery may thus be considered as the diameter of a foveal cone. From our concept of physiologically useful flux we know that for this high brightness the width of the useful ribbon inside the perimeter of the target does not exceed 1 minute. Therefore it cannot be as great as 2 cones. It then seems reasonable to suppose that a visually independent section consists of a single foveal cone, and that this is our primary visual unit in the contrast

[7] G. Østerberg, *Topography of the Layer of Rods and Cones in the Human Retina* (Copenhagen, 1935).

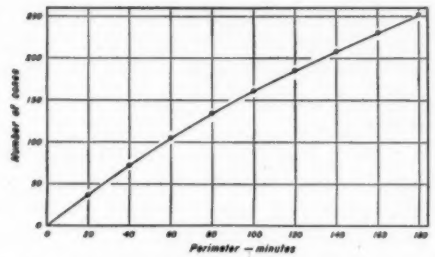

FIG. 14. Number of cones in the image perimeter as a function of the length of the perimeter (from Østerberg).

recognition of targets. If we accept this, then k which appears in Eq. (14) can be considered as the perimeter of the retinal image of the target as measured in cone diameters.

With this in mind we may examine two experimental consequences of the assumptions of Case III. The first concerns the shape and slope of the frequency-of-seeing curves for different targets. We saw that these are different for different targets. Since the frequency-of-seeing curves should be described by Eq. (14) it follows that if we put $n=4$ for all of them, and give k specific values corresponding to the number of cones in the perimeter of the target, Eq. (14) should describe all the data in Figs. 3 to 13. This turns out to be so.

To determine the number of cones k in the perimeter of the target image we have used the excellent measurements of Østerberg.[7] From his data we have constructed Fig. 14 which relates the length of the perimeter in minutes to the number of cones covered by it. Among the various target shapes there are slight differences in number of cones. These differences may well appear in visual measurements involving special research designed for this purpose. In our present investigation these differences are within the accuracy set by other factors, and an average value is quite adequate. These average values are the ones given in Fig. 14.

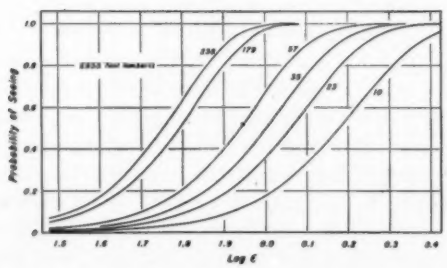

FIG. 15. Computed probability of seeing as a function of $\log\epsilon$, the expected number of quanta absorbed, for images having various members of cones around the perimeter. Target background brightness, 2950 foot-lamberts.

In Figs. 2 to 7 and 8 to 13, the average image perimeters are given. For each perimeter we have obtained from Fig. 14 the corresponding number of cones k, to be used in computing the curve from Eq. (14) when $n=4$ for all of them. The resulting computed curves are shown in Fig. 15 for the 2950 foot-lambert data and in Fig. 16 for the 17.5 foot-lambert data. The solid lines in Figs. 2 to 7 and 8 to 13 are these curves, traced on to the measurements. In every case the fit is satisfactory within the limits of experimental error. The demand that the slope of the curve become steeper as the target perimeter increased is also satisfied. Therefore this first consequence of the assumptions of Case III is fulfilled by the data.

The second consequence of Case III appears in the fact that as the number of cones increases, not only does the frequency-of-seeing curve change in shape, becoming steeper, but it shifts to the left on the abscissa, thus moving to lower values of the expected average number of quanta ϵ absorbed per cone. Since $\Delta E/E$ is proportional to ϵ this consequence demands that $\Delta E/E$ should decrease as the target perimeter increases. We know this to be true from the measurements, since $\Delta E/E$ varies inversely as a fractional power of the perimeter, the fraction being between $\frac{1}{4}$ and $\frac{1}{3}$. If we study Eq. (14) and compare the values of ϵ_t in Figs. 15 and 16 (ϵ_t is defined as that value of ϵ for a probability of 57 percent seeing) we find that ϵ_t varies inversely very nearly as the $\frac{1}{3}$ power of the value of k, the number of cones in the perimeter of the target. The second experimental consequence of Case III is therefore also fulfilled.

It is valuable to compare precisely the way in which measurements and theory agree in this particular case of the dependence of $(\Delta E/E)_t$ on the perimeter of the target. For the low and high brightness measurements we have the average values of $(\Delta E/E)_t$ from Table III for the data of Figs. 2 to 7 and 8 to 13. From Figs. 15 and 16 we can take the values of ϵ_t for each value of k. The

relation between ϵ_t and $(\Delta E/E)_t$ for the two brightness levels is shown in Fig. 17.

Strictly, the two ought to be related by a straight line inclined at 45°. This is almost true for the 17.5 foot-lambert data. The line for the 2950 foot-lambert data is steeper than 45° and this corresponds to the experimental relation between perimeter and $(\Delta E/E)_t$ as being a $\frac{1}{5}$ power. These deviations, however, are insignificant by comparison with the general agreement of theory and data. Within the accuracy of the present measurements the assumptions involved in Case III lead to a description of cone vision in the fovea which agrees with the experiments. They may therefore be accepted as an adequate first-order explanation of foveal vision relating contrast recognition of targets of various shape and size.

TABLE III. Retinal image perimeter; average retinal threshold contrast $(\Delta E/E)_t$; expected number of quanta absorbed by a cone, ϵ_t from the ΔE field and ν from the E or background field, and δ the probable deviation of ν.

Retinal perimeter (minutes)	Average threshold contrast $(\Delta E/E)_t$	Expected number of quanta ϵ_t—from ΔE field	ν—from background	Probable deviation of $\nu-\delta$
	2950 foot-lamberts—background brightness			
6.3	0.0238	1.62	68.0	5.56
12.5	0.0170	1.23	72.5	5.75
19.0	0.0169	1.07	63.3	5.36
31.0	0.0150	0.93	61.3	5.29
115.0	0.0132	0.66	50.3	4.79
168.0	0.0120	0.60	50.0	4.77
	17.5 foot-lamberts—background brightness			
9.4	0.0281	1.40	50.0	4.77
13.5	0.0248	1.18	47.6	4.64
20.4	0.0245	1.05	42.8	4.41
32.0	0.0239	0.91	38.1	4.16
98.0	0.0170	0.69	40.5	4.28
169.0	0.0153	0.61	39.6	4.24

IX. THRESHOLD CONTRAST AND THE "NOISE LEVEL"

All of our experiments consist in observing a target against its background. We have measured the contrast required for such a target to be recognized as brighter than its background, and we have worked out a theory which describes the measurements in terms of the number of light quanta which have to be absorbed during a "look" by the cones *in addition* to the quanta which they continuously absorb from the background. Since the background brightness is constant we have tacitly assumed up to now that the number of quanta absorbed by the cones from the background is also constant. However, just as the absorption of quanta from the target ΔI field is subject to statistical fluctuation, so also are the quanta absorbed from the background. We must now consider this fluctuation as well and see what bearing it has on the measurements and theory.

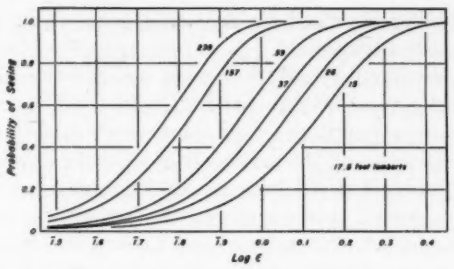

FIG. 16. Computed probability of seeing as a function of $\log\epsilon$, the expected number of quanta absorbed, for images having various numbers of cones around the perimeter. Target background brightness, 17.5 foot-lamberts.

In sound it has long been recognized that in order to be heard, a particular sound signal must be about as intense as the random sounds which produce a noise background or "noise level." The same term has been borrowed for use in electronics to describe the random fluctuations in background voltage which limit the intensity of an added signal so that it can be distinguished from its background. "Noise level" is so descriptive a term that for lack of a better one, we may also use it to describe the statistical fluctuation in quanta absorbed by the retinal elements from the light background. Obviously an illuminated target will be recognized as brighter than its background only when the number of quanta absorbed by the cones from it during a "look" is equal to or larger than the random fluctuations in

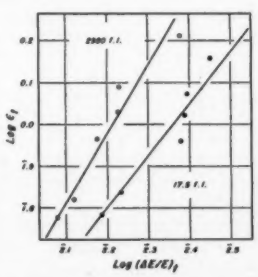

FIG. 17. Relationship between expected number of quanta absorbed, ϵ_t and the retinal threshold contrast $(\Delta E/E)_t$.

number absorbed by the same cones from the steady background.

We have found that even against the high background brightness of 2950 foot-lamberts, 4 or more quanta are required to be absorbed by a single cone on the perimeter of the retinal image in order for an increase in brightness to be recognized. It is therefore imperative to inquire what relation these 4 or more quanta bear to the random fluctuations or "noise level" of the quanta absorbed from the background during a "look."

Let ν be the expected or average number of quanta absorbed from the background E field during a "look." It will be recalled that ϵ is the expected or average number of quanta absorbed from the ΔE field in the same time. Then the ratio of ϵ/ν is equal to $\Delta E/E$ as experimentally determined, and the equation

$$\nu=\epsilon/(\Delta E/E)_t \qquad (15)$$

can serve for the computation of ν.

In Fig. 17 we possess the corresponding pairs of values of ϵ_t, the expected average number of quanta required for the different perimeters and the experimentally determined values of $(\Delta E/E)_t$ both for 57 percent correct seeing. These pairs of values are given in Table III. In the table are also given the computed values of ν corresponding to the number of quanta absorbed per cone per look from the background. Before commenting on these numbers let us complete the noise level computations from them.

For any process that occurs at random, if p is the chance of success in one "trial," and q is the chance of failure in one trial, then for m trials the most probable deviation from the expected number of successes is

$$\delta=0.6745(mpq)^{\frac{1}{2}} \qquad (16)$$

in terms of standard probability considerations. Even the roughest computations show that compared to the number of quanta incident on a cone at high and even at low intensities the number absorbed is extremely small.[2] Therefore p in Eq. (16) is extremely small, so that with practically no error q can be taken as unity, since $p+q=1$. In Eq. (16) m is the number of trials, which here means the number of quanta incident on a cone during a look. Also ν is the number of successes, which here means the number of quanta absorbed by a cone during a look. Therefore the probability of absorption of a single incident quantum of light is $p=\nu/m$, which when substituted in Eq. (16) converts it into

$$\delta=0.6745(\nu)^{\frac{1}{2}}. \qquad (17)$$

This says essentially that the "noise level" is proportional to the square root of the number of *absorbed* quanta per cone per look.

From the values of ν in Table III one may then compute the values of δ in terms of Eq. (17). The resulting values of δ are also given in Table III. They turn out to be about 4.4 and 5.3 quanta for the 17.5 and 2950 foot-lambert backgrounds respectively, which are approximately the same as the 4 quanta we have found necessary for seeing a target. Thus even at the higher brightness the minimum number of quanta required to make a target visible against a background is practically equal to the "noise level" or the most probable random fluctuations to be expected in the background field.

It is a fairly general rule that no detecting instrument can perceive a signal which is much below the noise level. Therefore even at the relatively high brightness of 2950 foot-lamberts, the cones do about the best that can reasonably be expected of them.

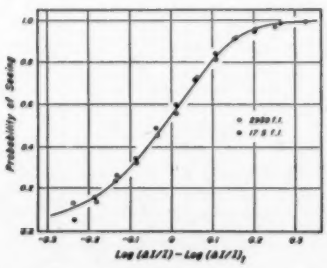

FIG. 18. Average probability of seeing, as a function of $\log(\Delta I/I)-\log(\Delta I/I)_t$ for the background brightnesses 2950 and 17.5 foot-lamberts.

X. BRIGHTNESS AND THE NUMBER OF QUANTA

It is an important experimental fact shown by the data in Figs. 2 to 7 and 8 to 13 that the shapes of the two series of frequency-of-seeing curves are essentially the same for the two levels of brightness of background. Thus, though the light in-

tensities of the background differ by a factor of 109, the shapes of the curves for seeing comparable images remain the same.

This identity is apparent by mere inspection of the figures. It is rendered quantitative by the fact that we used the same Eq. (14) with $n=4$ to describe the curves through the measurements. Indeed the identity of the frequency-of-seeing measurements at the two background brightnesses was evident to us as one of the earliest regularities of the data. In the beginning we averaged all the measurements at each brightness, using as in Section III $\log\Delta I/I-\log(\Delta I/I)_t$ as abscissas. Both sets of averaged measurements are shown together in Fig. 18. There is no doubt of their identity.

Such an identity means that the number of retinal events involved in recognizing a contrast in the form of a target is the same at the two background brightnesses. In terms of our hypothesis it says that at both brightnesses the same number (4 or 5) of additional quanta have to be absorbed by a cone regardless of the number of quanta it is already absorbing from the background. Evidently this number of quanta is set to be about the magnitude of the noise level of the very high background brightness and is kept at a constant value for all light intensities below this.

This conclusion is similar to that reached by the photochemical theory of contrast recognition.[8] This theory assumes that for any given target, a contrast is recognized when the added light ΔI initiates the same rate of photo-chemical change regardless of the photo-chemical equilibrium already established by the background. The photo-chemical change produced during an exposure can be expected to equal, approximately, the product of this rate and the critical exposure time. If the critical exposure time were independent of the background brightness, then the total photo-chemical change produced during an exposure would be independent of background brightness which is the conclusion already reached. Actually, the critical time of exposure changes slowly with changing background brightness so that the chemical theory leads to a conclusion which is similar to but not identical with the conclusion of this investigation. Indeed, so similar are the two conclusions that it may be difficult to distinguish between them.

Visual Acuity as Measured with Various Orientations of a Parallel-Line Test Object*

G. C. Higgins and K. Stultz
Eastman Kodak Company, Rochester, New York

(Received May 13, 1948)

Visual acuity has been measured in terms of the reciprocal of the angle in minutes subtended by the individual lines in a parallel-line test object at the limit of perception of the lines. Both clear and opaque lines in this test object were of equal width. It was found that the limit of perception of the lines in such a test object depends upon the orientation of the lines. Visual acuity, measured with the lines passing diagonally through the visual field at an angle of 45 degrees to the horizontal, is between 10 and 20 percent lower than that measured with the parallel lines passing vertically or horizontally through the visual field.

INTRODUCTION

During the process of making visual acuity measurements with a parallel-line test object, it was observed that the values obtained were a function of the orientation of the test object. Visual acuity measured with the parallel lines passing diagonally through the visual field at an angle of 45 degrees to the horizontal was found to be appreciably lower than that measured with the lines passing through the visual field either vertically or horizontally. We do not pretend to be intimately familiar with all of the literature on visual acuity. However, a careful examination of that part of the literature to which we have access does not reveal any reported data indicating the dependence of visual acuity on the orientation of the parallel-line test object. We feel, therefore, that it may be of interest to report our preliminary data on the variation of visual acuity as measured with different orientations of a parallel-line test object.

EXPERIMENTAL PROCEDURE AND RESULTS

The test object was made by photographing a parallel-line halftone screen in which the clear and opaque lines were of equal width. This halftone screen is one in which only one set of parallel lines is present, the orthogonal set of parallel lines normally present in halftone screens being absent. The resulting transparency, which was made on a very fine-grain photographic material, was placed in a projector and an enlarged image of the test object was viewed on a rear-projection screen. Both the projector and the screen are part of a new graininess instrument which will be described in detail at a later date.

The circular rear-projection screen, which has a diameter of 7.5 cm, is located in the center of the 280 cm-square front wall of the observation room. The area surrounding the projection screen consists of diffusing screens which are illuminated from behind by banks of lamps. The ceiling, the floor, and the two side walls of the observation room are white and the back of this room is closed by means of a black drape. The observer's station is located 200 cm from the front wall of the observation room and, at this viewing distance, the projection screen subtends an angle of 2 degrees in the observer's visual field and the entire illuminated front wall of the observation room subtends a visual angle of approximately 70 degrees.

An enlarged image of the test object was presented to the observer at ten different magnifications. As the magnification of the image was varied, the luminance of the rear-projection screen remained fixed at 50 ft-L, with no sample in place. The diffusing screens, which surround the rear-projection screen and fill the remaining area in the front wall of the observation room, were adjusted to a luminance of 2 ft-L. The images at ten different magnifications were presented to the observer in five different random orders. He was asked to state whether he could definitely perceive the individual lines in the test chart. Employing binocular vision, the observer was required to make one hundred judgments, that is, each magnification of the parallel-line test object was presented to the observer ten different times. From these data, the fre-

* Communication No. 1197 from the Kodak Research Laboratories.

quency of perception of the individual lines was determined for each magnification.

The parallel-line test object was oriented with the lines passing vertically through the visual field, and each of three observers made one hundred judgments, as described above. These measurements were repeated with the parallel lines passing horizontally through the visual field and with the parallel lines passing diagonally through the visual field, at an angle of 45 degrees to the horizontal. The three psychometric curves shown in Fig. 1 were obtained by plotting the frequency of perception of the individual parallel lines at each magnification against the corresponding angle in minutes subtended by a single line in the test chart. Each curve represents one of the three orientations of the test object. The angle of the lines with respect to the horizontal is indicated on each curve. The value of visual acuity as measured at each orientation of the test object was taken as $1/\alpha$, where α is the angle in minutes subtended by the single line in the test object when the lines were just perceptible 50 percent of the time. These values of α were taken directly from the psychometric curves shown in Fig. 1. The data plotted in Fig. 1 represent the composite readings for all three observers or 300 observations for each orientation of the test object.

The values of visual acuity as measured at the various orientations of the parallel-line test chart are shown in the first line of Table I. The values of α' are shown in the second line of Table I and the maximum percent variation between the values of visual acuity is shown in the last column of the table. It is clear from Fig. 1 and Table I that the individual lines in the parallel-line test object are appreciably more easily perceived when they are oriented either vertically or horizontally than they are when they pass diagonally through the visual field at an angle of 45 degrees to the horizontal.

Observations were also made with test-pattern fields which varied in visual angular diameter from approximately ten minutes to three degrees, and in all cases the parallel lines were definitely more easily perceived when they were oriented either vertically or horizontally than they were when they passed through the visual field diagonally at an angle of 45 degrees to the horizontal.

TABLE I. Variation of visual acuity as measured with various orientations of a parallel-line test object. Measurements were made with a constant viewing distance.

	Inclination of parallel lines with respect to horizontal			Variation
	0°	90°	45°	
$1/\alpha'$	1.02	1.00	0.90	
α'	0.98	1.00	1.11	12%

Similar results were obtained with both monocular and binocular vision. The perceptibility of the diagonal lines was improved, and the perceptibility of horizontal and vertical lines diminished when the observer merely tilted his head. In addition, when the circular test field was changed to a square field the same results were obtained, irrespective of the orientation of the edges of the square with respect to the direction of the parallel lines. Moreover, with either the circular or the square test field, the phenomenon was observed, irrespective of whether or not the surrounding screens were illuminated. While the data reported in the previous section are quantitative, it should be noted that the data reported in this paragraph are only qualitative, since sufficient observations were not made to establish the quantitative differences in visual acuity as measured under these diverse viewing conditions. On the other hand, the change in the ease of perception of the individual lines in the parallel-line test object as it was rotated was so easily noticeable that quantitative measurements were not necessary to establish the presence of these variations.

In order to eliminate possible complications introduced by the projection screen and projection optics, a print of this parallel-line test object was made on photographic paper. The

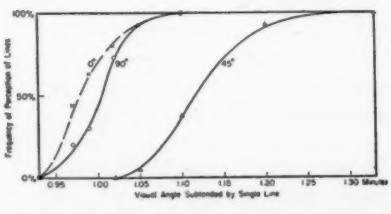

FIG. 1. The influence of the orientation of parallel-line test object upon the perception of the individual lines. The inclination of the lines with respect to the horizontal is shown on the curves.

individual black-and-white lines on the print were 0.4 mm wide and the entire circular test object was 7.5 mm in diameter. This print was mounted in the center of an octagon which had been cut from gray cardboard. The parallel sides of this octagon were 35 cm apart. The mounted print was placed in a special print-judging room and the viewing distance at which the individual lines were just perceptible was determined when the parallel lines passed vertically, horizontally, and diagonally through the visual field at an angle of 45 degrees to the horizontal. The angles, α, in minutes, subtended by the individual lines when they were just perceptible, were computed from these viewing distances and these values of α, together with visual acuity in terms of $1/\alpha$, are given in Table II. The maximum percent variation between the values of visual acuity is given in the last column of this table. It is clear from the data shown in Table II, that, as reported in the previous section, the individual lines in a parallel-line test object are more easily perceived when they pass through the visual field either vertically or horizontally than they are when they pass diagonally through the visual field at an angle of 45 degrees to the horizontal.

TABLE II. Variation of visual acuity as measured with various orientations of a parallel-line test object. Measurements were made with a variable viewing distance.

	Inclination of parallel lines with respect to horizontal			Variation
	0°	90°	45°	
$1/\alpha'$	0.98	0.97	0.70	
α'	1.02	1.03	1.42	29%

An ophthalmologist examined the eyes of the three observers. Two of these observers had normal vision without correction and the third had normal vision with correction. Special care was taken to ascertain that astigmatism was not responsible for the reported effect. In addition to the three observers who made the quantitative measurements, twelve different individuals made observations which showed that the individual lines in the parallel-line test chart were more easily perceived when they passed through the visual field either vertically or horizontally than when they passed through the field at an angle of 45 degrees to the horizontal.

CONCLUSIONS

Visual acuity measured with a parallel-line test object is appreciably lower when the lines pass through the visual field at an angle of 45 degrees to the horizontal than when they pass through the visual field either vertically or horizontally. The qualitative manifestation of this phenomenon can be seen quite easily by rotating a halftone print in a newspaper. If the area being examined in this print is of moderate uniform density, the halftone dots will appear as an array of lines when they are aligned either vertically or horizontally, but this systematic array will disappear when they pass through the visual field diagonally. The workers in the graphic arts are aware of this decreased visibility for diagonal lines and customarily make halftone prints with the two orthogonal sets of parallel lines passing diagonally through the visual field.

The data reported in this paper are preliminary and are part of a series of measurements which are being made to determine the factors which affect the perception of nonuniformity in a pattern. The complete investigation will be reported later.

JOURNAL OF THE OPTICAL SOCIETY OF AMERICA VOLUME 38, NUMBER 9 SEPTEMBER, 1948

Multi-Prism Spectrographs with Glass Optics by Carl Zeiss, Jena

G. HANSEN*
Oberkochen, Germany
(Received April 26, 1948)

A new three-prism spectrograph following the original prism system of Foersterling is described.

I. SINGLE- OR MULTI-PRISM SPECTROGRAPH?

THE resolving power of a spectrograph depends on the base length of the prism, or, in the case of a multi-prism spectrograph, on the sum of the base lengths; hence, in a prism spectrograph, the same resolving power can be obtained with a variable number of prisms. If, instead of one prism of large base thickness, m prisms are used, each having a base length of $1/m$ of the single large prism, then the angular dispersion is m-times larger than that in the case of the single prism. For that reason the focal length of the camera can be reduced to $1/m$, if a spectrum of equal length is desired. The diameter of the camera objective being reduced in the same ratio, the luminosity of the spectrograph will remain unchanged. A multi-prism arrangement requires only the fraction $1/m^2$ of the material needed for a single prism.

An advantage of the single-prism spectrograph is its ability to cover a large range of the spectrum with a single exposure and without adjustment. It has the disadvantage that, if high resolving power is required, expensive optical parts and a long focal-length lens are necessary. On the other hand, points in favor of the multi-prism spectrograph are that, even with maximum resolving power, considerable raw material and production costs are saved and that a short focal-length lens can be used. Disadvantages of the multi-prism apparatus are that it covers a small range only, that higher requirements are placed on the camera objective because of the large image angle, and that mechanical devices are necessary to bring the prisms and lenses into the correct position each time. The mechanical system for the moving parts in a multi-prism spectrograph presents the main difficulty of design. An entirely satisfactory solution of this problem has not been given previously. The designs prior to 1900 were meant to be spectroscopes only. The accuracy of the complicated mechanism was not enough to allow the satisfactory photographing of spectra. In some cases the design required that in order to change over from one spectral range to the other, each single element—prisms and camera—had to be freshly adjusted; in particular, changing the apparatus from single to double passage of the rays required a complete re-adjustment.

II. ZEISS THREE-PRISM SPECTROGRAPH WITH PRISM SYSTEM OF FOERSTERLING'S DESIGN

In order to explain the idea underlying the design of the new Zeiss prism spectrograph "G 50," it is advisable to describe its predecessor with three prisms, designed by Foersterling. A large number of these instruments have been manufactured in the same design since 1926; they are being used in all parts of the world. This instrument is semi-automatic. The angle between collimator and camera remains constant. The three prisms have a base length of 7 cm each and are simultaneously adjusted by turning a handle, so that the central ray of each color passes through them at minimum deviation. Figure 1 shows a diagram of the path of the rays for a camera with a 1300-mm focal length. This camera is designed for double passage of the rays. The effective prism thickness is therefore 40 cm. The apparatus can be equipped with a set of cameras of shorter focal length (84 cm, 27 cm, 12 cm), using in each case a collimator and single passage of the rays. Figure 2 depicts this arrangement on a movable stand with adjustable height. The light enters through the slit, which is situated near the plate holder, and, after passing through the prisms, is reflected by a plane mirror .This apparatus has the following disadvantages:

(a) The central prism consists of two parts. Light which enters near the top of the prism and

* Translated by S. Meyer.

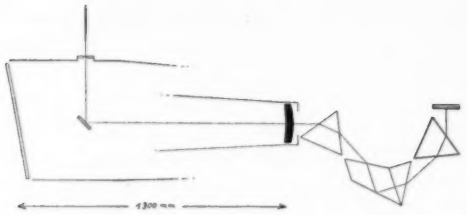

FIG. 1. Zeiss three-prism glass spectrograph with prism system of Foersterling's design and with Littrow camera of 1.3-m focal length (diagram).

has a smaller refractive index than the central ray is totally reflected at the contact plane of the two prism parts, with a resultant disturbing reflection in the middle of the spectrum. This reflection can be eliminated if the spectral prism is made from one piece. The complete prism set cannot be made out of quartz because the disturbing effects of birefringence in the central prism cannot be eliminated.

(b) When longer focal lengths are used, the arrangement of collimator and camera at right angles is impracticable, requiring too much space. Changing over from single to double passage of rays calls for moving either the source of light or the spectrograph.

(c) The apparatus is only semi-automatic. Adjustment of the camera extension and of the inclination of the plate holder must be effected separately for each wave-length.

The "G 50" spectrograph was designed with a view to the following requirements: a full, automatic spectrograph with a set of prisms for which quartz could be used and which had no disturbing reflections; with compact dimensions even when using collimators of long focal length; and with a simple method of change-over from single to double passage of rays without adjustment of the source of light.

FIG. 2. Zeiss three prism spectrograph with 1.3-m camera.

III. EARLIER MULTIPLE-PRISM ARRANGEMENTS

A

The first automatic prism spectrograph was designed by L. M. Rutherfurd,[1] a New York lawyer and amateur astronomer. In his design, only the movement of all the prisms was automatically controlled. The first design incorporating automatic adjustment of the telescope as well as of the prisms, was published by J. Browning[2] in 1870. These arrangements, although satisfactory for visual observation, did not guarantee reproducible adjustment of all movable parts. In 1904, Fabry and Jobin published a description of an apparatus with double passage of rays and with automatic adjustment of two prisms and a mirror. This design, for the first time, incorporates the condition necessary for the correct kinematic solution of the problem: each of the movable elements rotates around a fixed axis. The spectrograph of Fabry and Jobin still has some disadvantages: the three movable elements require three rotating axes; the distances between the single prisms is rather large and changes at each adjustment to an unnecessarily large degree; the transfer of the rotating movement from one axis to the others is effected with the help of curved surfaces which slide on one another. In a prism spectrograph it is important to keep the number of rotating axes small and to make the coupling between them as simple as possible.

B

(a) *The New Prism System*

The prism system of the "G 50" spectrograph consists of three identical prisms and a plane mirror. These four elements have only three rotating axes[3] (Fig. 3). The prisms 1 and 3 rotate around axis S_1, the central prism 2 around S_2, and the plane mirror M around S_3. The axes S_2 and S_3 rotate at a speed which is three times that of S_1. The total deviation of the prism system is 180°

[1] L. M. Rutherfurd, Am. J. Sci. (II) **39**, 129 (1865).
[2] J. Browning, M.N.R.A.S. **30**, 198 (1870).
[3] G. Hansen, Physik. Zeits. **43**, 213 (1942).

for the ray at minimum deviation. The direction and position of the central ray are fixed and independent of the color. The reproducibility of the adjustment is dependent on the precise rotation of the mirror. The light passes through all the prisms at minimum deviation; small deviations from the correct position are therefore of no consequence. The rotating axis S_1 passes through the connecting line from the center of the face of the first to that of the last prism. This connecting line is at right angles to the entering and emergent rays. The rotating axis is situated halfway between the central rays of the incoming and emerging beams. Thus, to a first approximation, the rotation of both prisms does not cause a displacement of the prism faces at right angles to the path of rays. The rotating axis S_2 for the central prism may be located in various ways. In Fig. 3 it is located so that the neighboring rear corners of prisms 1 and 2 are as close together as possible. Contact is made only at the two extreme positions. Between these positions small displacements occur. In order to obtain the desired effect, the axis S_2 is placed so that the connecting line from S_1 to the rear corners of the prisms passes through it. The distances between the rear prism-corners and S_1 and S_2, respectively, have the ratio of 3/1. Since the angular rotations of prisms 1 and 2 are in a ratio of 1/3, the rear corners travel almost equal amounts.

It is important that the path of the rays in the whole prism system be made as short as possible. The shortest path is obtained if the ray which enters the top of prism 1 after being reflected by the mirror just passes the left rear corner of prism 2. This requirement introduces a relation between the prism angle φ and the total deviation δ:

$$\cot\varphi/2=\tan\delta/2\cdot(2\cos\delta-\cos 2\delta)\cdot\cos^{-1}2\delta.$$

(*b*)

The above relation holds only if the prisms remain in their initial position, as illustrated. If the prisms are rotated from their central position by an angle of $\Delta\epsilon$, the above relation changes somewhat, and the prism angle becomes dependent on the size of $\Delta\lambda$ or on the change of the index of refraction which corresponds to this difference in wave-length. In the Table I the

TABLE I.

n	φ $\Delta n=0$	$=0.05$	$=0.10$
1.40	84.3	85.3	86.0
1.50	73.7	74.4	75.2
1.60	64.9	65.5	66.2
1.70	57.7	58.2	58.7
1.80	51.8	52.2	52.6

prism angle φ is given for different values of n and Δn. When $\Delta n=0$ the difference a between the centers of the incoming and out-going beams is

$$a=b\cdot\sin\delta/2\cdot\cos^{-1}2\delta,$$

where b is the base length of the prisms.

(*c*) *Axis of Rotation of the Mirror*

The axis of rotation of the mirror must be so placed that the central ray for the extreme position of the prism system toward the red travels from the center of the exit face on prism 2 to the center of the entrance face on prism 3. The computation of the position of the center of rotation can be made analytically without special difficulty. The following table shows, for $\Delta n=0$ and for three different values of n, the coordinates of the mirror axis. A rectangular system of coordinates is used, with the y axis parallel to the

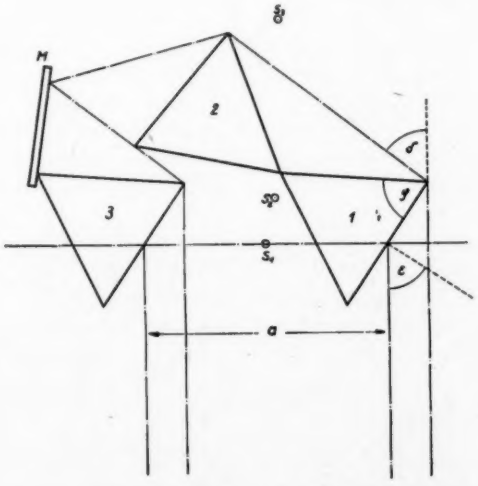

FIG. 3. Prism system of the "G 50" spectrograph: S_1=axis of rotation of prisms 1 and 2; S_2=axis of rotation prism 3; S_3=axis of rotation mirror M; a=distance between collimator and camera axes.

TABLE II. Axis of rotation of mirror (prism base = 1); $\Delta n = 0$.

n	x	y
1.40	−0.745	+1.242
1.60	−0.767	+1.501
1.80	−0.791	+1.779

central ray before it enters prism 1. The origin coincides with the point where this ray enters prism 1. (See Table II.)

IV. THREE-PRISM SPECTROGRAPH "G 50"

A. Single and Double Passage of Rays

Figure 4 is a sketch of the path of rays in the Zeiss spectrograph "G 50." Light source and slit can remain fixed when either single or double passage of the rays is used. With the single passage of rays, the light from the slit travels to the mirror M_1, from there to the collimator lens L_2, through the prism system, and then through the camera objective L_1 to the camera. The spectrum is produced on the plate P. When the light is to traverse the prisms twice, mirror M_3 is inserted in the path of rays. Furthermore, the light after passing the slit is displaced and raised about 15 mm with the help of two reflections in a parallelopiped prism. In this way it falls on mirror M_2, which is located somewhat above the plane of the drawing. Now the light first enters the camera objective L_1, which in this case serves as collimator lens, passes once through the prism system to the mirror M_3, which is slightly tilted downwards, is reflected from there, and passes for the second time through the prism system. The spectrum is produced on plate P as before.

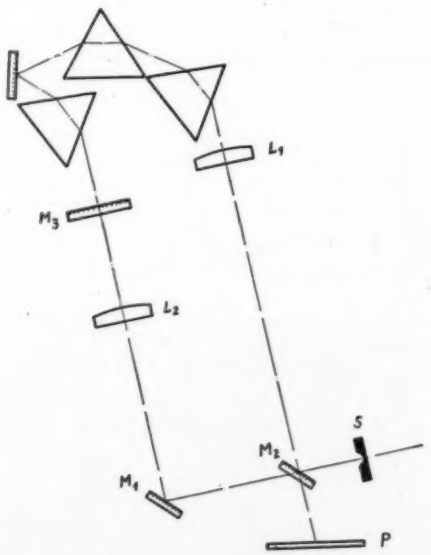

FIG. 4. Path of rays in the "G 50" spectrograph: S = slit; L_1 = camera lens; L_2 = collimator lens; M_1 = mirror; M_2 = mirror above the plane of optic axis for double light passage; M_3 = mirror for double light passage, to be swung out for single light passage.

B. Focusing

(a) The common drawback of spectrographs with double passage of rays (autocollimation) lies in the disturbing reflections occurring at the lens system which serves as collimator as well as camera objective. For this reason, lens systems are used with the smallest possible number of glass-air surfaces. With the simple lens the two reflections can easily be neutralized. C. B. Brackett suggested in 1882 making the inner surface of the lens (facing the slit) concave with a radius approximately equal to its focal length. In this way the first surface of the lens forms a real image of the slit at the plane of the plate, which can be moved away from the spectrum by very slightly tilting the lens around the horizontal axis. The reflection at the second surface is always a real image and in this case occurs at a distance of about one-third of the focal length. It can be easily removed by a very small diaphragm at the image point.

If it is desired to replace the prisms of the spectrograph with others of a different material, the only practical procedure is to exchange the whole optical system—prisms and lenses. In this case the distance between slit and lens is rather strongly dependent on the wave-length, because for each material the index of refraction depends on the wave-length. Since the relation between the distance from slit to lens and the index of refraction is controlled by the external form of the optical parts, the relation between prism rotation and lens distance remains constant for all materials, provided that the outer form of the optical parts remains the same for the various substances. Hence a mechanism can be used which both rotates the prisms and changes the distance be-

tween slit and lens. If the slight influence exercised by the finite thickness of the lens on the relation between its focal length and the index of refraction is neglected, it is easy to design a mechanism which effects a linkage between the lens displacement and the prism rotation in a mathematically exact way. In order to keep such a mechanism as simple as possible, the element which makes the angular rotation proportional to the sine of the angle of emergence is omitted and this rotation is made directly proportional to the angle itself. The resulting simple and nearly accurate mechanism is difficult to make, however, because a bar with an exact straight edge is required which is rotated around the prism axis with the help of a lever, the length of which should approximately be equal to the focal length. For an apparatus of the type of "G 50" with a focal lens of 2 m, such an arrangement would be unwieldy. A mechanism was designed, therefore, with a straight stationary bar and with a lever of shorter length to transfer the rotation to the prism table. This mechanism is sketched in Fig. 5. A lever is attached to the mount which carries the prisms and lenses. This lever turns faster than the prism carrier, in the ratio of $v/1$. The lever carries a roller at one end that slides along a bar which forms the angle γ with the optical axis of the spectrograph. The lever in its central position makes the angle β with the optical axis. The length of the lever is l. The factor A, shown in the illustration, is then as follows:

$$A = l \cdot \sin(\gamma - \beta) \cdot \sin^{-1}\gamma.$$

If the mechanism is moved from the central position by an amount Δs, the change of β which is v-times as large as the change of the prism position will be correct. The change of A is equal to the change of focal length of the lens, which corresponds to the difference in the index of refraction. The difference in index of refraction of course requires change in the angle of incidence of the prism. The change of the incident angle must be adequately linked with the change of A by the mechanism by a proper selection of the angle and dimensions. For the range from $n=1597$ to $n=1670$ and $v=6$, the following values are found at 1000-mm average focal length:

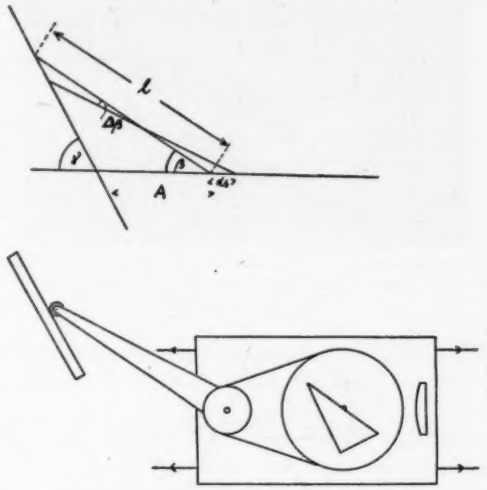

FIG. 5. Mechanism for rotation of prisms of "G 50" spectrograph (diagram).

$$A = 256.47,$$
$$l = 381.90,$$
$$\beta = 32.8°.$$

The values of A and β are given for the mean value of $n=1.63407$.

(b) Figure 6 shows the mechanism of the "G 50" with the correct dimensions for the extreme blue and red settings. The axis of rotation for the central prism has not been placed at a point where the adjacent rear corners touch in the two extreme positions. The axes of the prisms are rather far apart in order to make possible a more convenient mechanical arrangement. The linkage between them is effected by steel ribbons. The lever which transfers the movement to the prisms rotates twice as fast as the mounting of the plane mirror and six times as fast as the mount for the first and third prisms. The movement of the whole prism system is initiated at the contact point between turning lever and bar. Collimator and camera lenses are displaced with respect to each other by the amount of the distance between the central rays so that lenses of equal focal length can be used. The dimensions of the apparatus are: prism base for all three prisms, 10 cm each; average focal length, 200 cm. The mechanism must control the distance between lenses and slit or plate for each position of the

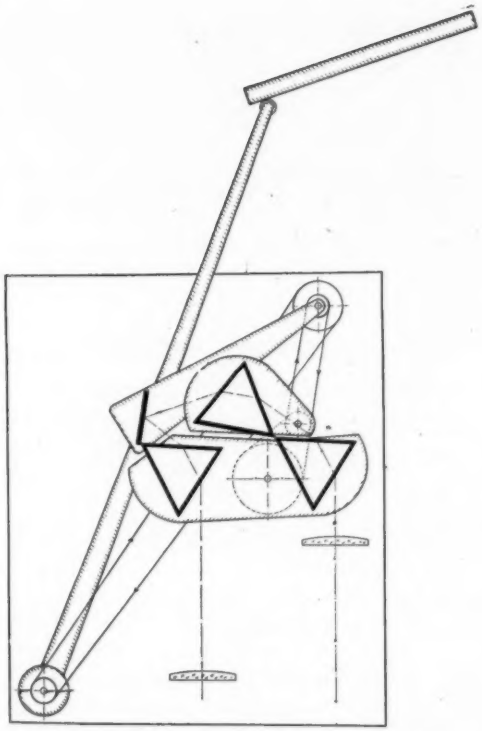

FIG. 6. Mechanism of the "G 50" spectrograph for extreme red and blue positions, respectively.

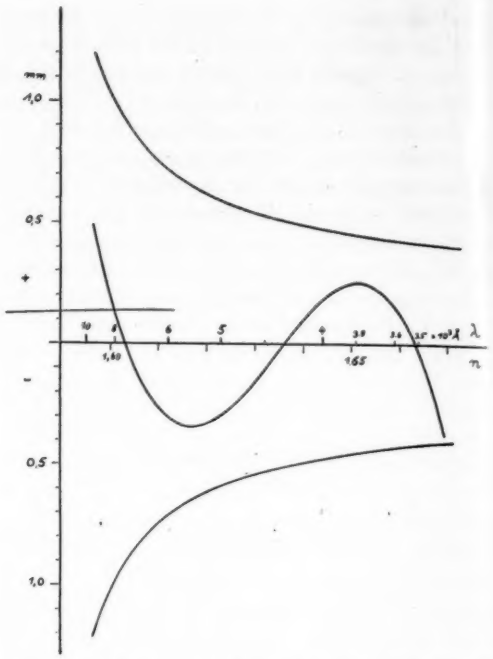

FIG. 7. Deviation curve of the mechanism of the "G 50" spectrograph; the two outer curves show the allowable deviation.

prisms in such a way that any lack of focus caused by improper adjustment remains negligible. The depth of focus is equal to the product of wave-length and the square of the aperture ratio (the ratio of focal length to the diameter of the camera objective). Considering the change of wave-length and of aperture ratio, a definite tolerance for the adjustment error of the instrument can be established for each wave-length. Figure 7 shows the curve of error for the mechanism and allowable error for each wave-length. It shows that the amount of deviation between 10,000 and 3500A remains well within the permissible tolerances. The test of the complete instrument showed, in fact, that a focusing error could not be found.

(c) The first experimental model showed one defect which should be eliminated. The linkage between the axis of the rotating lever and that of the plane mirror is effected by a steel ribbon of almost 16-cm length. The elasticity of the steel ribbon, which is kept taut by a strong spring, together with the comparatively large inertia of the mirror carrier, proved to be a rather strong source of oscillations. To eliminate these, the steel ribbon was replaced by a linkage, as shown in Fig. 8. The steel ribbon produces an exactly proportional transfer of the rotating movement to the rotating lever at a ratio 1/2. Although the mechanical linkage does not give exactly proportional rotation, the deviations can be used to reduce the error of the mechanism still farther by about 50 percent.**

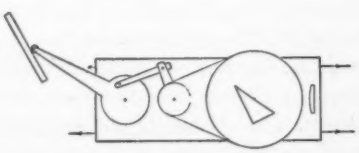

FIG. 8. Intended changes of mechanism of the "G 50" spectrograph (diagram).

** The test of this improvement on the only available experimental model of the "G 50" was made impossible by the end of war and the occupation of Jena.

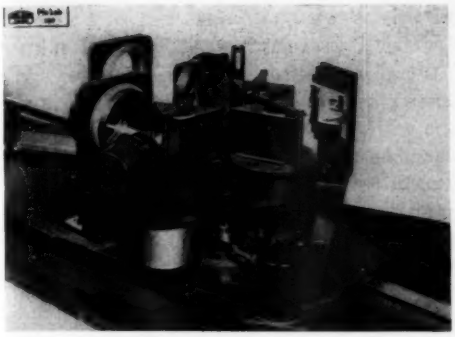

FIG. 9. Prism system of the "G 50" spectrograph, with prism of 100 mm base length (mirror M_3 of Fig. 4 is inserted).

C. Construction

Figure 9 shows the prism arrangement in the central position. It shows the ribbon connection between the mirror carrier and the carrier of the central prism. In the background toward the center is the large round plane mirror inserted in the path of rays. It can be rotated around the vertical axis and is kept in position by a small permanent magnet. This very simple arrangement has proved its merits. Figure 10 depicts the mechanism for tilting the plate holder. The relation between the inclination of the plate holder and the wave-length is different for single and double passage of the rays. A curved template is used for controlling the inclination. The curved template can be used at two different angles to the axis of the spectrograph and in both cases produces the correct inclination of the plate holder with sufficient accuracy. The plate holder itself is turned against a stop when switching over from single to double passage of the rays, since the angle of the plate holder is different when used for single passage of the rays from that used for double passage of the rays. Figure 11 also shows the movable curved template. Figure 11 shows the complete apparatus without hood. The wave-length drive is transmitted to the carrier at the far side of the apparatus where, with the help of a spindle, it actuates the turning lever for the prism movement along the guiding bar. This mechanism is built under the base plate and is not visible in the illustration. Figure 12 shows the apparatus as seen from the slit side, with protecting hood in place. In order to switch over from single to double passage of the light beam, three operations are necessary:

1. By pressing a button behind the slit, a prism with two reflections is inserted, which lifts the path of rays.
2. The plate holder is adjusted to the correct basic angle by turning it against a stop.
3. The curved template for the movement of the plate holder is placed in a different position

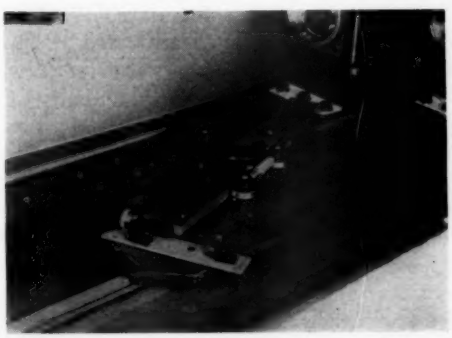

FIG. 10. Curved template to govern the plate holder movement.

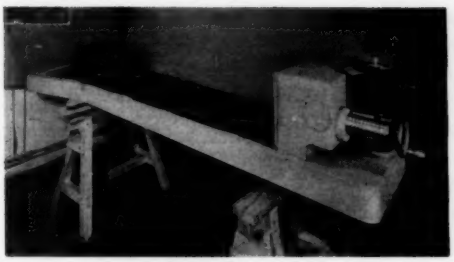

FIG. 11. General view of the "G 50" spectrograph without the hood.

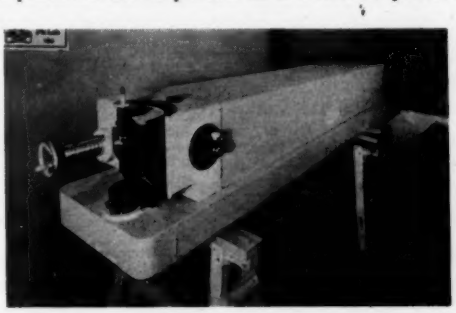

FIG. 12. Zeiss "G 50" spectrograph.

for double passage of the rays. A change of focusing is not necessary. Prism rotation and change of focus are always effected automatically.

The apparatus can be used for the range of approximately 10,000 to 3700A. The resolving power for single passage of the rays is approximately 5600 at 10,000A; for double passage of the rays, 250,000 at 3700A.

The "G 50" spectrograph was designed in 1939 and a model was completed in November 1941. At the request of Professor Gatterer, Castel Gandolfo, Italy, a similar apparatus ("G 80") and prisms with the thickness of 15 cm was designed. This apparatus had a 30° prism instead of the plane mirror at autocollimation, as requested by Professor Gatterer. Focusing was done with the help of a curved template, which was made without difficulty in the shops at Jena. The "G 80" ordered by Professor Gatterer was almost completed in October 1946 and was at that time removed to Russia, when the Zeiss Works were dismantled as reparations. The "G 50" described above may be in the United States.

JOURNAL OF THE OPTICAL SOCIETY OF AMERICA VOLUME 38, NUMBER 9 SEPTEMBER, 1948

Formation of Optical Images by X-Rays

PAUL KIRKPATRICK AND A. V. BAEZ
Stanford University, Stanford, California
(Received March 12, 1948)

Several conceivable methods for the formation of optical images by x-rays are considered, and a method employing concave mirrors is adopted as the most promising. A concave spherical mirror receiving radiation at grazing incidence (a necessary arrangement with x-rays) images a point into a line in accordance with a focal length $f=Ri/2$ where R is the radius of curvature and i the grazing angle. The image is subject to an aberration such that a ray reflected at the periphery of the mirror misses the focal point of central rays by a distance given approximately by $S=1.5Mr^2/R$, where M is the magnification of the image and r is the radius of the mirror face. The theoretically possible resolving power is such as to resolve point objects separated by about 70A, a limit which is independent of the wave-length used. Point images of points and therefore extended images of extended objects may be produced by causing the radiation to reflect from two concave mirrors in series. Sample results are presented.

INTRODUCTION

THE literature of x-rays contains many passages deploring the supposed impossibility of focusing x-rays with lenses or mirrors. Both the difficulty and the regret are easily appreciated. A satisfactory x-ray microscopy would open up fields of investigation closed to the optical microscope because of its restricted resolution, and to the electron microscope because of the limited penetrating power of electrons. X-ray spectrometers and diffraction instruments would probably have evolved along simpler or more advantageous lines had their designers possessed the means of optical control available to workers with light in other spectral regions.

X-RAY LENSES

Roentgen's[1] first experiments convinced him that x-rays could not be concentrated by lenses; thirty years later his successors understood why. X-ray refractive indices are less than unity by an amount δ which for common solids and x-rays of general practice has a value of the order of 10^{-5}. It may readily be shown that the focal length f of a single refracting surface of radius R is approximately R/δ. For several surfaces in series, arranged cooperatively, we have $1/f=\delta(1/R_1+1/R_2+\text{etc.})$. To make a successful lens we require a large δ and slight absorption. Unfortunately ma-

[1] W. C. Roentgen, *Sitzungsberichte der Würzburger Physikalischen-Medicinischen Gesellschaft* (1895).

terials of large δ are also strong absorbers, the absorption coefficient increasing much more rapidly than δ with increasing atomic number. An element of low atomic number, such as beryllium, is indicated.

In choosing a usable x-ray wave-length we note that δ is proportional to λ^2 and the absorption coefficient to λ^3. This makes long waves undesirable. For concreteness of argument let the wave-length be that of the K_α lines of molybdenum (0.71A), which in beryllium gives $\delta = 1.13 \times 10^{-6}$. For one refracting surface we shall have $f \approx 10^6 R$. If a radius of one centimeter be assumed it is found that about one hundred lens surfaces in series would be required to bring the focal length down to one hundred meters. This would produce a cumbersome and very weak lens system of poor transparency. These discouraging considerations incline us toward other methods.

IMAGES WITHOUT RAY DEVIATION

Optical imagery of a sort may be had without ray deviation, as the pinhole camera and the shadow picture demonstrate. The production of pinhole images of x-ray targets and focal spots is an old art, and one which, but for intensity difficulties, might be extended to objects emitting secondary x-radiation. Figure 1 shows an image of this kind which was made with an unusually small pinhole and therefore shows more focal-spot detail than is usually seen. Objects not self-luminous might be imaged by pinhole photography by placing them between a broad x-ray source and the pinhole. The fatal limitation of this form of imagery is the complete incompatibility of high resolving power with high speed. Both are controlled by the size of the pinhole. Resolution is linearly improved as hole diameter is decreased, but this same change diminishes the mean illumination of the image *parabolically*. The method is therefore unpromising.

A shadow picture technique which has been proposed by Zworykin[2] and others requires the production of an exceedingly fine focal spot for the radiation source. It is not stated that the method has been tried.

An alternative proposal, more readily put to practice, involves the use of a small hole located outside the window of a conventional x-ray tube. Radiation from the focal spot within passes through this hole in a divergent beam which may be intercepted by shadow-producing objects on its way to the photographic emulsion. Figure 2 is a shadow image of this kind in which a copper

FIG. 1. Pinhole image of target of a deep-therapy x-ray tube. The focal spot is a crude copy of the cathode filament structure.

FIG. 2. X-ray image of copper gauze of 200 meshes per linear inch, formed by a shadow projection method. The x-rays diverged from a small hole and passed through the gauze on the way to the film, producing a 98-fold magnification.

[2] Zworykin, Morton, Ramberg, Hillier, and Vance, *Electron Optics and the Electron Microscope* (John Wiley and Sons, New York, 1946), p. 111.

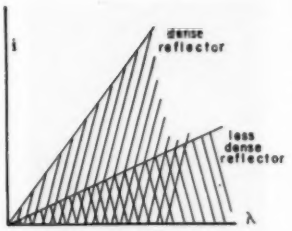

FIG. 3. Shaded areas represent conditions of wave-length (λ) and grazing angle (i) for which total reflection of x-rays occurs.

gauze of 200 meshes per linear inch was used as object. The hole which served as the effective radiation source was the intersection of two crossed slits in contact. The initial magnification was 98 and the exposure, with a molybdenum target at 35 kv, was 1.2 ampere hours. The shadows appear to be sharp to five or ten μ at the object. Evidently this process suffers from intensity limitations like those of the pinhole method described above.

X-RAY MIRRORS

It remains to consider the possibility of producing x-ray images with mirrors. There are two distinct kinds of x-ray reflections, *viz.*, the reflection from crystals with which the name of Bragg is familiarly associated, and the external total reflection which takes place at surfaces which are either crystalline or amorphous when the tangential angle of incidence is sufficiently small. Reflection of the latter type is highly efficient, and even complete for certain radiations, but the limitation of the angle of incidence to values under one degree has heretofore completely discouraged the development of x-ray catoptrics.

FIG. 4. Line images of a short and narrow slit from which x-rays diverged to a spherical concave mirror of 11-m radius. Grazing angle of incidence about 0.01 radian. The film receiving the reflected radiation was placed at eight successive positions, which included a position of good focus.

Bragg reflection admits of convenient angles of incidence but suffers from severe intensity limitations because of its essential wave-length selectivity. Only the most perfect of crystals could be considered if high image quality were required, and it has not been demonstrated that even these would suffice. We consider that good image formation by crystal reflection is an interesting possibility but that total reflection methods offer the greater promise.

When a parallel beam of x-rays of the familiar sort is incident upon a smooth surface at a small grazing angle i those components of the beam possessing wave-lengths in excess of a critical value λ_c will be reflected with almost complete efficiency, while shorter wave-lengths will not reflect at all. The critical value, as given with good accuracy by classical dispersion theory, is $\lambda_c = (ci/e)(\pi m/n)^{\frac{1}{2}}$, where c is the speed of light in cm/sec, e and m are the electronic charge and mass in electrostatic units and grams respectively, i is expressed in radians and λ_c in centimeters, and n is the total number of electrons per cubic centimeter of the reflector. Figure 3 summarizes the situation in a simple manner. For soft x-rays or reflectors of high atomic number the sharpness of the critical wave-length for a particular angle (or of the critical angle for a particular wave-length) is somewhat impaired; the "total" reflection does not achieve totality and the forbidden reflection does not remain at zero intensity.

Probably the possibility of forming x-ray images by reflection from a portion of an ellipsoidal surface has occurred to many. There is no record that it has ever been done and it is very doubtful that it has been tried. Production of the required surface, that of a very eccentric ellipsoid, would present a difficult problem to optical workers. We therefore prefer to see what may be done with spherical surfaces and moderate departures therefrom.

It is obvious that x-rays may be focused[3] by concave spherical mirrors, though, with such oblique incidence as is necessary for reflection, a strong astigmatism must be expected. By an extension of ordinary optical principles to this unprecedented obliquity it is found that a narrow bundle of rays from a point source will, upon reflection, give rise to two focal lines whose positions derive from two focal lengths. Meridian-rays (in a plane containing the radius of curvature R of the mirror at the point of incidence) focus according to a focal length $f_m = R \sin i/2$, while sagittal rays (in a plane normal to that of meridian rays) possess a focal length $f_s = R/2 \sin i$.

The astigmatic difference here is great, the ratio of the two focal lengths being $1/i^2$ or about 10,000 in possible x-ray cases. The extreme weakness of such a mirror for sagittal rays makes it practically equivalent to a circularly cylindrical surface. The meridian focal line is readily demonstrated. Figure 4 shows a series of such lines obtained by reflecting x-rays at a platinum-coated glass mirror for which $R = 11$ m and $i = 0.0102$ radian. The distance from the effective source (a fine slit parallel to the focal lines) to the center of the mirror was 9.8 cm, and the distance from mirror to photographic film was increased in steps, producing at each step one of the parallel lines of the figure. The progressive improvement and deterioration of the focus is clearly shown.

GEOMETRICAL THEORY OF THE IMAGE

We discuss here the location of the image formed by grazing reflection of meridian rays at a spherical reflector, and also the sharpness of that image as affected by both geometrical and diffraction considerations. This is, as shown in Fig. 5, a two-dimensional problem. Given a circular reflector of radius R, illuminated at a small grazing angle i by a narrow bundle of radiation from a point source P, we seek to determine the location of Q, the image of P. The object and image distances, p and q, are measured from an arbitrarily selected point O on the surface of the reflector. Consider a point N situated

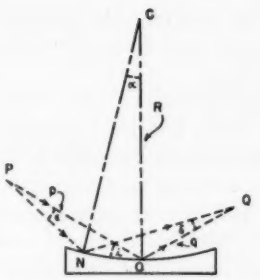

FIG. 5. Reflection of radiation from a spherical mirror at small grazing angles. Meaning of symbols used in the text is shown.

upon the reflector near enough to O so that $NO \ll R$. The chord NO subtends at the center of curvature C an angle α. The image Q is at the intersection of the reflected rays from N and O. These rays meet at an angle δ, while the angle between the incident rays is designated by ϵ.

Application of the law of sines to the triangles PNO and QNO yields

$$p\epsilon = R\alpha(i + \epsilon - \alpha/2) \tag{1}$$

and

$$q\delta = R\alpha(i - \delta + \alpha/2), \tag{2}$$

in which small angles have been identified with their sines. Eliminating δ and ϵ by the relation $\delta + \epsilon = 2\alpha$, which follows from the law of reflection, and introducing the symbol $a = \alpha/i$, we obtain

$$\frac{1}{q+2af} + \frac{1}{p-2af}\left(\frac{2-a}{2+a}\right) = \frac{1}{f(1+a/2)}, \tag{3}$$

in which the substitution $f = Ri/2$ has been employed. Evidently for vanishingly small α this becomes $1/q + 1/p = 1/f$, which agrees with the statement above that $R \sin i/2$ is a focal length,

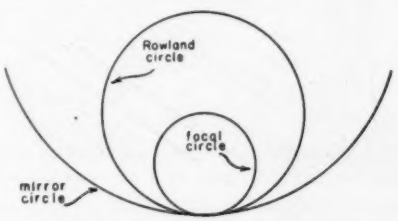

FIG. 6. Outside circle represents profile of a mirror for which intermediate circle includes conjugate foci of unit magnification and inside circle is the locus of principal focal points.

[3] W. Ehrenberg, Nature **160**, 330 (1947). This brief communication describes the formation of line images by reflection of x-rays from a point source at a gilded glass plate which had been bent so as to form an approximate circular cylinder.

and, taken in combination with the law of reflection, locates the image for a mirror of restricted aperture.

For the special case of unit magnification the object and image will be found at points on a circle passing through the point O of the mirror. This property of spherical mirrors is familiar in connection with the concave grating, the locus being known as the Rowland circle. In the present application there are three significant circles having radii in the ratios 1:2:4 as shown in Fig. 6. The outer circle is an extension of the arc of the mirror, the intermediate one is the locus of object and image for unit magnification, while the smallest circle contains the infinity of principal focal points of that portion of the mirror lying near the intersection of the three circles.

It is clear from Fig. 6 that the focal surface is extremely oblique to the focused rays. An inclined object conforming to the Rowland circle would give rise to a symmetrically inclined image lying along the opposed side of the same circle. This would be bad enough, but the image of a plane object disposed *normally* to the principal incident ray would be even more oblique. We shall return to this matter at a later point.

The argument of the two paragraphs just above pertains to ray bundles or mirror apertures so narrow that α may be neglected. In such cases no problem of focal unsharpness arises, but in the approximation where small quantities of the order of a are retained but terms in a^2 are discarded as being negligible in relation to unity, it is found that the image of a point suffers from a considerable spherical aberration. This may be investigated by returning to Eq. (3) and investigating the variation of q with α. Let the value of q for vanishingly narrow beams be hereafter designated by q_0, and let M stand for q_0/p, the magnification of the image. Be it noted that $f/p=M/(M+1)$. Equation (3) may be written in the form

$$q/q_0=(M+1)^{-1}[1-2a+(M+a/2-a^2M)(1-\tfrac{3}{2}aM)^{-1}]. \quad (4)$$

Upon dropping the term a^2M this becomes

$$q-q_0=\frac{q_0a}{M+1}\left[\frac{1+3M^2}{2-3aM}-2\right]. \quad (5)$$

Evidently the wandering of the focus with increasing a (hence, increasing α) is accentuated at high magnification and diminishes as the angle of incidence is increased. For this and other reasons it is desirable to use the highest feasible grazing angles. It was to obtain such angles that the mirrors described earlier were coated with platinum.

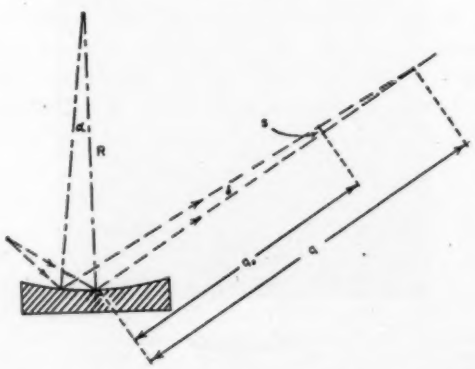

FIG. 7. Detail of ray intersections at the image of a point, formed by a spherical mirror illuminated at a small grazing angle.

FIG. 8. Image formation with an elliptical mirror. The spherical aberration of Fig. 7 is avoided. The bundle shown includes all rays from a point object whose grazing angle of incidence does not exceed a critical value i. Magnification is unity.

The image impairment caused by this aberration is not measured by $q-q_0$ but by the small distance S by which the aberrant ray misses the image point formed by rays for which $\alpha\to 0$. Figure 7 shows the manner in which rays of positive α pass the focus of rays for which α is vanishingly small.

As a matter of fact, reflected rays resulting from both positive and negative values of α pass above the focus of central rays, a fact which insures a goodly concentration of rays close to the focus. Such a focus will be sharp and intense on the side which is below in Fig. 7, fading off on the side above.

We are concerned here with the distance S,

which is evidently given by $S=(q-q_0)\delta$. From Eq. (1) and $\delta+\epsilon=2\alpha$ we obtain

$$\delta=\alpha\left[\frac{2-3aM}{M+1-2aM}\right]. \tag{6}$$

Combining Eqs. (4) and (5) we have

$$S=\frac{3Mpa\alpha}{M+1}\left[\frac{M^2+2aM-1}{M+1-2aM}\right], \tag{7}$$

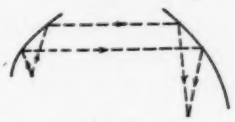

FIG. 9. Image formation by two parabolic mirrors with incidence at sub-critical grazing angles. The spherical aberration of Fig. 7 is removed and magnification is possible.

an expression able to withstand certain simplifying approximations. For values of α small enough to justify the neglect of a in respect to terms of the order of unity Eq. (7) simplifies to

$$S=(3/2)RM\alpha^2\left[\frac{M-1}{M}+2a\frac{M}{M+1}\right]. \tag{8}$$

The quadratic dependence upon α is favorable to the reduction of image impairment without total loss of light-gathering power.

We shall ultimately be concerned with cases in which the magnification is high. If the conditions $M\gg1$ and $a\ll1$ be imposed upon Eq. (7) the following simple approximations emerge.

$$S/M=(3/2)R\alpha^2=3\cdot k^2/2R, \tag{9}$$

where k is a radial distance on the face of the mirror, subtending at the center of curvature the angle α. When α is the maximum value possible for a given mirror k becomes r of Fig. 10.

Equations (9) are solved explicitly for S/M since this quantity is a better measure of the confusion which results from spherical aberration than is S alone. S/M is the linear measure of the extent of the object which simultaneously sends rays to a single point at the image. So long as magnification is high and α small it is evident that this spherical aberration is controlled almost entirely by the dimensions of the reflector. Small mirrors of long radius clearly favor good image

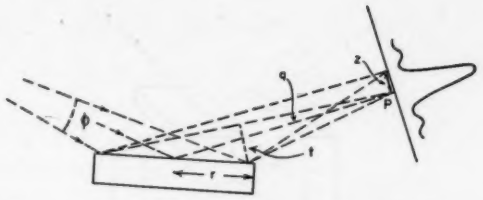

FIG. 10. Limitation of resolving power of a spherical mirror by diffraction. Grazing angle of incidence is small. Diffraction pattern of a point object is represented.

definition, though they are lacking in speed. Equations (9) indicate that a spherical mirror 4 mm in width, with a radius of 10 m, should resolve object features separated by about one wave-length of visible light, assuming adequate diffraction resolution. This relatively good definition occurs in spite of the extreme obliquity of the geometrical focal surface to the plane of the photographic emulsion upon which the image is to be recorded. This obliquity is so great that it would be quite impracticable to tilt the film to fit it.

The image which has thus far been discussed geometrically is a diffraction pattern, and the resolving power of a geometrically ideal x-ray mirror will naturally be finally limited by wave considerations. It is probable that elliptical or parabolic mirrors will permit a much closer approach to geometrical ideality than do spherical mirrors. We therefore consider next the resolving power of a mirror without geometrical aberrations, seeking to obtain a theoretical upper limit of resolution which may be approached but not surpassed by real x-ray mirrors.

THEORY OF RESOLVING POWER

We take up the problem of resolving two small, luminous spots, each of which fills the mirror with coherent x-radiation. This situation is not realized when an opaque, perforated plate is interposed between an x-ray target and the mirror, unless a perforation is so small that the central maximum of its diffraction pattern covers the entire mirror. The assumed conditions could be realized by using a well-designed condensing system to illuminate the perforations, and they would be fulfilled in the observation of self-luminous spots such as emitting points on the

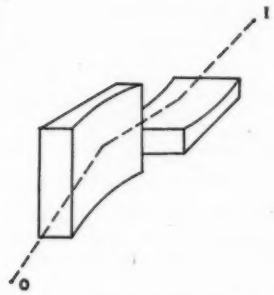

FIG. 11. Arrangement of concave mirrors to produce real images of extended objects with incidence at small grazing angles.

anode of an x-ray tube or small objects emitting secondary x-rays.

Consider first a reflector whose meridian section is a portion of a very eccentric ellipse with semi-axes a and b, where $a>b$. A point object placed at one focus will give rise to a line image passing through the other. For maximum resolving power the plane angle including the bundle of rays proceeding from the object and destined for reflection should be as great as possible. This maximum angle ϕ is limited by i, the angle of total reflection. The reflectible bundle is that embraced by ϕ in Fig. 8 and its approximate value is given by $\phi=2(i^2-b^2/a^2)^{\frac{1}{2}}$. In principle this angle might be doubled by using a portion of the upper half of the ellipse, but this plan is experimentally unattractive. Since the mirror is symmetrically located between the foci no magnification is produced, but we are now bending all efforts to favor resolving power, so this fact will be overlooked. Evidently the aperture angle ϕ may approach but not exceed $2i$.

An alternative reflector of possible merit is the parabola. Two parabolic cylinders arranged as in Fig. 9 may form a perfect line image of a point with complete compatibility of high angular aperture and high magnification. The maximum possible aperture ϕ (using one side of the parabola) may be shown to be $2i$, as in the case of the ellipse.

Figure 10 represents a mirror of width $2r$ bringing to a focus at a distance q rays of wave-

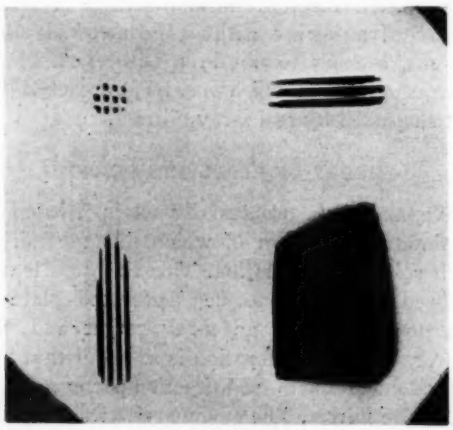

FIG. 12. Pattern produced by mirrors arranged as in Fig. 11. Object was a monel screen having 350 meshes per linear inch. In addition to the full image of the screen two partial images, each formed by one mirror, and a large spot caused by direct radiation appear above.

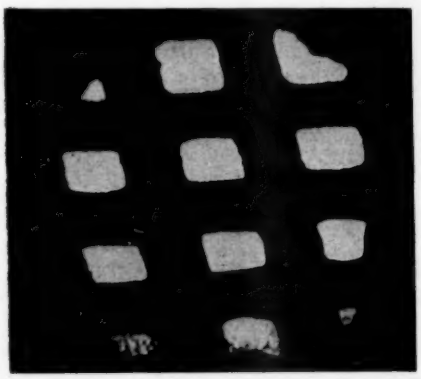

FIG. 13. Further enlargement of the full image shown in Fig. 12 showing definition limited only by photographic grain.

length λ from an object point (not shown) which is situated at the left. The focal point P is at the maximum of a diffraction pattern, as suggested by the intensity graph near it. Evidently $\lambda/t=z/q$, where z is the linear separation of the intensity maximum from the adjacent minimum, and t is the projected aperture of the mirror as seen from the focus. But $t=p\phi$ where p is the object distance and ϕ is the aperture angle discussed above. Hence $z/q=\lambda/\phi p$.

It will be assumed that two object points separated by a distance y will just be resolved if their geometrical images are separated by the distance z. In these circumstances, by the law of reflection, $z/y=q/p$. Combining this with the

final equation of the foregoing paragraph we obtain $y=\lambda/\phi$. If, as shown above, $2i_c$ is the maximum possible value of ϕ the minimum separation of resolvable objects will be $y=\lambda/2i_c$. Now the maximum possible value of i is given by the theoretical expression $i_c=\lambda[ne^2/\pi mc^2]^{\frac{1}{2}}$. The electron density n attains its highest known

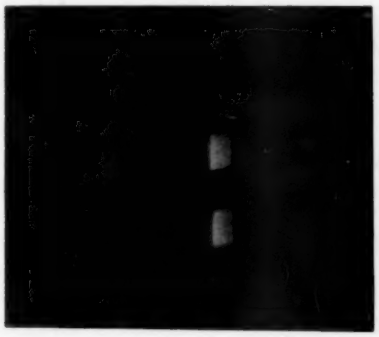

FIG. 14. Image of monel screen (350 meshes per linear inch) formed at a magnification of 29 diameters by a system like that of Fig. 11.

values in the platinum metals, for which $i=7\times10^5\lambda$ approximately. This proportionality of i to λ makes the maximum resolving power of the instrument independent of wave-length and fixes the minimum resolvable distance at about 70 angstrom units.

TWO-DIMENSIONAL IMAGES FORMED BY CROSSED MIRRORS

Two cylindrical lenses in the crossed position possess the focusing properties of a single lens of axial symmetry. Similarly two x-ray mirrors may be positioned as shown in Fig. 11 to produce point images of point objects, and therefore real, extended images of extended objects.[4] In Fig. 11 is shown a broken ray taking the path of reflection by both mirrors which is necessary for image formation. In practice radiation will also get through the system after reflection from the first or the second mirror only. In addition there will be a ray which misses both mirrors, so in general four spots will be seen on the observer's fluorescent screen or recorded upon the photographic emulsion.

[4] Paul Kirkpatrick and A. V. Baez, Bull. Am. Phys. Soc. 23, 10 (1948).

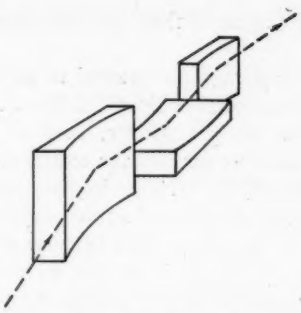

FIG. 15. Arrangement of concave mirrors to produce real images of extended objects with incidence at small grazing angles. This combination obviates a type of image distortion inherent in the arrangement shown in Fig. 11.

These four spots appear in Fig. 12, an exposure obtained with two platinized glass mirrors figured to a radius of 21.9 meters. The object was a piece of monel wire gauze having 350 meshes per linear inch. The x-ray magnification in this case was unity, the scale of the figure being the result of subsequent photographic enlargement from the original plate. Figure 13 presents a further enlargement of the portion of Fig. 12 containing the full image of the screen. The definition is as good as the photographic grain of the original plate could permit.

Figure 14 shows the image of the same gauze at an original x-ray magnification of 29 diameters. The mirrors were separately focused by adjustment of their angles of incidence so that they produced their partial images at the location chosen for the photographic plate. Both the object and the plate were approximately normal to the radiation bundles incident upon them. Any attempt to fit the plate to the true focal surface would have produced an extreme distortion of the recorded image. Theory and experience agree that rather good images (of small objects) may be had without such precise focusing. The definition of the image in Fig. 14 is limited more by the grain of the plate than by optical image defects.

Another type of distortion (anamorphotism) results from the non-coincidence of the two mirrors. Each mirror controls, by its object and image distances, the magnification of one coordinate of the image, and these magnifications are naturally not equal. They may be rendered equal by a moderate tilting of the film (which also brings it somewhat closer to the true focal sur-

face) or by the use of three mirrors disposed as in Fig. 15.

An earlier paragraph referred to the difficulty of producing a single ellipsoidal mirror. We now remark that such a mirror, even if perfectly figured, would be far inferior to the two-mirror combination of Fig. 11. The single ellipsoid would produce a perfect image of a point object situated at a focus of the ellipse, but because of its great transverse curvature it would produce badly elongated images of other points, even of points very close to the focus. Two elliptical mirrors arranged as in Fig. 11 would have a useful field thousands of times larger than would a single ellipsoid of like light-gathering power.

PROPOSED EXTENSIONS

It is clear that an x-ray microscope is now a definite possibility. Such an instrument would have a maximum resolving power somewhere between those of the optical and electron microscopes, and would be peculiarly applicable to the study of objects not readily penetrated by light or electrons. It would be much simpler in construction and operation than is the electron microscope and would not require that the materials observed be placed in a vacuum.

Many problems must be solved before a useful instrument may be constructed. It is not yet known that the figure and polish of optical surfaces produced by current methods is good enough for these purposes. We believe that x-ray reflections provide a more sensitive test of the quality of optical surfaces than do other known methods. Elliptical and parabolic surfaces are being studied both theoretically and experimentally. They will almost certainly be superior to spherical surfaces when methods for producing them shall have been brought under control.

A start has been made upon the construction and testing of *compound* systems, in which the image formed by one combination like that of Fig. 11, becomes the object for the next. Combinations of reflecting components offer unexplored possibilities for the removal of image defects and rectification of field obliquity. Reflecting condensers for the x-ray illumination of objects need to be developed, and with them x-ray tubes with very small, high-powered focal spots and transparent windows.

So far all experiments have been conducted with copper or tungsten x-rays which had emerged from glass tube windows. The wavelengths of the reflected radiations were of the order of one Angstrom unit. Longer waves have many advantages: the resulting increased critical angle of reflection will reduce image aberration, tend to rectify the obliquity of field, accommodate larger objects, and improve light gathering power. Surface irregularities will diminish in importance as wave-length increases. Degrees of contrast in thin and light objects improve with the softening of radiation. Absorption by air becomes serious beyond 1.5A and air paths will need to be replaced by tubes containing hydrogen or helium.

It remains to remark that these optical methods are immediately applicable to the focusing of neutrons and such other particles as may be found to exhibit external total reflection.

We are happy to acknowledge the cooperation of Dr. G. D. Hanna, of the California Academy of Sciences, who worked most of the mirrors used; to Mr. Allen Newell, Mr. Walter Kerttula and Mr. Wilson S. Geisler, Jr., who collaborated at various stages of the work; and to Mr. Leonard Rieser, Jr., who suggested the optical focusing of neutrons.

The Transmission of Powder Films in the Infra-Red

R. L. HENRY*
Johns Hopkins University, Baltimore, Maryland
(Received April 5, 1948)

Infra-red transmission measurements on dry films of quartz and zinc sulfide powders are presented. The effects of particle size, layer thickness, and the optical constants of the materials are discussed.

GENERAL INTRODUCTION

DRY powder films consisting of small particles adhering to transparent plates have been shown to possess spectral transmission curves widely different from those of the same materials in bulk. A great variety of transmission curves can be obtained throughout the visible and the infra-red regions of the spectrum by employing various materials and by varying the particle size and the layer thickness. By dispersing the powders in transparent liquids still other transmission characteristics can be obtained.

The possibility of using powder films as infra-red filters was suggested by Pfund.[1] These filters fall into two classes—those composed of powder materials exhibiting selective absorption in the spectral region being employed and those composed of transparent powder materials. Part A of this paper deals with crystalline quartz powders in the infra-red from 1μ to 14μ as an example of the first class. Part B deals with zinc sulfide powders throughout the same spectral region. In this region the absorption by small particles of zinc sulfide is too small to be of any consequence.

Apparatus

For the transmission measurements on the powders a rocksalt spectrometer, whose optical design is shown in Fig. 1, was employed. The radiation source G is a water-jacketed Globar. M_1 is an on-axis parabolic mirror 50 cm in focal length. Fixed slits 0.6 mm wide were placed in a hollowed-out place in the back of the plane, perforated mirror M_2. The entrance slit was curved to compensate for curvature by the prism. The spectral slit-width was calculated to vary with wave-length as tabulated in Table I.

By rotating the Littrow mirror M_3, various parts of the spectrum could be made to fall on the exit slit. A Bi, Bi—Sn compensated thermopile in conjunction with a Leeds and Northrup Type R galvanometer was used as the radiation detector. Evacuating the thermopile increased the sensitivity by a factor of ten, approximately. This was accomplished by means of a charcoal trap which was heated and pumped out overnight and then cooled with liquid nitrogen when readings were to be taken. Deflections were observed on a 50-cm scale at a distance of 9 meters from the galvanometer and could be read to 0.5 mm.

Since the slits were made wide enough to produce deflections of a few centimeters at 13μ, the sensitivity of the galvanometer had to be reduced considerably at shorter wave-lengths to keep the deflections under 50 cm. This was accomplished by means of two dial resistance boxes, one in parallel and one in series with the galvanometer. In this way the galvanometer could be kept slightly underdamped at each sensitivity.

The effects of contaminating radiation were made negligible by means of a series of selectively transparent shutters and filters.

Preparation of the Powder Films

The quartz powder films were formed by making a suspension in amyl acetate and then letting the powder settle onto a polished rocksalt

TABLE I.

λ	Spectral slit-width
1μ	0.03μ
2	0.12
3	0.17
4	0.14
6	0.10
8	0.08
12	0.05

* Now Assistant Professor at Carleton College, Northfield, Minnesota.
[1] A. H. Pfund, J. Opt. Soc. Am. 24, 143 (1934).

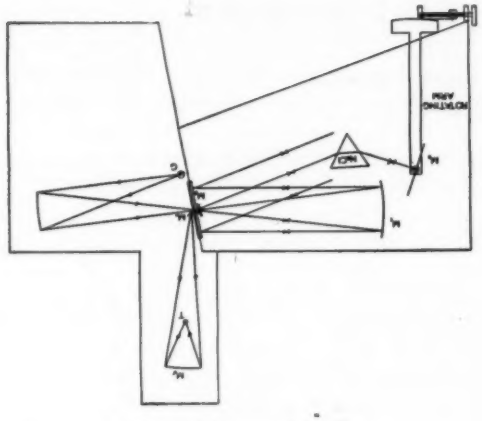

FIG. 1. The spectrometer.

disk. After the powder had settled for a few hours (as much as a day for the 1-μ particles), the liquid was siphoned off until the surface was only a millimeter or so above the powder film. The remainder of the liquid was evaporated away under a bell jar at a pressure of a few cm of Hg. Care had to be taken to avoid boiling.

From the mass of the powder deposited (determined by weighing the rocksalt disk before and after deposition), the area of the disk, and the density of quartz, it was possible to calculate the thickness of the powder film by means of the following relationship: $t=m/a\rho$, in which m = mass of powder, a = area of rocksalt disk, and ρ = density of quartz (2.66 grams per cm^3). The disks were about 2.95 cm in diameter. The thinnest film of quartz used was 1.1μ thick, which corresponded to a deposition of 2.0 mg of quartz. From the area of the rocksalt disk and the area of the bottom of the container in which the settling out was to take place, it was possible to calculate how much powder to put into suspension to deposit a layer of a given thickness.

Toward the end of the work with the quartz powders it was found that the rocksalt disks could be lifted out of the shallow liquid without destroying the films if sufficient care were taken. The films could then be dried rapidly by fanning. Not only was this method faster than evaporating to dryness under a bell jar, but it was the only way found to make acceptable thin films of the smallest particles (1μ in diameter).

The zinc sulfide powder films were formed in much the same way as the quartz films. The zinc sulfide powder had a greater tendency to form aggregates, however. To break them up the powder was mulled into a smooth paste with amyl acetate on a glass plate. This paste was put directly into a flask containing amyl acetate to form the suspension. The suspension was then shaken vigorously. Since the zinc sulfide powders were not weighed before making the suspension, it was not possible to determine in advance how thick the resulting film would be. However, by making a master suspension, pouring various amounts into beakers, and diluting to equal volumes, it was possible to obtain suspensions whose relative concentrations were known. In this way the relative thicknesses of the films could be predicted. The films were dried by lifting them out of the shallow liquid (after the level had been brought down almost to the disk by siphoning) and fanning them dry. The mass of powder deposited was determined as with the quartz by weighing the rocksalt before and after deposition. From the mass of powder on the disk, the area of the disk, and the density of zinc sulfide (4.1 g per cm^3), the thickness of the layer could be calculated.

Method of Making Transmission Measurements

The rocksalt disk with the film to be investigated was placed about 2 cm from the entrance slit in a converging cone of radiation corresponding to an aperture of f:4.2. A clear rocksalt disk could be substituted for the one supporting the powder film. The procedure was to run through a portion of the spectrum taking galvanometer deflections at certain wave-lengths with the powder film and then with a clear rocksalt disk. Usually this was followed by measurements on a second powder film. When these three runs had been made, another region of the spectrum was investigated in the same fashion. Occasional checks were made of the output of the source and the sensitivity of the thermopile.

PART A: QUARTZ POWDER FILMS

Introduction

In 1930 Pfund[2] published a set of curves showing the relative energy from a Nernst lamp

[2] A. H. Pfund, Phys. Rev. **36**, 71 (1930).

transmitted by powder films of various materials. In this collection of curves was one for crystalline quartz powder 2.5μ in average particle diameter. It exhibited a rather narrow peak at about 7.3μ with a very sharp drop on the long-wave side produced by true absorption. Except for the sharper long-wave cut-off, the curve for quartz looked much like those for the other materials, such as zinc oxide and magnesium oxide. In a later paper Pfund[3] showed that the transmission maximum exhibited by a film of coarse quartz powder at 7.3μ is produced by a special set of circumstances. The transmission peak for the powder film occurs at the same wave-length as the reflection minimum of quartz, at which wave-length the reflecting power is practically zero. It was suggested that wave-lengths shorter than 7.3μ are reflected by the many faces of the powder particles, producing an apparent opacity. A similar transmission maximum was shown to occur for calcite powder films at about 6.15μ, that is, at the wave-length for which a polished plate of calcite exhibits a reflection minimum.

TABLE II.

Figure	Particle size d_3	Particle size d_1	Layer thickness
2	0.99μ	0.58μ	1.1μ
			6.0
			9.6
			12.6
3	6.6	5.4	2.3
			3.4
			6.2
			14.8
4	15.5	13.5	4.1
			6.7
			14.9
5	28.1	24.8	7.8

Barnes and Bonner[4] pointed out that these transmission maxima are actually examples of the Christiansen filter effect, which is well known in the visible. The transmission peak occurs at a wave-length for which the refractive index of the powder is equal to that of the surrounding medium. Quartz has a refractive index of unity at about 7.4μ. Barnes and Bonner showed that the

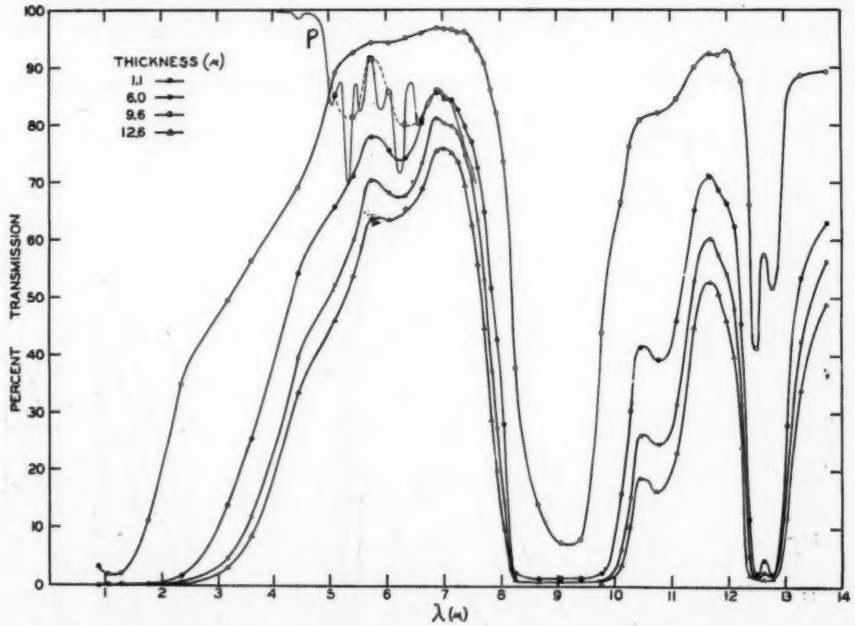

FIG. 2. The four main curves are for quartz powder films of 1-μ particles. Curve P is for a solid plate of quartz 12.6μ thick.

[3] A. H. Pfund, J. Opt. Soc. Am. **23**, 375 (1933).
[4] R. B. Barnes and L. G. Bonner, Phys. Rev. **49**, 732 (1936).

transmission band was shifted to a shorter wave-length when a quartz powder film was immersed in CCl_4, and actually occurred at a wave-length for which quartz and CCl_4 have the same refractive index. The effect of the particle size upon the shape of the transmission curve of the dry powder was studied to some extent. Barnes and Bonner also found infra-red Christiansen peaks for a number of other crystalline powders in air and for a few immersed in liquids.

The purpose of the work to be reported here was to investigate more thoroughly the transmission of dry films of crystalline quartz powders for a wide range of particle sizes and layer thicknesses and to do it for the wave-length range from 1μ to 14μ.

Results

Transmission curves were obtained for quartz powder films of four different particle sizes and various layer thicknesses. A tabulation of the films measured appears in Table II. We follow the customary notation and denote by d_3 the average diameter from which the surface area may be calculated by means of the relation $S=6/\rho d_3$, where ρ is the specific gravity of the powder. With d_3 in microns S will be in square meters per gram. The symbol d_1 denotes numerical average diameter. The closer d_1 is to d_3, the more uniform is the sample. For the purpose of referring to the various sizes the value of d_3 will be used. The 0.99-μ particles will be called 1-μ particles.

All of the curves shown in Figs. 2 through 5 show maxima near 7μ and 12μ. Another common characteristic is the great opacity at 9μ and 12.6μ produced by the true absorption of quartz. The curves for the 1-μ particles are strikingly different from those for the larger particles, however. This was to be expected since the 1-μ particles are small compared to the wave-length throughout practically the whole region studied, whereas the larger particles are about the same as, or larger than, the wave-length. One of the most noticeable features of the curves is the greater transparency of the 1-μ particles between 1μ and 6μ and between 10μ and 12μ as compared with the larger particles. In order to show the effect of particle size alone, we have superimposed in Fig. 6 curves for three powder films having the same thickness

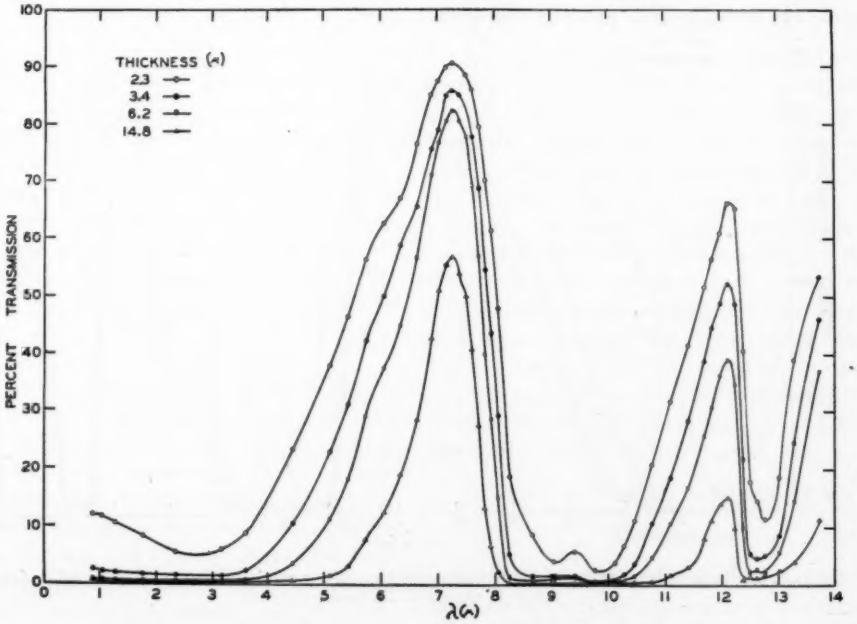

FIG. 3. Transmission of quartz powder films, 6.6-μ particle size.

(4.1μ) but composed of particles of three different sizes. The curve for the 15.5-μ particles is just a re-plot of the one in Fig. 4. The other two, however, were obtained by graphical interpolation from experimental data on films of other thicknesses. A corresponding set of curves for a thickness of 12.8μ is shown in Fig. 7.

As was found by Pfund and Barnes and Bonner, films of coarser particles are quite opaque to the shorter wave-lengths. One explanation that has been suggested is that these larger particles act like little mirrors to reflect the incident radiation out of the direct beam. It was pointed out by Barnes and Bonner that for the observed opacity to be produced in this fashion alone a large number of reflections would be required, since the reflecting power of quartz in this region is less than four percent. It is found experimentally (Fig. 5) that a powder film of 28.1-μ particles only 7.8μ thick transmits less than ten percent of the incident radiation up to 6.2μ. It is seen that such a film, consisting of large particles separated by open spaces, cannot provide enough reflecting surface to reduce the intensity of the direct beam to this extent by reflection alone. Another example is the 4.1-μ thickness of the 15.5-μ particles (Fig. 4).

When the transmission maxima for coarse quartz powders at about 7.4μ came to be recognized as Christiansen filter peaks, the role played by refraction was emphasized, since the Christiansen effect in the visible had been successfully explained on this basis. According to this explanation, the amount of energy removed from the direct beam depends upon the extent to which the incident wave front is broken up by the particles because of retardation of those parts of the wave front passing through the particles. The larger the particles and the larger the refractive index, the greater is this effect. Scattering, reflection, and absorption also occur. If the particles are small compared to the wave-length (as the 1-μ quartz particles are in this example), there are no refraction effects to speak of, and the film derives whatever opacity it possesses from scattering and true absorption. The scattering by these 1-μ particles is weak between 4μ and 7.4μ, both because the particles are small compared to the wave-length and because the refractive index is not far from unity.

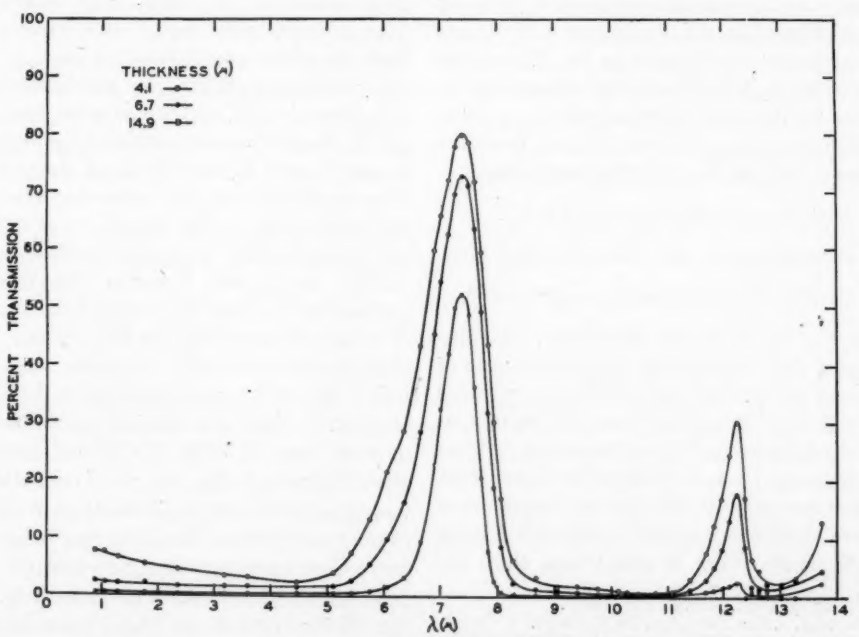

FIG. 4. Transmission of quartz powder films, 15.5-μ particle size.

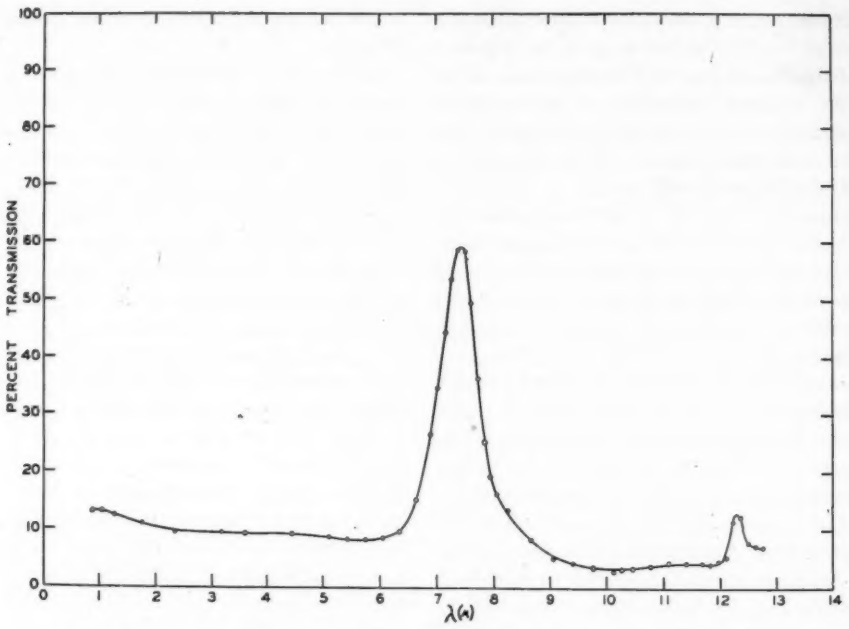

FIG. 5. Transmission of quartz powder film, 28.1-μ particle size, 7.8-μ layer thickness.

The refractive index plays a vital role in determining the transmission of powder films. In Fig. 8 is shown the dispersion curve of quartz (for the ordinary ray) from 1μ to 14μ. The values from 4μ to 8μ are by Nichols,[5] and those from 8μ to 10μ are by Boeckner.[6] To extend the curve to 14μ, refractive indices were calculated from the well-known formula for the reflecting power,

$$R=[(n-1)^2+k^2]/[(n+1)^2+k^2],$$

which, when solved for the refractive index, gives

$$n=[(1+R)/(1-R)]\pm[(4R/(1-R)^2)-k^2]^{\frac{1}{2}},$$

in which k is the extinction coefficient. The plus sign is used since the minus sign gives values of n less than unity. The reflecting power values were taken from Reinkober[7] and the extinction coefficients from Stein.[8] The transparency of the powder films near 7.4μ is easily understood from the dispersion curve. At first glance it would seem that there should be another transmission peak for quartz powder films at about 9.3μ, since the refractive index is unity here also. The reason no peak occurs is, of course, that quartz absorbs very strongly in this region. It is conceivable that just the right combination of particle size and layer thickness might show a small maximum at this wave-length. Of the powder films investigated, the only one that showed any indication of a peak near 9.3μ was the 2.3-μ thickness of the 6.6-μ particles (Fig. 3). Unfortunately, the density of readings in this region is not sufficient to make any definite statement possible.

The relationship between the transmission curves and the dispersion curve from 10μ to 12.5μ is worthy of comment. In this region, as on the short-wave side of the 7-μ peaks, the refractive index gets smaller as one goes to longer wave-lengths. It does not become unity, but it does decrease rapidly from 11μ to 12μ, producing a sharp decrease in the amount of refraction by the larger particles and an increase in transparency of the powder films. The refractive index does not come close enough to unity to produce a sizable peak for the film of 28.1-μ particles (Fig. 5) or for the thickest film of the 15.5-μ particles (Fig. 4). Part of the reason for the smallness of the

[5] E. F. Nichols, Phys. Rev. **4**, 297 (1897).
[6] C. Boeckner, J. Opt. Soc. Am. **19**, 7 (1929).
[7] O. Reinkober, Ann. d. Physik **34**, 343 (1911).
[8] W. Stein, Ann. d. Physik **5**, 36 (1939).

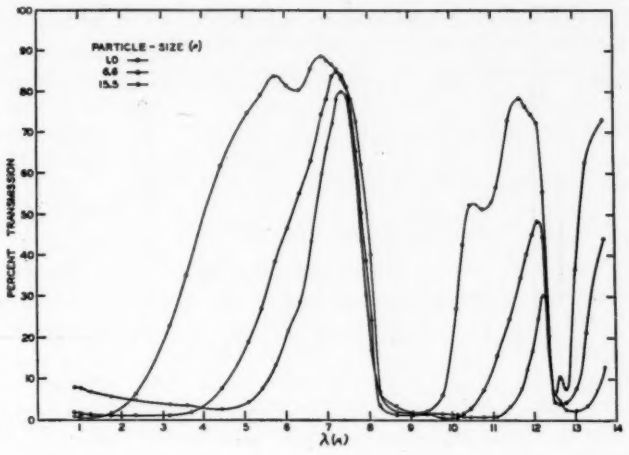

FIG. 6. Transmission of quartz powder films, 4.1-μ layer thickness, three different particle sizes.

maxima exhibited by these films is that quartz absorbs rather strongly at 12.2μ. The other films do show peaks of considerable height, however. The 6.6-μ particles (Fig. 3) show the drop in refractive index by their sharp increase in transparency between 10.5μ and 12μ. The rise is even sharper for the 15.5-μ particles, the transmission being kept low up to 11.5μ by the high value of the refractive index and the large size of the particles. The 1-μ particles (Fig. 2) are so small compared to the wave-length that they have very little effect on the incident waves throughout this region except through true absorption.

The similarity between the peaks near 7μ and those near 12μ is striking, particularly for the 6.6-μ and 15.5-μ particles. In each case a drop in refractive index is responsible for the peak. At 7.4μ the refractive index becomes unity and we have what are called Christiansen peaks. We would not call the maxima near 12μ Christiansen peaks, but it must be admitted they are closely related.

As has been mentioned previously, the opacity of these quartz powder films around 9μ and 12.5μ is produced by the strong absorption of quartz. Here true absorption is dominant, covering up the powder effects almost completely. In other regions true absorption plays a smaller part, but at all wave-lengths beyond 5μ it is a factor of considerable importance.

In Fig. 2, a calculated transmission curve for a solid plate of quartz 12.6μ thick is shown for com-

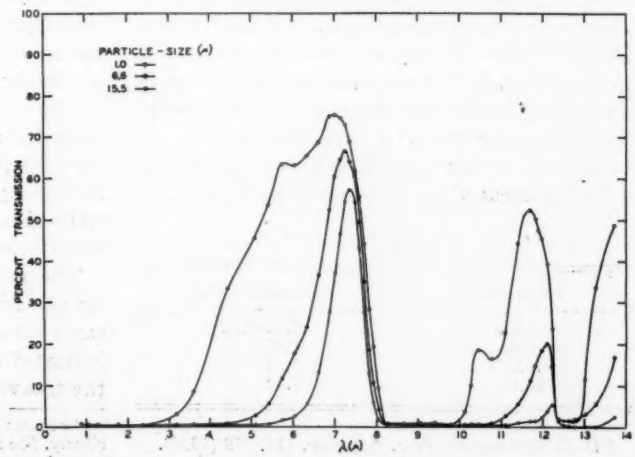

FIG. 7. Transmission of quartz powder films, 12.8-μ layer thickness, three different particle sizes.

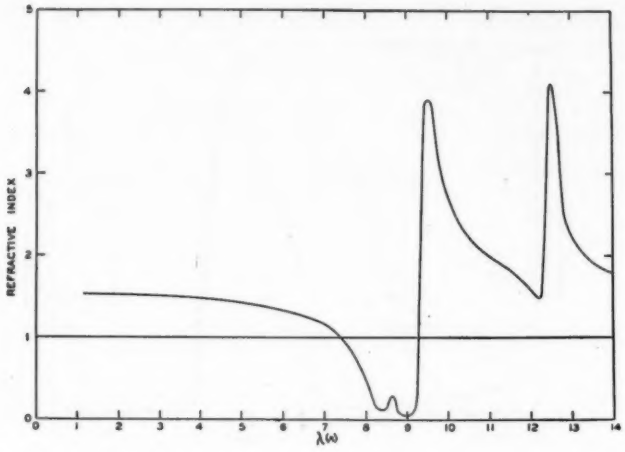

FIG. 8. Dispersion of quartz (ordinary ray).

parison purposes. The solid curve represents the percent transmission calculated from absorption coefficients published by Drummond.[9] The percent transmission plotted here represents the average of the percent transmission for the ordinary and the extraordinary ray. Since readings were not taken closely enough together on the powder films to show up such rapid variations in the region from 5μ to 6.5μ, a curve (dotted) was plotted to show what the transmission of this hypothetical quartz plate would be at the wave-lengths for which readings were taken on the powder films. To obtain each plotted point for the dotted curve, the graphical average of the solid curve over a wave-length interval equal to the spectral slit-width of the spectrometer was used. The resulting curve compares very favorably with a transmission curve for quartz published by Nichols.[5] It is seen that the dips at 6.3μ in the curves for the 1-μ particles (Fig. 2) can be accounted for on the basis of true absorption. The curves for the 6.6-μ particles (Fig. 3) show inflections at this wave-length as does also the 4.1-μ thickness of the 15.5-μ particles (Fig. 4). All except the thinnest of the films of the 1-μ particles show small inflections at 5.3μ, which match up with the dip in the transmission curve for quartz in bulk at this wave-length.

TABLE III.

Particle size	Wave-length of peak
1.0μ	6.9μ–7.0μ
6.6	7.25
15.5	7.38
28.1	7.42

It is seen from the graphs[10] that the transmission peaks do not occur at the same wave-length for different particle sizes. The smaller the particles, the greater the shift toward shorter wave-lengths. The peaks near 7μ are located as listed in Table III. The reason for this shift is evident from Fig. 2, which shows that the transmission of quartz decreases very rapidly beyond 6.9μ. Since the 1-μ particles have such small powder effects in the region from 6.9μ to 7.4μ, the effect of true absorption becomes a dominant one, with the result that the peak which would otherwise occur at 7.4μ does not show up. The same argument applies to the case of the 6.6-μ particles, the only difference being that the shift from 7.4μ is smaller. Here, as for the 1-μ particles, the Christiansen effect is somewhat covered up by absorption effects. The 15.5-μ and the 28.1-μ particles (Figs. 4 and 5), however, exhibit rapidly increasing transparency between 6.9μ and 7.3μ, in spite of the increasing absorption of the quartz. The Christiansen effect is very evident for them.

The positions of the peaks near 12μ are affected by the true absorption of quartz in much the same manner as those near 7μ. They occur as indicated in Table IV. For comparison purposes the transmission of a plate of quartz 12.8μ thick

[9] D. G. Drummond, Proc. Roy. Soc. **153**, 318 (1936).

[10] Figures 6 and 7 show the effect of particle size most clearly. See also Fig. 5.

is shown in Fig. 9. The curves for the ordinary and the extraordinary ray are traced from a paper by Stein.[8] The dotted curve is simply an average of these two. It is seen that the transmission maximum of the quartz plate occurs at 11.7μ, coinciding almost exactly with the maxima for the powder-films.

In the absorption region around 12.5μ quartz is seen to exhibit considerable dichroism (Fig. 9). The transmission minimum for the ordinary ray occurs at 12.4μ, whereas that for the extraordinary falls at 12.8μ. Because of the random orientation of the powder particles, the transmission of the powder should be something like the average of that for the ordinary and the extraordinary ray. Hence the transmission of the quartz powders should be compared to the dotted curve in Fig. 9. The powder films show only one minimum near 12.5μ, except for the two thinnest films of the 1-μ particles. No curves are available for quartz plates thinner than 12.8μ. It seems reasonable, however, that the average of the curves for the ordinary ray and the extraordinary ray for a quartz plate 2μ or 3μ in thickness might show two minima.

The dips in the curves for the 1-μ particles at 10.8μ are probably caused by true absorption also, although there is no indication of minima here in the curves for the quartz plate. The reason for this absence of minima at 10.8μ in Stein's curves probably lies in the fact that he used a spectral slit-width of about 0.35μ in this region.

TABLE IV.

Particle size	Wave-length of peak
1.0μ	11.7μ
6.6	12.1
15.5	12.25
28.1	12.3

Supplementary Discussion

In the preceding discussion the effects of the birefringence of quartz have been considered only in connection with the different absorptivities of quartz for the ordinary and the extraordinary rays. The extent to which the existence of a second refractive index for quartz affects the transmission characteristics of quartz powder films in the infra-red has not been discussed. In a strict sense there should be no true Christiansen effect for birefringent powders since there will be no regularly transmitted light for any wave-length. On the other hand, there is some evidence that the effect of the second refractive index is small. For example, the transmission peaks for quartz powder films of coarse particles fall very near 7.4μ, the wave-length at which the ordinary refractive index is unity.

It is of some interest to consider whether, after making the simplifying assumption that only the ordinary refractive index of quartz need be considered, it is possible to work out an expression which will give the transmission of quartz powder films as a function of wave-length, refractive index, particle size, layer thickness, and absorp-

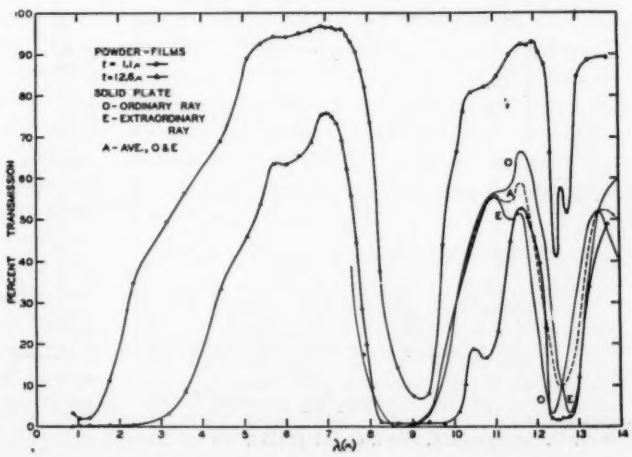

FIG. 9. Transmission of quartz powder films of 1-μ particles (two thicknesses of film) together with the transmission of a solid quartz plate 12.8μ thick.

tion coefficient. In this connection there came to the attention of the author a paper by N. K. Sethi[11] in which he derived an expression of this kind for Christiansen filters in the visible. He obtained good agreement with experimental data on filters of glass particles in various liquids. Since the derivation was based only upon the wave theory of light and upon the theory of probability, the resulting expression should be applicable to quartz powder films in the infra-red. With the introduction of a factor to take account of the absorption by the powder particles, Sethi's equation is modified to read

$$I = I_0\{[\exp(-k_0 t)+\exp(-k_e t)]/2\} \times \exp(-ctd_3[(n_0-1)/\lambda]^2),$$

in which I = intensity of the transmitted radiation, I_0 = intensity of the incident radiation, k_0 = absorption coefficient, ordinary ray, k_e = absorption coefficient, extraordinary ray, t = thickness of layer in microns, d_3 = diameter of quartz particles in microns, n_0 = ordinary refractive index, λ = wave-length in microns, c = a constant which may depend upon the arrangement of the particles, but is otherwise an absolute one. Sethi found that for his filters in the visible $c = 7$. Here the constant was also taken to be 7, since there was no *a priori* reason for using any other value.

For the region from 2μ to 7.6μ, k_0 and k_e were obtained from Drummond's paper,[9] and for the region from 9.7μ to 12.2μ they were taken from Stein's paper.[8]

In Figs. 10–18 the curves based on this equation are shown together with the corresponding experimental curves. The region from 9.7μ to 12.2μ is included because the optical effects here are identical with those in the region between 2μ and 7.6μ. The agreement between the theoretical curves and the experimental ones is striking. No serious attempt was made to try other values of the constant c to see whether a better over-all fit could be obtained. In general, the agreement is better for the larger particles. It is noticeable that the thicker films give better agreement than the thinner ones.

For the three larger particle sizes the theoretical maxima occur at the same wave-lengths as the experimental ones, except for the $15.5\text{-}\mu$ particles at 12.2μ. The values from the equation are in doubt at 12.2μ since the absorption coefficients are not known accurately here. The most noticeable discrepancy is in the difference in the heights of the peaks, particularly for those in the $7\text{-}\mu$ region. It seems reasonable to suppose that the birefringence of quartz is responsible for this.

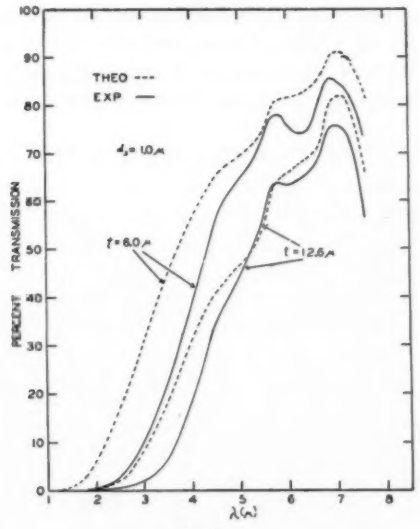

FIG. 10.

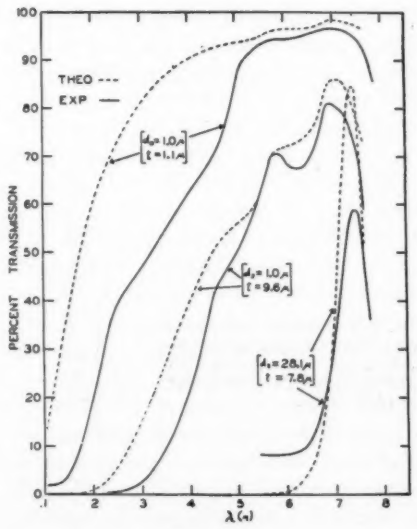

FIG. 11.

[11] N. K. Sethi, Ind. J. Phys. **6**, 121 (1921).

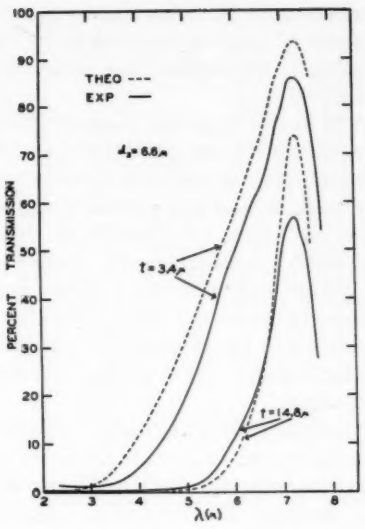

FIG. 12.

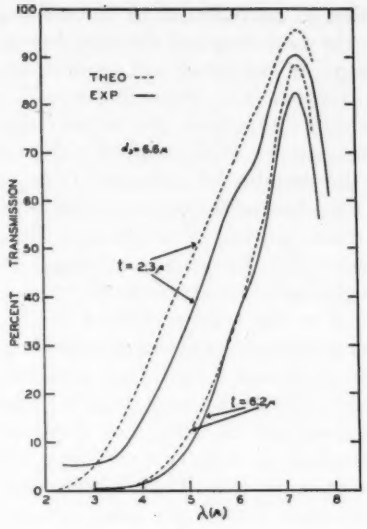

FIG. 13.

Transmission of quartz powder films.

PART B: ZINC SULFIDE POWDER FILMS

Introduction

The amount of light transmitted by a dispersion of transparent particles in a transparent fluid depends upon the amount of light scattered and reflected by the particles. Hence, the important factors are the refractive indices of the two components, the size of the particles, and the amount of powder in the dispersion. The arrangement of the particles may also have some effect. For example, a film of powder particles adhering to a transparent plate which is placed in a liquid may not have the same optical characteristics as would a suspension of the same amount of powder dispersed throughout the liquid. Another important question is that of the effect of the state of aggregation of the particles. It was originally intended to make a more or less thorough investigation of these various factors for dry films of zinc sulfide in the infra-red, then to measure the transmission of the same films immersed in carbon disulfide and carbon tetrachloride, and finally to investigate suspensions of zinc sulfide powder in these liquids. Unfortunately, time did not permit as thorough an investigation as was desired. Nevertheless, it is hoped that some light may be shed on this interesting subject.

The optical properties of dispersions of transparent powders have been thoroughly discussed previously,[12–18] and although there are several points yet to be cleared up, certain salient facts are evident. These are presented here to serve as a basis for an understanding of the present work. In the first place, a dispersion of particles which are all small compared to the wave-length of the light throughout the region investigated will obey Rayleigh's law of scattering very closely. The transmission will be low for short wave-lengths and high for long wave-lengths. If the investigation is carried out in the infra-red so that the particles are large enough to be measured easily microscopically, and yet small enough to fulfill Rayleigh's condition, the scattering follows the d^3/λ^4 law very well.[19] It has also been established that an increase in the refractive index of the surrounding medium is equivalent to a decrease in the size of the particles.

[12] G. F. A. Stutz and A. H. Pfund, Ind. Eng. Chem. **19**, 51 (1927).
[13] G. F. A. Stutz, J. Franklin Inst. **210**, 67 (1930).
[14] A. H. Pfund, J. Opt. Soc. Am. **24**, 143 (1934).
[15] D. L. Gamble and C. E. Barnett, Ind. Eng. Chem. (Anal. Ed.) **9**, 310 (1937).
[16] A. H. Pfund, J. Opt. Soc. Am. **29**, 10 (1939).
[17] D. H. Clewell, J. Opt. Soc. Am. **31**, 521 (1941).
[18] C. E. Barnett, J. Phys. Chem. **46**, 69 (1942).
[19] It is a d^6/λ^4 law if the number of particles is kept constant, but d^3/λ^4 if the mass concentration is kept constant.

A dispersion of particles which are all large compared to the wave-length of the light throughout the region investigated will exhibit non-selective scattering. The transmission will be rather constant throughout the entire region since the transparency of the dispersion depends only upon the amount of reflection from the faces of the particles and the amount of refraction by the particles, neither of which is a highly selective effect like Rayleigh scattering. The amount of light reflected out of the direct beam is proportional to the total surface of the particles. If several suspensions having the same mass concentration of powder material but containing different sizes of particles are investigated using the same wave-length of light, the suspension having the smallest particles (but still large compared to the wave-length) will show the greatest opacity. The reason is that the total surface of the particles is greatest for the suspension containing the smallest particles, and is, in fact, proportional to $1/d$.

Finally, between the Rayleigh and the non-selective regions is a region in which the particles are about the same size as the wave-length. Experimentally, this region can be investigated in either of two ways. Either the mass concentration and the wave-length can be kept constant and the transmission of suspensions (or films) of various sized particles measured, or the transmission of a given suspension (or film) can be measured throughout the spectral region in question.

The first of these two methods yields the result that for a given powder material and surrounding medium there is one particle-size which produces the most opaque suspension. This fact was first used by Stutz and Pfund[12] as the basis of a method for determining the average particle-size in paint pigments. In a later paper Stutz[13] showed that over a small range, at least, the particle size for which the transmission was the lowest is proportional to the wave-length of the light used.

It is not difficult to "explain" the occurrence of this minimum. As particle size is increased on the Rayleigh side, the scattering increases as d^3. As the particle size decreases from very large particles the scattering increases as $1/d$. It seems reasonable that somewhere between these two regions there should be a scattering maximum and, hence, a transmission minimum. Clewell[17] has developed a semi-empirical equation which provides a connecting link between the d^3/λ^4 region and the $1/d$ region. Starting with the observed fact that powder suspensions show transmission minima for particle diameters approximately equal to $\lambda/2$, he arrives at the conclusion

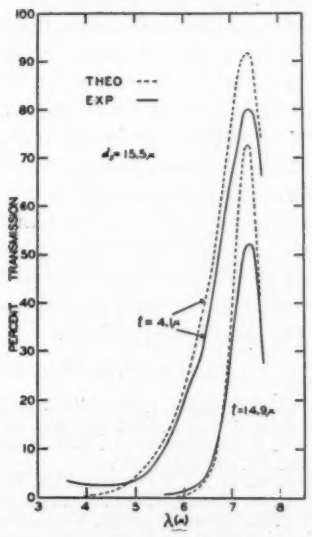

FIG. 14.

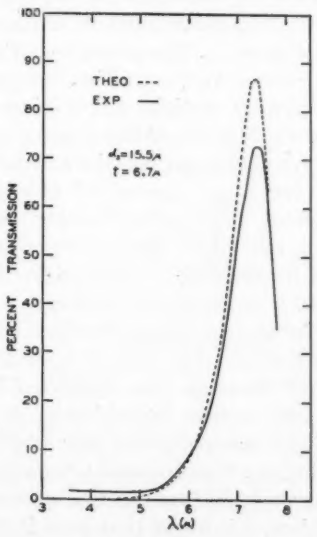

FIG. 15.

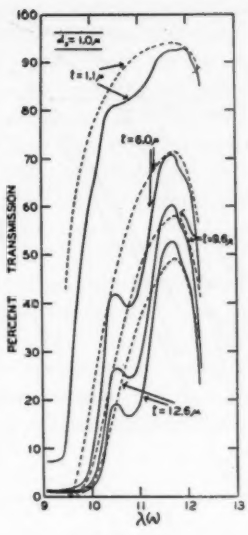

FIG. 16.

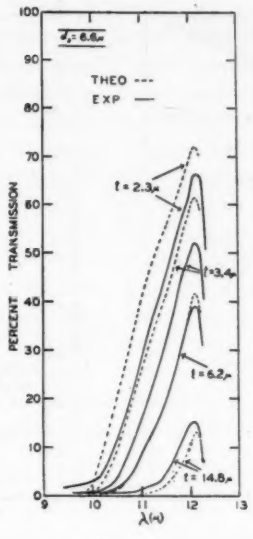

FIG. 17.

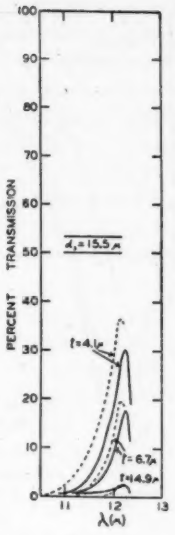

FIG. 18.

Transmission of quartz powder films.

that diffraction effects are responsible for the optical characteristics of the suspensions in this intermediate region. In connection with the argument, he points out that this is also the smallest particle that can be resolved by a microscope, a limitation placed on the instrument by diffraction. The intermediate region has now been given a name; it is the "diffraction region."

The other experimental approach, as mentioned above, has been to measure the transmission of a given powder suspension (or powder film) throughout a spectral range large enough so that two, or perhaps all three, of the regions are covered. The experimental evidence here is not completely clear as yet. Some investigators have found that there is a transmission minimum for some wave-length in the diffraction region, and others have failed to find it. A contributing factor here was that some of the investigators were looking for the minimum, whereas others were concentrating on the Rayleigh region. The search for this minimum came about as a result of the calculations by Stratton and Houghton[20] on the scattering of light by water droplets in the air, the calculations for which were based on the theory of Debye[21] and Mie.[22]

An interesting effect which has some bearing on this question was found by Pfund.[16] He produced some dry powder films composed of patches one particle in thickness ("mosaic films"), which exhibited pronounced transmission minima. The minimum for each film shifted toward shorter wave-lengths when the film was immersed in a liquid. The effect was explained on the basis of interference (colors of mixed plates). When the same particles were thoroughly dispersed, the minimum vanished in almost every case. How-

TABLE V.

Figure	Particle size d_3	Particle size d_1	Layer thickness
19	1.07μ	0.86μ	0.2μ 0.4 0.7 1.1
20	2.4	1.9	0.3 1.2 2.1
20	7.4		0.5 1.1

[20] J. A. Stratton and H. G. Houghton, Phys. Rev. **38**, 159 (1931).

[21] P. Debye, Ann. d. Physik **30**, 57 (1909).
[22] G. Mie, Ann. d. Physik **25**, 377 (1908).

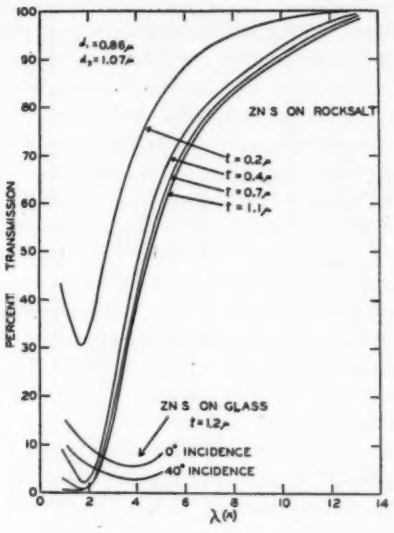

FIG. 19.

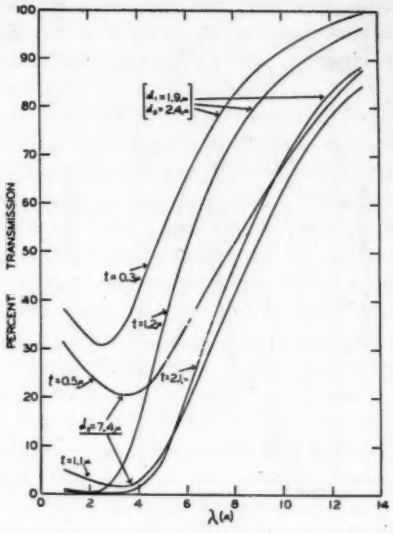

FIG. 20.

Transmission of ZnS powder films. (Reference has been made to the curves shown in these figures in a paper by J. R. DeVore and A. H. Pfund, J. Opt. Soc. Am. **37**, 826 (1947). At that time the material presented here was contained in an unpublished dissertation.) Those in Fig. 20 are on rocksalt. The effect of absorption and reflection by the supporting plate has been eliminated.

ever, one or two examples were given of thoroughly dispersed powders that showed a shallow minimum of the Stratton-Houghton kind.

Results

In Figs. 19 and 20 are shown transmission curves for the dry powder films of zinc sulfide on rocksalt tabulated in Table V. It is seen that minima do occur for the thinner films. Their positions are as mentioned in Table VI. For the smallest particles, $d_1=\lambda/2$, within the experimental error, as Clewell's equation predicts. Neither of the larger particle sizes gives any agreement. The writer is not in a position to explain this.

It is believed that these are not mosaic films and that the minima are not produced by interference. The powder particles were seen under the microscope to be well dispersed on the rocksalt plates, rather than in little "islands."

TABLE VI.

d_2	d_1	λmin
1.07μ	0.86μ	1.75μ, 1.80μ
2.4	1.9	2.5
7.4		3.4

The test would have been to measure the transmission of the same powders first in layers immersed in carbon disulfide and then dispersed throughout a cell containing carbon disulfide. Unfortunately, time did not permit this.

Earlier in the investigation some zinc sulfide films were formed whose transmission minima came at considerably longer wave-lengths than the minima listed in the Table VI. Some of these earlier films were laid down on microscope cover slips and some on lithium fluoride plates. The 1-μ particle size showed a minimum at about 3.8μ and the 2-μ size at about 4.4μ, as compared with 1.8μ and 2.5μ for the films on rocksalt. One possible explanation for this difference is that the films on glass and lithium fluoride may have contained aggregates of particles. The position of the minimum in each case may be determined by the size of the aggregates, rather than by the size of the particles. The nature of the surface upon which the powder is deposited may affect the degree of aggregation.

The transmission of one of the films formed on glass is shown in Fig. 19. Two different angles of incidence were used to test whether or not the

minimum was produced by interference. No shift was observed, indicating that the film was not of the mosaic type. Since all of the films were formed in much the same manner (by allowing a powder to settle out of a liquid), there is good reason for believing that no mosaic films were produced. This indicates that the minima were probably of the Stratton-Houghton variety.

Conclusion

It is apparent from the above presentation that the question of the transmission of dry powder films of transparent materials is not settled. One fact is clear, however. Sufficiently thin, dry powder films of a non-mosaic type do possess transmission minima. In each case the minimum occurs at a wave-length of the order of magnitude of the particle size. One question left to be answered is the effect of the degree of aggregation of the particles. Some evidence is presented that aggregates of particles act like larger particles as far as the transmission of the film is concerned.

The author wishes to express his appreciation to Professor A. H. Pfund for suggesting the subject of this paper and for continual guidance during the experimental work, and to Professor John Strong for building the thermopile and for many helpful suggestions. The author also wishes to thank Dr. C. E. Barnett and Mr. J. R. DeVore of the New Jersey Zinc Company for furnishing the graded quartz and zinc sulfide powders.

JOURNAL OF THE OPTICAL SOCIETY OF AMERICA VOLUME 38, NUMBER 9 SEPTEMBER, 1948

The Quantometer, A Direct Reading Instrument for Spectrochemical Analysis

M. F. Hasler, R. W. Lindhurst, and J. W. Kemp
Applied Research Laboratories, Glendale, California

(Received April 22, 1948)

A description of the quantometer, a direct reading instrument for spectrochemical analysis is presented in this paper. The spectrometer equipped with movable receivers is discussed from the standpoint of basic optical, mechanical, and electrical design. An arrangement of four bridges with three receivers on each, allows up to twelve receivers to be moved and positioned so as to receive light from a great variety of line arrays in the spectrum range covered by the instrument. The limitations in this respect are presented for instruments utilizing 24,400 line per inch gratings and 36,600 line per inch gratings, both with a 1.5 meter radius of curvature. The basic electrical circuits and constants are given in detail for the receiver units, the low and high voltage power supplies, the sensitivity controls, and the recorders. The recording console is described especially with regard to the interchangeable panel method of direct reading, suitable for the analysis of a wide variety of alloys of the same base material. General operating methods are discussed in some detail. Adjusting and testing the instrument are explained and the precision of the unit as a light-measuring device is indicated.

NOW that the direct reading instrument, termed the Quantometer, has been accepted in industry both for research and production control, it would seem desirable to have a complete description of this instrument in the permanent literature. This is an appropriate time to do this, as the original instrument has been modified to meet various demands required by its commercial application which in general has improved it markedly. Thus the instrument to be described represents not only four years of basic development work, but two years of modification as succeeding instruments have been produced to do specific jobs for industry. Since nothing has been published on this instrument except for a preliminary paper in 1944,[1] a full description will be attempted at this time, plus a discussion of the testing and adjustment of the unit.

A Quantometer installation consists of three basic instruments—a spectrometer, a recording console, and a source unit to excite the spectra of the samples to be analyzed. Since any source unit of sufficient intensity and precision can be

[1] M. F. Hasler and H. W. Dietert, J. Opt. Soc. Am. **34**, 751 (1944).

used with the Quantometer, a description of the unit recommended for this purpose will be provided in another paper.

THE SPECTROMETER

One of the first things noted in working with direct-reading instruments, which have considerable spectrum range, is that many lines which prove most suitable for direct reading, furnishing maximum analytical range, sensitivity, and accuracy, are not those recommended for spectrographic use in the literature. This is due to certain limitations of the spectrograph which are not shared by the Quantometer and *vice versa*.

In the first place the region of the spectrum from 2100A to 2400A, wherein the photographic emulsion loses sensitivity and contrast rapidly with decreasing wave-length, is open to regular use by employing 1P28 multipliers in a direct reading instrument. Likewise the visible region from 4000A to 6000A, which is often shunned by spectrographers because of contrast variations, behaves in a regular manner with direct reading instruments. In the second place, the necessity of exposing in such a manner as to bring the weakest lines to a visible density on the photographic emulsion, places many restrictions on the use of intense lines in spectrography, which again are not shared by direct reading. Many lines considered much too intense for the former, prove ideal for the latter. Third, where photographic emulsion is employed, there is the

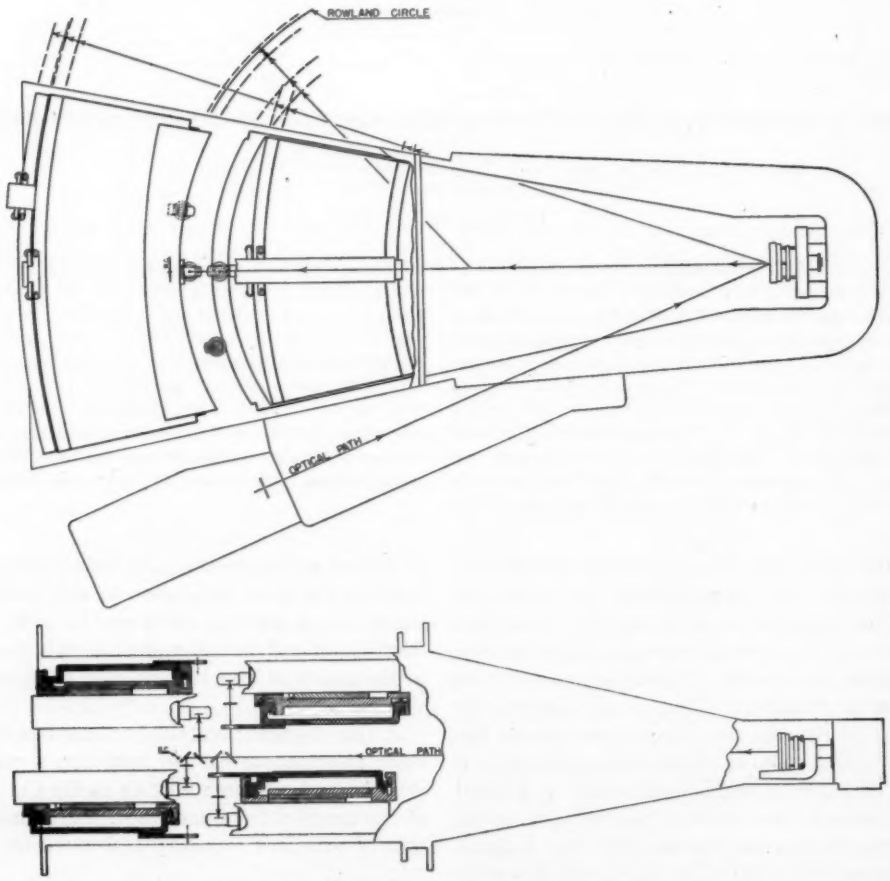

FIG. 1. Schematic drawing of the spectrometer.

difficulty of accurately comparing the intensity of lines which provide greatly different densities or which differ widely in wave-length. No comparable difficulties exist in direct reading as the sensitivities of multiplier phototubes can easily be adjusted over a factor of a hundred and their response is always a linear function of intensity regardless of the wave-length of incident light. On the other hand, a practical direct reading instrument using wider receiver slits than entrance slit will provide a lower ratio of line to background intensity than a spectrograph of the same dispersion employing the same width entrance slit. This has likewise encouraged the use of more intense spectrum lines for direct reading.

In view of all these factors it was recognized very early that it would be wise to develop a spectrometer that would possess the maximum of flexibility with regard to choice of wave-lengths, and yet would be stable and rugged, so that it could be used effectively for routine testing as soon as suitable methods of analysis were developed. These considerations led to the design of the spectrometer shown schematically in Fig. 1. The top view shows that the receivers move along two separate circles, one concentric with the Rowland circle, the other centered at the grating. The former keeps the slit in focus and the latter keeps it in exact alignment with the grating. The side view shows positions of four bridges which are mounted in the spectrometer. It also shows one receiver on each of these bridges so that the optical path in connection with each of these can be readily seen.

The standard instrument is supplied with sets of one, two or three receivers on each of the four bridges making a total of four, eight, or twelve receivers for the complete instrument. The spectrometer can be fitted with either of two gratings, one with 24,400 lines per inch, the other with 36,600 lines per inch. In order to cover the most satisfactory range with each grating, different entrance beam castings, providing different angles of incidence, are mounted to the frame, depending on which grating is to be used in a particular instrument. The specifications of these systems are shown in Table I.

The mechanics of the receiver carriage are also indicated in Fig. 1. A *T*-shaped assembly, formed by three rollers bearing against curved

TABLE I. Optical specifications of quantometer.

Grating specifications		Spectrometer specifications			
Lines per inch	Radius of curvature in meters	Entrance beam angle	Range A	Dispersion, A per mm in 1st order	Resolution with 100μ receiver slit, in A
24,400	1.5	22° 38′	2000–6000	6.9	0.7
36,600	1.5	29° 18′	2060–4730	4.6	0.5

ways centered at the grating, keeps the receiver pointed in the proper direction at all times, irrespective of its position on the Rowland circle. The straight ways on the carriage allow the receiver portion to follow the Rowland circle by means of a bearing riding on a curved track concentric with the Rowland circle and thus keep the slit in focus. A precision screw of twenty threads per inch, pivoted at one side of the spectrometer frame, moves the carriage around on the circular tracks. Each screw is equipped with a numbered dial and a revolution counter as shown in Fig. 2. Calibration of these screws then allows the receivers to be placed very accurately with respect to the spectrum.

With regard to the optical paths to the receivers, Fig. 1 shows these quite clearly. In each case, the plane mirror at 45° merely changes the direction of the beam and does not effect its focus. The spectrum line imaged at the slit, passes through this opening and falls directly on the sensitive cathode of the multiplier-phototube. The position of the multiplier with respect

FIG. 2. Intensity meter and lead screws used for positioning receivers with respect to spectrum lines.

TABLE II. Wave-length dispersion for receiver lead screws.

Grating lines per inch	Units of dispersion	Receivers 1	2	3	4	5	6	7	8	9	10	11	12
24,400	A/revolution	7.5	7.7	11.1	11.5	8.0	8.1	11.9	12.7	8.8	9.0	12.7	13.2
	Revolutions/A	0.133	0.130	0.090	0.087	0.126	0.123	0.080	0.079	0.114	0.111	0.080	0.076
36,600	A/revolution	5.0	5.1	7.3	7.6	5.3	5.4	7.9	8.4	5.6	5.7	8.4	8.8
	Revolutions/A	0.200	0.195	0.137	0.131	0.190	0.185	0.127	0.120	0.179	0.175	0.119	0.114

to the slit and the divergence of the beam provides a beam width at the cathode of 0.070 inch. Provisions are made to allow movement of the multiplier across the beam so that the point of highest sensitivity can be chosen. Contrary to the results published by Saunderson, *et al.*,[2] no sharp narrow maximum of high sensitivity was found, but rather a broad plateau which usually extends one-eighth of an inch. Thus it is a relatively simple matter to set the multiplier correctly in the beam. This method of illuminating is considered far superior to using a diffusing screen and having the multiplier pick up the scattered light from it. In general the ratio of multiplier sensitivity to dark current is such, in commercially available multipliers, that as high a spectrum line intensity as can be obtained is usually desired. Therefore reducing the intensity at the multiplier by a factor of from 2 to 3, as would be done by a diffusing screen, does not seem desirable.

To facilitate focusing the receiver slit, the whole electrical sub-assembly including multiplier can be removed, and a telescope fitted in its place. The telescope is provided with a prism at the far end so that by looking through the eyepiece one can see an image of the slit. Also, by changing the focus of the telescope one can view the grating image through the slit, and use the slit as a knife-edge tester. This serves to tell when the receiver slit is at the correct distance from the grating, for as the receiver is moved across the line image, the grating will appear to darken simultaneously if in correct focus. Also by examining the slit image one can see whether the line image is exactly parallel to it and adjust the slit rotation accordingly. The most convenient way to perform these optical tests is with a mercury spectrum line obtained from a test lamp provided with the Quantometer. The strong blue line at 4358A is quite convenient as it is near the middle of the range of the spectrometer and yet can be observed visually.

After all of the receivers have been carefully focused by means of the visual test, the instrument is calibrated for wave-length. This is also done with the mercury lamp, the relationship between wave-length and screw settings being readily determined. These calibration curves are very nearly straight lines. They can be readily plotted on large-scale graph paper so that the screw setting of a particular line can be determined to within a few tenths of a revolution, which corresponds to a few angstroms. Table II shows the wave-length dispersion for each of these screws. Receivers 1, 5 and 9; 2, 6 and 10; 3, 7 and 11; and 4, 8 and 12 are respectively on separate bridges. This accounts for the similarity of the dispersion values in each set of three.

It is apparent from the above that any receiver can be placed very close to a given spectrum line merely by referring to the calibration chart. To permit exact positioning of the receiver slit so that the line image falls exactly within it, an intensity meter is provided which may be plugged into the final counting portion of any receiver circuit. This arrangement is also shown in Fig. 2. This meter is used to profile the lines in the vicinity of the region determined from the chart. By sparking a sample which is high in the element to be detected, it is usually a simple matter to find the correct line. The exact positioning of the receiver is then done by manual profiling wherein one notes the position at which about half the maximum intensity is obtained on one side of the line and then goes over and determines the position where the same intensity is obtained on the other side of the line. The position midway

[2] Saunderson, Caldecourt, and Peterson, J. Opt. Soc. Am. **35**, 681 (1945).

between those two points is then used as the correct point for the receiver. It is necessary to employ this method rather than to determine the position of maximum intensity directly, because of the variable instantaneous intensity of even the best sources. In general this maximum point can be determined in about one minute per receiver.

It is quite obvious that if minor mechanical vibrations are not to effect the quantitative results, the spectrum line image must fall entirely within the receiver slit and must not intercept the edge of the slit. In general the line image is made about one-half as wide as the receiver slit, that is, 50 microns as compared to a 100 micron receiver slit width. Thus if the image is at the center of the receiver slit, this allows a movement of about 25 microns before the image starts to intercept the side of the slit. This feature of adjusting the individual receivers to the correct spectrum lines is one which has proved to be extremely valuable, not only in research work where lines must be easily found, but in production control where it is essential that the receivers be exactly positioned with respect to the various lines. Thus the screw device described above serves a dual purpose, the importance of which cannot be over-emphasized.

The next point to be considered is the possible line arrays which can be used simultaneously. The first thing in this connection is the closeness of lines in the spectrum which may be utilized. As indicated in Fig. 1 there is no mechanical interference between receivers on separate bridges. Thus four of them on separate bridges can be clustered quite closely, the only limitation being an optical one, caused by the widths of the mirrors on the various receivers. These widths are predetermined by the width of the beam starting at the grating and converging to a line image at the receiver slit. Those mirrors closest to the grating must be the widest to intercept the full beam. Table III shows the mirror widths of the various receivers and the shadow effect caused by each. The minimum difference of wave-length between lines which may be selected for any two receivers is determined solely by the widest mirror involved and is the value in Angstroms shown. The minimum distance of approach between two receivers on the same bridge in terms of wave-length is also given. With these facts for both types of gratings, the possibility of setting up on any particular line array can be readily determined.

TABLE III. Mirror widths of various receivers and wave-length differences for receiver positions of closest approach.

Receivers	Width of mirrors in mm	Wave-length difference for receiver positions of closest approach: With 24,400 line per in. grating, Different bridges	With 24,400 line per in. grating, Same bridge	With 36,600 line per in. grating, Different bridges	With 36,600 line per in. grating, Same bridge
1, 5, 9	1.6*	**	490A	**	325A
2, 6, 10	2.4	18A	490A	12A	325A
3, 7, 11	3.9	30A	750A	20A	500A
4, 8, 12	5.2	41A	750A	28A	500A

* Effective width—a much larger one is actually used.
** Between any two receivers on different bridges, the wave-length difference of closest approach is determined entirely by the receiver with the largest mirror and is the value shown.

BASIC CIRCUITS

Before describing the recording console in detail it may be well to discuss the various circuits involved in the Quantometer. The basic integrating circuit used depends on charging a small condenser between two voltages, which are respectively the ignition voltage and the extinction voltage of a neon lamp. Operation is as follows: light causes the multiplier to pass output current which charges a small condenser up to the ignition voltage of the neon lamp, say 80 volts. When the neon lamp discharges, current from the condenser flows through a resistor and provides a voltage pulse. This is amplified by the first tube in the receiver circuit from which it is passed on to a thyratron. The final output from this thyratron is a fairly high energy pulse which is used to operate an electromagnetic counter. With the discharge of the condenser, the voltage drops to the point where the neon tube is extinguished, say 75 volts. However, immediately that extinction occurs, the condenser again starts to charge and the process is repeated. High accuracy demands that the discharge time be a very small fraction of the charging time. This system provides an extremely simple method of measuring very low currents. The main advantages are: first, freedom from all zero drift, as zero current provides a zero count; second, extreme stability, as the counting rate is determined entirely by the characteristics of the neon

lamp and nothing else; third, great sensitivity, as currents of the order of a hundredth of a microampere can be readily measured; and fourth, excellent proportionality of count rate with charging rate.

The top section of Fig. 3 shows the receiver circuit in some detail. It will be noted that an argon irradiating lamp is used in order to insure a definite ignition voltage for the neon lamp. This helps greatly to provide a reliable counting operation. By selection with an oscillograph, neon lamps can be readily chosen to provide a constant proportionality between counting rates and charging rates. Counting rates as low as one every two seconds and up to 60 per second or over a factor of better than a 100 to 1 can be readily obtained. This usually corresponds to charging currents of about 0.03 microampere to 3 microamperes though different tubes give somewhat different count rates.

The circuit diagram of the low-voltage supply is shown in the middle section of Fig. 3.

Since it only furnishes voltage for the amplifier and counter which handle pulses exclusively, voltage regulation is not particularly important for this unit. However to be on the safe side it is powered from a Sola, or magnetic-type regulator. The important point in connection with this supply is that it reduces 60 cycle ripple to a very low value. This is necessary in order to eliminate any possible pick-up by the integrating circuit. It is found that such pick-up tends to cause an interlock between the counting rate and sub-multiples of 60 cycle which can cause error. However the constants shown for the supply minimize this effect so that it does not introduce any appreciable error.

The high-voltage supply which powers the multipliers must be very constant in its output voltage, as any variation is magnified five-fold in multiplier gain variation. Thus only a few hundredths of a percent variation is allowable. This degree of regulation is obtained by using a three-fold correcting system. First the high voltage supply is powered from a Sola regulator. Next the output from the main transformer is rectified by an 8005 tube which also acts as a voltage control element. The grid of this tube is powered from a bridge circuit in such a manner as to minimize such fluctuations. Lastly, the output of this system is then fed into a bank of VR tubes which provides additional regulation. The net result is a very high degree of stability and independence from line fluctuations. The dia-

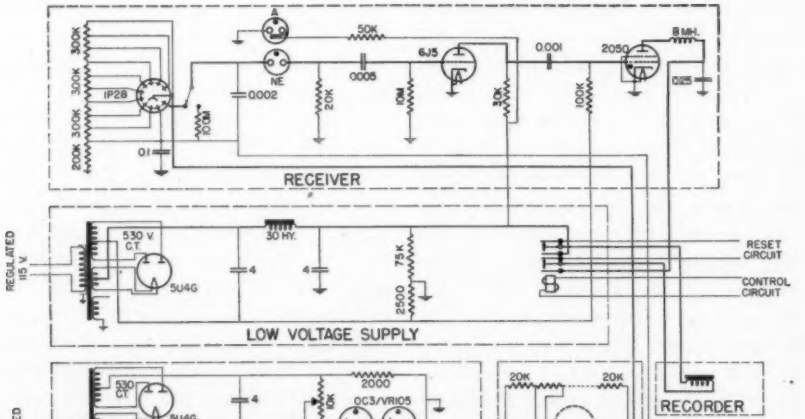

FIG. 3. Circuit diagrams for electrical components constituting a single channel.

gram of this system is shown in the bottom section of Fig. 3.

The sensitivity-control circuit, consisting of two, forty-step tapped resistors which are connected in series, is shown in Fig. 3. The coarse control has 20,000 ohms per step, the fine control 500 ohms per step accurate to 0.1 percent. Thus the fine control just bridges the gap between one-coarse control step. These controls, employing taps and precision wire-wound resistors with a low temperature coefficient, provide a very accurate and stable arrangement for varying the voltage applied to the first eight stages of each multiplier. By means of the coarse control a one hundred-fold over-all change in sensitivity can be obtained, while by means of the fine control a change as small as 0.25 percent can be made. Thus this provides a practical method for varying the sensitivity of the multipliers. A pair of such controls is used with each multiplier.

The recording circuit is very simple. It consists of an electromagnetic counter connected in series with the plate circuit of the thyratron in each receiver circuit. The counting rate is controlled entirely by the quantity of light falling on the multiplier and the sensitivity of that multiplier. The latter is controlled with the sensitivity controls mentioned above.

Interconnecting circuits appear rather complicated when first viewed in the instrument, however, in reality they are rather simple for any one receiver-recorder combination. The complexity arises from the twelve-fold replication needed to measure the intensity of twelve spectrum lines simultaneously. Fig. 3 shows the basic interconnections including the sensitivity controls. Wherever possible Cannon, plug-type connectors are utilized so that any of the units described above such as the receivers, high-voltage supplies, sensitivity controls, low-voltage supplies, recorders, etc., can be disconnected from the circuit at a moment's notice. This allows rapid replacement of units if trouble develops in any part. It also allows the offending unit to be located very rapidly by a systematic interchange of units which are operating, with suspected units. Obviously it is of the utmost importance that a direct reading instrument upon which the whole analytical load of a plant is placed, should be easily and rapidly serviced. The above mentioned system allows this.

RECORDING CONSOLE

The recording console houses the low voltage power supplies, the high voltage supply, the sensitivity controls, and the recorders. The recorders are motor-driven electromagnetic counters. A pawl and a ratchet wheel with thirty teeth, allows a 12° advancement of the wheel with each count. The motor operates stalled and provides a torque on the wheel which is ample to drive a sixty-inch tape over sprockets. Even with this appreciable load on the counters, counting rates up to sixty per second can be handled easily. In fact, reset to zero is effected by means of a sixty-cycle pulsing circuit. Terminators and zero stops are provided by small snap fasteners attached to the tapes. These activate standard micro-switches mounted on or near recorders.

The present tape system utilizes a sixty inch tape with pointers every twelve inches. Each of these pointers is of a different color for ease of identification. The tape passes from the recorder down to the front of the console, up the front of the console, and back to the recorder. The vertical path at the front of the console is twelve inches in height so that a pointer is always visible. Two numbered scales with appropriate color designations are mounted on a plastic panel on each side of an opening. The percentage composition is then read directly on the scale of the color corresponding to that of the pointer in view.

The great advantage of this last mentioned system over a previous one is that working scales can be readily changed for all elements merely by interchanging panels. This makes for a very rapid method of changing the instrument to analyze a variety of alloys which possess a common major constituent. This procedure will be described in more detail when the operation of the instrument is considered. Figure 4 shows a typical working scale panel at the front of the console.

METHOD OF OPERATION

The method of operation of the Quantometer is quite straightforward. A control circuit is powered with 230 volts a.c. from the source

unit whenever a discharge is started to the sample to be analyzed. This circuit operates a prespark or prerecording timer which can be set at any value from zero to sixty seconds. At the end of the prerecording time, this timer closes the relays in the various low voltage supplies which in turn close the recorder circuits starting the recorders. The integrated intensity of each of the spectrum lines upon which the receivers are focussed is then measured by the separate recorders. Termination of the recording period is affected by the internal standard line. When its integrated intensity is such as to produce 590 counts, the stop on the recorder tape activates a micro-switch which terminates all recording by stopping the operation of the source unit. Without calculations of any kind, all other recorders can be read directly as to percentage composition, providing, of course, that the instrument has been previously calibrated.

This method of working to a constant integrated intensity of the standard line rather than to a standard time, eliminates all necessity of comparing the various line intensities to the standard after the recording cycle is completed, such as is sometimes done in other instruments.[2] With the Quantometer, completion of the discharge to the sample completes the recording, and data can be taken immediately. This is of considerable advantage in cases where a high rate of sample analysis must be continuously maintained.

FIG. 4. The recording console equipped with interchangeable, working-scale panel.

Where two types of sources are utilized, a selection circuit must be provided within the source unit to power the selection relays in the recording console. These may, for instance, automatically operate certain preselected recorders when a spark-like source is employed and others when an arc-like source is used. Still other recorders may be operated by both sources. In this way complete flexibility is provided in the operation of the unit.

STANDARDIZATION

The standardization of the Quantometer is a straightforward procedure. All of the receivers are accurately centered on the various spectrum lines, the intensities of which are to be measured. The source unit is adjusted to provide certain definite conditions of operation. The time of prespark is decided upon and the prerecording timer is set at this value. The total time of recording, usually between 20 and 30 seconds, is decided upon. A standard sample is chosen which possesses relatively large amounts of most of the elements to be determined. This sample then has its spectrum excited under the standard conditions and the operations of the various recorders are noted. Any tendency for the tapes to move in jerks means possible jamming of the recorders and indicates that lower counting rates should be employed. Reduction of the sensitivity of the multipliers involved is readily done by adjusting the proper tapped sensitivity controls. If the recorder, measuring the intensity of the internal standard line, appears to advance the tape in a smooth manner, then the total recording time appearing on a precise electric clock can be noted. Comparing this to the standard time decided upon, will indicate the direction and amount which the sensitivity controls must be adjusted. One step on the coarse control varies the multiplier sensitivity approximately 10 percent though this value varies from multiplier to multiplier and also depends upon the position of the control. The fine control provides forty steps between each of the coarse steps.

With the more obvious adjustments completed, the standard is again analyzed. The recording time is read and if within one or two seconds of the desired time, the counts obtained on each of the other recorders are noted. To facilitate this reading, a recording panel provided with simple count tables is furnished. From these readings sensitivities are adjusted so that the highest percentage of each element to be determined can come within the 600 counts which constitute one cycle of a tape. With the instrument thus adjusted, all standard samples are analyzed two or three times each, preferably in rotation rather than repeatedly so that any long term drifts of the instrument will be detected and averaged out. These results are plotted as counts—which really represent intensity ratios to the internal standard line—*versus* various percentage compositions. Two typical working curves thus obtained are shown in Fig. 5.

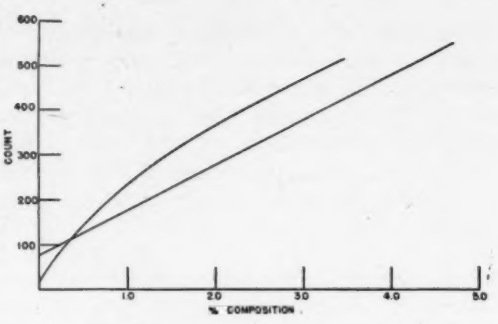

FIG. 5. Two typical curves obtained by the count method of linear recording.

The linear one represents the ideal type where the intensity of the spectrum line is changing linearly with respect to the amount of the element present. The non-linear one is the type obtained from spectrum lines which show a marked amount of self-absorption. The count at zero percentage is made up of the sum of optical background and dark current. In general, multipliers with a sufficiently high ratio of sensitivity to background are selected so that combined with the intense sources recommended, this dark current is less than 20 percent of the optical background. At this level small changes in dark current have practically no effect on the analytical accuracy. This method of eliminating the effect of changing dark current—that is by making the dark current a small part of the total current being measured—seems much more desirable than going to complicated alternating current amplifiers as has been proposed,[3] as any such complication must be repeated for each receiver.

Having obtained working curves for each of the elements to be determined, the next step is to prepare the working tables. These are typed on color designated strips of paper to match the colored pointers on the tapes. Numbers are spaced apart vertically the distance the tape travels in two counts. In the case of linear working curves, it is best to make two counts equal a simple number such as 0.001 percent, 0.002 percent, 0.005 percent, 0.01 percent, 0.02 percent and so on, the choice depending upon the range to be covered. A typist can then prepare such a table very readily. In the case of non-linear scales a percentage value must be determined from the curve for every two counts. These tables are cemented to one of the detachable plastic panels and the instrument is ready for direct reading after the sensitivity controls and the zero-control tabs on the tapes have been adjusted.

The procedure for adjusting them is simple. Since changing the sensitivity of the multiplier changes the slope of the working curve but does not affect its shape, analysis of two standards, one low, the other high in the element being considered, provides the data. The difference of count obtained from these two samples is compared to the difference which should be obtained from the working table. The sensitivity is adjusted to correct for this difference. The standards are again analyzed to check the change made. If their difference in count is correct but the actual count of each differs from the values on the table by a constant, the pointers on the tape are moved this constant distance by varying the zero tab along the tape. Analysis of any standard or sample should now be possible by direct reading from the tabulated working scales. This may appear to be complicated but any other system which professes to calibrate by a single adjustment is overlooking the fact that four variables are being considered—line intensity,

[3] K. G. Kessler and R. A. Wolfe, J. Opt. Soc. Am. **37**, 133 (1947).

optical background, multiplier sensitivity and multiplier dark current—and ways must be provided to correct for changes in each. In actual practice the main variable seems to be multiplier sensitivity. Thus usually an adjustment of this sensitivity by checking a single standard, which is typical of the analysis being made, suffices to keep the whole system in calibration.

TESTING THE QUANTOMETER

From the above it should be apparent that though analyzing samples is a simple, rapid affair, the apparatus used to obtain these results is fairly complicated. This complication lies not so much in the system employed, which is among the simplest conceived to date, but rather in the replication of this system up to twelve times. In any event rapid test methods must be available to ascertain that correct analyses are being obtained at all times. In the case of the Quantometer, testing equipment has been largely built into the unit so that it is available for instant use.

Starting at the receiver, the part most likely to fail is the multiplier-phototube. It may become gassy with age which would cause instability and erratic readings. To prove that erratic readings come from this source and not from some other, a switch and resistor is provided in each receiver. By rotating a knob the resistor is connected in the circuit in place of the multiplier. If reproducible counts are obtained for constant times, and the instantaneous count rate is stable as noted on the intensity meter, this is definite proof that the rest of the system is not producing the instability. This test also provides a very good measure of the accuracy of the integrating recording system of the Quantometer. Table IV shows deviations obtained from a typical set of data and illustrates the very high degree of reproducibility of this type of system.

TABLE IV. Reproducibility tests. Intercomparison of two receivers, providing deviations of the ratios of counts obtained from twenty runs.

Description of test	Standard deviations of count ratios
100 megohm resistors replacing multipliers in two receiver circuits	0.22%
Multipliers in two receivers measuring intensity of light from highly regulated tungsten filament lamp	0.31%
Multipliers in two receivers measuring intensities of 2270Å Ni line and 2370Å Fe line respectively, produced by high precision source	0.53%

With the supposed erratic operation narrowed down to the multiplier tube and its immediate equipment such as sockets and resistors, another simple test can be performed. Actually in practice this test would usually precede that mentioned above. This is to place a constant light source as close to the grating as possible and use this to determine the over-all stability of the system. Such a system is provided in the form of a lamp mounted directly above the grating and supplied from a voltage regulator. The same tests that were performed with the resistor can be done with the lamp. Data collected in this way indicate the over-all accuracy possible when a multiplier is combined with the integrating-recording system under consideration. Results of such tests are also shown in Table IV.

The final test, of course, is to determine the reproducibility which can be obtained when measuring the light obtained from a typical source unit. In the case of the spark section of the High Precision Source unit, recommended for use with the Quantometer, light from 240 discharges per second, each of a few microseconds duration, must be integrated accurately. That this can be done effectively with the system employed is indicated by the excellent reproducibility figures for such a source shown also in Table IV.

In addition to having good reproducibility, it is very important that the integrating-recording system possess good linearity. This combined with the linearity of the multiplier output is the basis for the whole system. A simple means of checking this has been devised. A regulated incandescent lamp is placed in front of the primary slit and is aligned so that the image of the filament formed by the condensing lens falls in the center of the grating. The intensity of the light in the continuous spectrum measured at the receiver is found to vary linearly with slit opening. Using a linear plot of count *vs.* slit opening, a zero setting error of the slit does not effect results but obviously the slit head must read relative openings accurately. By this test and other electrical and optical tests which have been devised, it can be shown that a system of

this type can be produced which deviates from linearity in count rate by less than 1 percent over a hundred-fold range.

ADDITIONS TO THE QUANTOMETER

Two additions to the Quantometer have been devised which extend the analytical usefulness of the instrument.

The first is an attachment which allows eight additional semi-fixed receivers to be added to the maximum of twelve usually furnished. Two additional bridges are mounted in the spectrometer—one of which is used to mount eight small telescope-mirror assemblies—the other, eight mirror-receiver assemblies. These units are connected to a separate recording console which provides a recorder, low voltage supply, and sensitivity control for each of the eight receivers plus a single high voltage supply for the group.

Lines throughout the whole range of the spectrometer can be focused upon these semi-fixed receivers providing that mirrors on the standard receivers do not intercept the lines desired. This arrangement greatly extends the analytical scope of the quantometer, allowing a greater number of elements to be determined simultaneously; and/or more percentage ranges of a single element, by utilizing several lines of that element for measurement.

The second addition also has to do with extending the useful percentage range of analysis. Often a spectrum line can be used over a thousand-fold change of intensity. This is considerably greater than the range of counting rate provided. Thus a means of quickly changing the count rate must be furnished if the whole range of intensity of a spectrum line is to be utilized. This can be done in two ways; either by changing the sensitivity controls of a receiver which changes the voltage applied to its multiplier, or by introducing a filter between the receiver slit and the multiplier to reduce the light intensity. The latter is favored in practice because the electrical stability of a multiplier may be impaired for a short time if its voltage is changed by a large amount. Thus a filter device has been developed which allows a filter to be moved in and out of the light beam in any receiver by a push button control on the outside of the spectrometer.

With these additional features the Quantometer can now provide a direct-reading instrumental solution to almost any analytical problem which can be handled by spectrochemical methods.

CONCLUSION

In concluding this description of the Quantometer and its mode of operation, it should be emphasized that this unit is ideal for research work. The over-all flexibility of the instrument, particularly the ease with which receivers may be moved to any point in the working range of the spectrum, offers definite advantages for this type of work.

As for plant control laboratories, many of the features discussed are well suited for production control applications. As pointed out in the beginning of this paper, an appreciable time must elapse before all the problems connected with the choice of the best source conditions for the analysis of a particular alloy, and the spectrum lines most suitable under those source conditions, are worked out. This, together with the usual differences encountered in the detailed analytical problems of one plant as compared to another, make the flexibility of the Quantometer a great asset in a control laboratory.

This flexibility also makes it possible for a laboratory to analyze large numbers of several entirely different types of samples, providing the individual samples do not have to be analyzed on a speed basis. This is possible as a Quantometer with twelve receivers can be changed from the analysis of one type of alloy, for instance, to the analysis of an entirely different type requiring a completely different set of spectrum lines, in a matter of one hour. To achieve this rapid change it is of course essential that the working scales and the exact method of analysis be developed previously.

It is hoped that this description of the Quantometer and its operation will stimulate further instrumental and method research in the field of direct-reading spectrochemical analysis.

Wide Range Analysis for Zinc Using Spectrographic Line Widths

E. JOHN EASTMOND AND BERNICE E. WILLIAMS
Western Regional Research Laboratory, Albany, California*

(Received April 5, 1948)

A spectrographic method has been developed for determination of zinc in biological ashes by use of line width as a concentration index. Synthetic standards and analytical samples, in the form of sulfates, are mixed with a potassium sulfate-graphite buffer containing barium and cadmium as internal controls. Samples are excited in a direct-current arc and spectra recorded with a Littrow quartz spectrograph. The contour of Zn 2138A is recorded with a recording microphotometer and the width determined at the maximum density of the control lines Ba 2255A or Cd 2288A. A plot of the logarithm of this width *versus* logarithm of zinc concentration prepared from standard samples containing 0.004 to 10 percent zinc serves as an analytical curve. Results determined by ordinary density measurements have been compared with those from width measurements. Although the two methods show comparable reproducibility of repeated exposures at the lower limit of the analysis range, the width method is more precise at higher ranges and has proven applicable even at concentrations where the line density method is limited by self-reversal and low photographic plate contrast. Concentrations as high as 10 percent have been determined, indicating possible application of such a method to the estimation of major constituents in such biological ashes or inorganic powders.

INTRODUCTION

CONSIDERABLE attention at this laboratory has been directed toward developing a spectrographic procedure for estimating, over wide ranges, the concentration of metals in the variety of different materials encountered. One of the chief difficulties was found in the estimation of zinc. In order to extend the lower limit of the analysis range to cover the small concentrations often occurring in the samples submitted, it was necessary to use the most sensitive zinc line at 2138.56A. However, the usable range of analysis with the usual line density methods was found to be quite limited. This is due to the tendency of the line to be easily self-reversed. Furthermore, the precision attainable was poor, probably partially due to the lack of control over self-reversal and partially to the low contrast of the photographic emulsion in this wavelength region resulting in only small changes in line density with changes in zinc concentration.

At the same time, as zinc concentration increased the increased *width* of the line was easily noticeable even after self-reversal had reduced the density at the center of the line. It appeared that a method such as suggested by Coheur[1] using line widths as a concentration index might be applicable to advantage in this instance. It should be noted, however, that his first method of measuring a broad line of the fundamental or control element at the varying maximum densities of the additional element is, in the present instance, subject to the same difficulties as the line density method. The procedure then has been to measure the varying width of the additional element, zinc, at the maximum density of a weak internal control line.

A comparison of results from intensity ratio measurements and line-width measurements has been carried out and the width results show better precision and an extended analytical range.

ANALYTICAL TECHNIQUE

Preparation of Materials

In order to make the method as generally applicable as possible, work was carried out with inorganic powders since most of our samples are either inorganic powders as received or reducible to this form. It has been found advantageous to convert the samples to sulfates whenever possible. Dry plant materials were sulfated by adding a solution of sulfuric acid in ethyl alcohol (1:9 by volume) and charred by burning off the alcohol. Solutions were dried and partially charred under

* Bureau of Agricultural and Industrial Chemistry, Agricultural Research Administration, U. S. Department of Agriculture.

[1] P. Coheur, J. Opt. Soc. Am. **36**, 498 (1946).

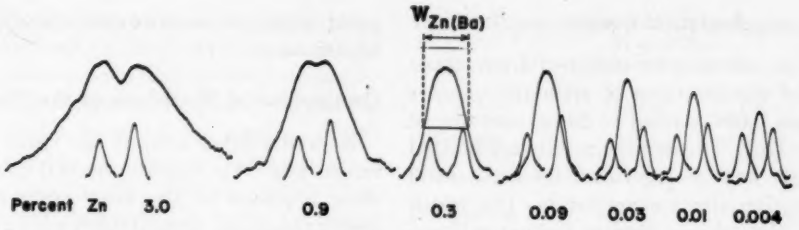

FIG. 1. Line contour recordings of typical exposures of synthetic zinc standards. The lines in each group of three are Cd, Zn, and Ba in that order from left to right. The measurement of zinc width at barium maximum, WZn(Ba), is illustrated for the 0.3 percent standard.

an infra-red lamp before sulfating. The char was further ashed in a muffle furnace at 450–500°C.

Standards were prepared from the following base approximating the qualitative composition of a typical sample: 2 percent sodium chloride; 4 percent calcium sulfate; 6 percent basic magnesium carbonate; 0.4 percent silicic acid; 10 percent potassium phosphate (Di-H); 77.6 percent potassium sulfate. Suitable aliquots of a standard zinc solution were added to portions of this base and the mixture dried and ground in a mortar.

A spectroscopic buffer-control mixture was prepared as follows: 10.000 g. high purity graphite powder, 3.000 g. potassium sulfate, 0.233 g. barium sulfate, 1 ml 0.01 percent cadmium solution. This mixture was also dried and ground in a mortar. The barium and cadmium are present in quantities sufficient to give lines suitable for use as internal controls for both density and line width measurements. The standards (or analytical samples) were mixed with this buffer-control in a ratio of 2:1 by weight.

Excitation and Photography

The 2:1 sample:control mixtures were tamped into the sample electrodes with a flat-ended nickel rod. The lower (+) electrode was cut with a $\frac{1}{8}$-inch center post with central sample cavity 2 mm in diameter and 4 mm deep. The upper (−) electrode was cut with a solid $\frac{1}{8}$-inch center post. Regular grade $\frac{1}{4}$-inch diameter spectroscopic graphite rods were used. The samples were excited with a 250-volt 15-ampere direct current arc.

The image of the arc was focused on a 13 mm diaphragm at the collimating lens of a large quartz prism Littrow spectrograph. The slit width used was 0.02 mm. Exposures were continued until the entire sample of approximately 15 mg was burned. Exposure times averaged about 50 seconds.

Type I-O ultra-violet-sensitized photographic plates were used and developed under standard temperature-controlled conditions. The emulsion was calibrated for intensity measurements by means of selected iron lines of known relative intensity. These relative intensities had been determined from a calibration curve established by use of a split-field filter[2] and preliminary curve procedure.[3]

Measurement of Densities and Line Widths from Spectrograms

A combined comparator, densitometer, and recording microphotometer[4] was used to measure both line transmissions and line widths. Transmissions were measured on the direct reading densitometer. Intensity ratios of zinc 2138.56A to barium 2254.73A or cadmium 2288.02A were calculated using the emulsion calibration curve and a standard calculating board. For width measurements, line contours were recorded on photographic plates with the 16 mm microscope objectives, a 0.5 mm slit and a 64X magnification on the recorder. The widths of the zinc line at maximum density of the same barium and cadmium lines were measured from this photographic recording by means of a small scale-magnifier (see Fig. 1).

---

[2] R. A. Sawyer and H. B. Vincent, J. Opt. Soc. Am. **33**, 247 (1943).
[3] J. R. Churchill, Ind. Eng. Chem. (Anal. Ed.) **16**, 653 (1944).
[4] P. A. Leighton, S. Smith, and F. C. Henson, Rev. Sci. Inst. **5**, 431 (1934).

Analytical Curves

Analytical curves were obtained from measurements of spectrograms of standard samples ranging from 0.004 percent to 10 percent zinc in the powder base. The density results are plotted in the usual way as logarithm intensity ratio *versus* logarithm zinc concentration. The width results are plotted in a similar fashion as logarithm of zinc width at the maximum intensity of the control line (width as measured on the recorded contour) *versus* logarithm of zinc concentration (see Fig. 2).

RESULTS AND DISCUSSION

Limitation of the Density Method

As has already been stated the density measurements are limited by self-reversal and lack of contrast effects. This is apparent in Fig. 1 where the height of the maximum (which is related to density) shows very little increase with zinc concentrations above about 0.03 percent. This is further emphasized by the steepness of the analytical curve seen in Fig. 2 above this point. The self-reversal at still higher concentrations is also apparent in both figures. The curve from intensity ratios has been dotted in above this point since it is obviously invalid over the higher range.

Comparison of Precisions of the Two Methods

Reproducibility tests in the lower part of the range, where the density method could be used, show precision of the same order only at the lowest point, i.e., around 0.004 percent zinc. (It is at this point that the density results should show their best precision since the density of the test and control lines are approximately equal. At the same point the width of the zinc line is determined near the tip and therefore will probably show lowest reproducibility). The precision of the width results gets progressively better than the density results as zinc concentration increases. Repeated exposures of the same sample at 0.03 percent indicate this. Density measurements showed standard deviations from the mean of 10 percent with barium as a control and 14 percent with cadmium. Width measurements on the same exposures show standard deviations of only 4 percent with barium and 5 percent with cadmium.

Additional tests have also been carried out in which known amounts of zinc were added to samples of inorganic powder of unknown zinc

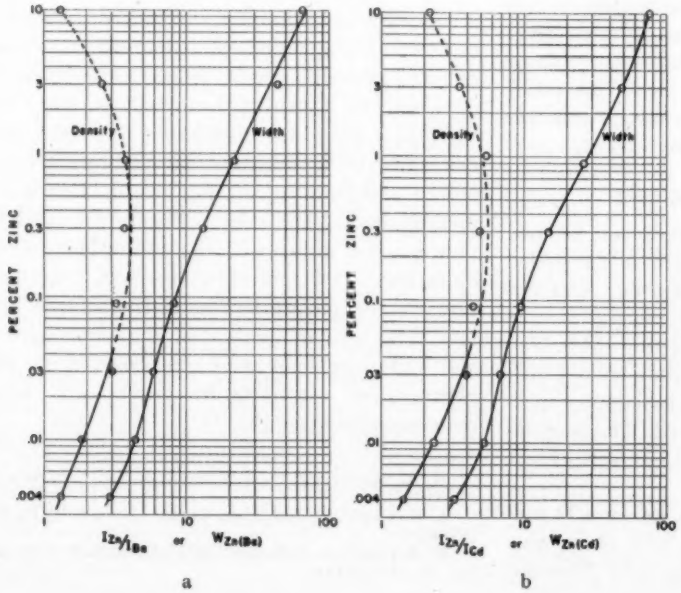

FIG. 2. Working curves as determined by intensity ratio and line width measurements with (a) barium as a control and (b) cadmium as a control. The zinc concentration is expressed as percent of the ash or inorganic sample before addition of buffer.

content and also to samples of agricultural plant material before ashing. We have been unable to observe increments with reasonable accuracy by line-density measurements even well within the apparently usable range of the working curve. On the other hand, the line width measurements on the same spectrograms give very satisfactory values for these increments even in the range beyond where the influence of self-reversal is apparent. Results from different tests of this sort are listed in Table I.

TABLE I. Results of tests with known amounts of Zn added to samples.

Material	Zn added	Zn observed Density	Zn observed Width
Potato ash	0.03%	0.024%	0.029%
(Zn added after ashing)	0.08%	0.039%	0.081%
Dried potato	0.0015%	0.0014%	0.0016%
(Zn added before ashing)	0.004%	0.0011%	0.0038%
Mixed agricultural ash	0.08%	—*	0.09
(Zn added to ash)	0.24%	—*	0.26

* Zinc concentrations not in workable density range.

Range of Analysis by Line-Width Method

The above results show that by use of the line-width method an analytical range of at least 1000-fold is possible with a single analytical procedure. The two methods generally used to extend the single procedure range of the density method to higher concentrations, namely (1) by use of a stepped sector to reduce density, and (2) by use of less sensitive lines, are not feasible in the present instance. The use of the sector is not applicable when the line is subject to self-reversal. The next most sensitive lines of zinc, 3345.02 and 3302.59A, are not only subject to interference from calcium and sodium commonly found in the samples under examination, but they lack sensitivity and do not appear in measurable density until a concentration of about 0.3 percent is reached.

The fact that concentrations as high as 10 percent have been determined is of interest since it indicates the possible application of a line width method to the estimation of major constituents in agricultural ashes or inorganic powders.

Report on Colorimetry and Artificial Daylight

Copies of the report of the U. S. Secretariat on Colorimetry and Artificial Daylight, prepared in connection with the I.C.I. meeting in Paris this summer, are now available. The following subjects are considered: (1) Proposed standard illuminant *E*, (2) definitions of colorimetric purity, (3) adequacy of standard observer for technical colorimetry, (4) definition of standard illuminants in the ultraviolet for the colorimetry of fluorescent materials, (5) illuminants for color matching, (6) specification of color-rendering properties, (7) color discrimination, (8) color terminology. The progress in colorimetry since the 1939 session is indicated by a bibliography of several hundred references. Copies of this report may be obtained by writing Dr. K. S. Gibson, Chairman, Tech. Com. 7, U. S. National Committee, I.C.I., National Bureau of Standards, Washington, D. C.

The Temperature Coefficient of the Refractive Index of Water*

J. B. HAWKES AND R. W. ASTHEIMER
Stevens Institute of Technology, Hoboken, New Jersey

(Received April 29, 1948)

A Jamin interferometer was used to measure the thermal coefficient of the refractive index of water for sodium light ($\lambda = 5893$A) from -5°C to $+25$°C. From this was calculated the index-temperature curve over the same range. The results agree with those found by the Bureau of Standards for water within the experimental error, which is between 1×10^{-6} and 2×10^{-6} index unit per degree centigrade. No differences were found between samples of water from different sources, nor was any change observed in the same sample over periods of weeks. No anomalies or irregularities in behavior were found in the average dn/dT. The possibility of a small consistent difference between the dn/dT *versus* T curves taken with rising and falling temperatures near 0°C is still under investigation.

IT is a mathematical commonplace that irregularities in the relationship between two variables have a more marked effect on the derivatives than on the function itself. For this reason anomalies in the index of refraction will more easily be found in the thermal coefficient of the index than in the index-temperature relation. At the same time the absence of irregular behavior in the thermal coefficient will have a correspondingly greater significance.

By the use of a Jamin interferometer described elsewhere,[1] measurements of the rate of change of refractive index with temperature, (dn/dT), have been made on water. Sodium light (5893A) was used. The water studied was triple distilled; the first distillation was conducted in a continuous-process copper still, the remaining two distillations being by batches, in Pyrex. At the end of the third distillation, which was in vacuum, the water was collected directly in the Pyrex cell, which was thereupon sealed from the outside air. However, a small amount of room air was sometimes included in the cell. The volume of this air was never over one percent of that of the water in the cell, and frequently much less. Measurements of dn/dT were started within a few minutes of sealing the cell. Direct continuous observation of dn/dT over a range of temperature was accomplished by counting the passing of interference fringes, during a corresponding known change in temperature. The details of the technique are described elsewhere.[1]

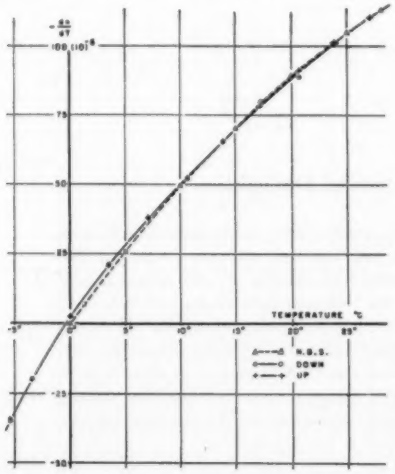

FIG. 1. Thermal coefficient of the index of refraction of water for $\lambda = 5893$A.

Measurements were made of dn/dT for water which had been kept in the Pyrex cell for periods from a few minutes up to a week or more. No difference in the refractive properties of water of different ages or from different geographical sources was found greater than the experimental error, which was estimated at 0.7×10^{-6} index unit per °C. Actually, the individual measurements were reproducible to 1.0×10^{-6} index unit per °C in the -10°C to 15°C range, and to about twice this figure in the range above this temperature.

RESULTS

The results are plotted in Fig. 1, in which are also shown the corresponding results obtained by

* Investigations carried out under Contract N6onr-247, Task Order I, of the Office of Naval Research.

[1] J. B. Hawkes and R. W. Astheimer, J. Opt. Soc. Am. **38**, 617 (1948).

Tilton and Taylor,[2] at the Bureau of Standards, using sodium light and a liquid prism. In the neighborhood of room temperature the agreement is well within the combined experimental errors. From 0°C to 10°C, however, the Tilton and Taylor curve lies slightly below ours. This small discrepancy may be due to the fact that Tilton and Taylor used a liquid prism surrounded by an air-filled space, all enclosed in a "thermostatted" cover. On the other hand, our surrounding air was at substantially room temperature at all times. The temperature changes in the air in the Bureau of Standards apparatus might have an effect of 1×10^{-6} index unit per °C, approximately the observed discrepancy. The difference between the values of dn/dT found by various investigators are plotted in Fig. 2. Here the values found

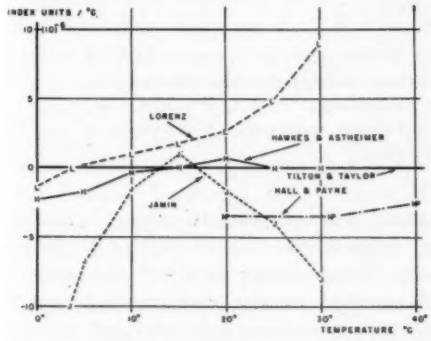

FIG. 2. Differences in dn/dT for water as measured by various observers.

by Tilton and Taylor are used as a norm. The results reported by Jamin[3] and by Lorenz[4] were obtained with the Jamin interferometer; those of Hall and Payne[5] were found with a liquid prism.

The dn/dT curve of Fig. 1 may be integrated graphically, taking the constant of integration as the refractive index of water at 20°C relative to air as found by Tilton and Taylor. The result is the index-temperature curve shown in Fig. 3. On this is plotted for comparison the direct measurements made at the Bureau of Standards. The agreement is almost perfect at all points.

[2] L. W. Tilton, and J. K. Taylor, J. Research Nat. Bur. of Stand. **20**, 419 (1938).
[3] J. Jamin, Comptes Rendus **43**, 1193 (1856).
[4] L. Lorenz, Kgl. Danske Vid. Sels. Math.-Fys. Medd. (5)8, 220 (1869).
[5] E. E. Hall and A. R. Payne, Phys. Rev. **20**, 253 (1927).

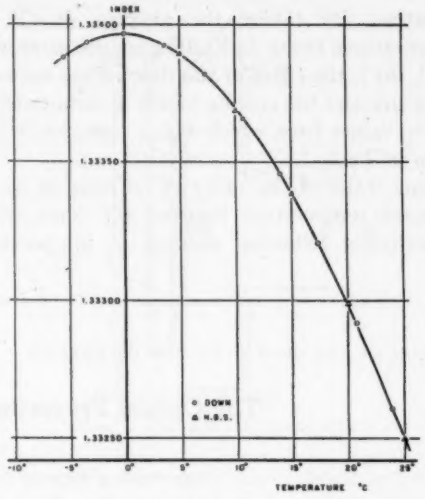

FIG. 3. Index of refraction of water for $\lambda = 5893$A.

DISCUSSION

In the course of this investigation measurements were made on distilled water from (a) the Hoboken, New Jersey, city supply, (b) the Brooklyn, New York, city supply, (c) freshly fallen snow. At least two successive distillations in Pyrex were carried out on each sample. No detectable differences were found. One sample was irradiated with strong 100 KC sound soon after distillation. No appreciable out-gassing or other effect, aside from a large surface agitation, was observed. The optical measurements on the sample after this treatment were indistinguishable from those of any other sample tested.

The thermal expansion of the Pyrex cell holding the water is the only systematic error for which the correction was large enough to require

TABLE I.

T °C	$-(dn/dT)\times10^6$ up	down	$-(dn/dT)\times10^6$ average
27.2	110.8	110.7	110.7
24.0	101.3	101.2	101.2
20.7	91.7	88.8(?)	(91.7)
17.3	78.8	80.0	79.4
13.9	66.1	65.6	65.8
10.6	53.1	52.6	52.3
7.1	37.5	37.8	37.6
3.5	20.9	21.4	21.1
0	2.3	2.3	2.3
−3.5	−20.5	−20.1	−20.3
−5.5	−33.6	−33.9	−33.7

attention. By taking the average dn/dT for temperatures rising and falling at the same rate (28°C/hr.), the effect of the thermal lag between the water and the cooling jacket is eliminated.

The values from which Fig. 1 was plotted are given in Table I.

Long waits of the order of an hour or so, at constant temperature between 0°C and 10°C, immediately following changes of temperature (for example, a drop of 20°C in five minutes) show a drift of the index no greater than 0.5 fringe per hour—corresponding to 1×10^{-6} index unit per hour. The possibility that at temperatures below 10°C the dn/dT *versus* T relation may be different for rising and falling temperatures is still under investigation. However, the *average* dn/dT as plotted in Fig. 1 shows no anomalies over the −5°C to +25°C range.

JOURNAL OF THE OPTICAL SOCIETY OF AMERICA VOLUME 38, NUMBER 9 SEPTEMBER, 1948

The Optical Properties of Ni, Co, Fe, Mn, and Cd

F. BUECHE
Department of Physics, Cornell University, Ithaca, New York
(Received April 28, 1948)

The reflectivities for evaporated metal films of Ni, Co, Fe, Mn, and Cd have been measured at five angles of incidence in the visible and near infra-red regions. From this data, the dielectric constant and conductivity of the metals were found by the method of J. R. Collins and R. O. Bock [Rev. Sci. Inst. **14**, 135 (1943)]. These data are shown graphically. A technique is described for obtaining smooth evaporated cadmium mirrors.

INTRODUCTION

THE optical properties of metals have been the subject of widespread study by many observers during the past half-century. However, with the application of quantum mechanics to the study of the solid state, the measurement of the dielectric constant (ϵ) and the conductivity (σ) of metals at optical frequencies has taken on a new significance in recent years. These constants are related to the index of refraction (n) and the extinction coefficient (k) by the relations

$$\epsilon=n^2-k^2 \quad \text{and} \quad \sigma=nk\nu.$$

Although such data are not easily related to the energy level densities within the metal except in certain special cases, it is, nevertheless, possible to obtain useful knowledge of the behavior of electrons in metals from their optical properties. Also, the reflectivities of metals are of value for purely optical reasons.

It was not until recently that satisfactory methods were proposed for investigating the dielectric constant and conductivity of metals in the infra-red. This spectral region is especially important when investigating the behavior of those metals whose valence electron bands overlap other filled energy bands of the solid. The metals studied in this research fall into this category of overlapping bands and, therefore, the method of measurement should allow one to make measurements extending into the infra-red.

METHOD OF MEASUREMENT

The method of measurement used was that employed by Collins and Bock.[1] They show that the equation for the reflectivity of monochromatic light (polarized parallel to the plane of incidence) by a plane metal surface may be expressed in terms of σ/ν and ϵ for the metal of the mirror as well as the angle of incidence used. Using this expression, Collins has prepared a voluminous set of tables listing many pairs of values of σ/ν and ϵ satisfying the equation for each of about two-hundred values of the reflectivity for incidence angles 50, 60, 70, 75, and 80 degrees. The calculation procedure, then, is to use the tabulated values to plot the curve coordi-

[1] J. R. Collins and R. O. Bock, Rev. Sci. Inst. **14**, 135 (1943).

nating ϵ and σ/ν for an experimentally determined reflectivity at a known angle of incidence. If, now, a second similar curve is plotted by use of the reflectivity determined at another angle of incidence, the graphical intersection of the two curves determines the values of ϵ and σ/ν for the metal at the particular frequency of light used. In practice, five such curves were plotted and an average intersection was used.

In the interest of greater instrumental stability, the optical arrangement proposed by Collins and Bock has been revised. Using their same basic mechanical apparatus, the optical system of the remodeled equipment is as shown in Fig. 1. The light source was a tungsten filament lamp (Sc). It, together with the collimating lens (L_1), was mounted on the movable arm of the reflectometer. The parallel light emerging from (L_1) was reflected from the metal mirror (MM'), plane-polarized with its electric vector parallel to the plane of incidence by the polarizing prism (N) and focused on the entrance slit (S_1) of the monochromater by the lens (L_2). After passing through the monochromater (which was equipped with two twin, off-axis, parabolic mirrors, M_1 and M_2, and a constant deviation prism, P), the light emerging from the exit slit (S_2) of the monochromater was focused upon the thermo-junction receiver (T). This receiver was replaced by a photo-cell in the visible spectral region. The response of these two receivers to the incident light was observed with the aid of a Zernike Z-c galvanometer.

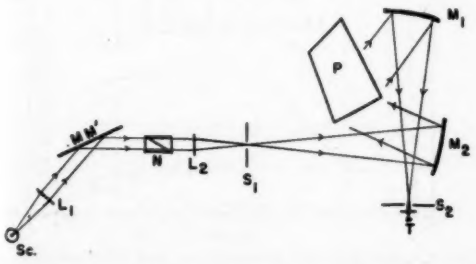

FIG. 1. The optical system used in measuring reflectivities.

PREPARATION OF THE MIRRORS

Standard high vacuum evaporation techniques were used in the preparation of the Ni, Co, Fe, and Mn mirrors studied. The evaporating system consisted of a twelve-inch glass bell jar mounted in a special groove on a heavy brass bed plate. The bed plate carried six high current electrodes and was connected to a liquid air trap and two mercury pumps in series. Outgassing of the system was accomplished by pumping with the evaporating filaments lighted for several hours before the evaporation was begun. The evaporation process itself was carried out very slowly in periodic bursts in order to avoid excess heating of the chamber. The pressures thusly maintained were read with the aid of a McLeod gauge. At no time was a mirror used which had been prepared at pressures in excess of 1×10^{-5} mm of mercury. In most cases, the pressure was lower than 5×10^{-6} mm of mercury as read by the McLeod gauge.

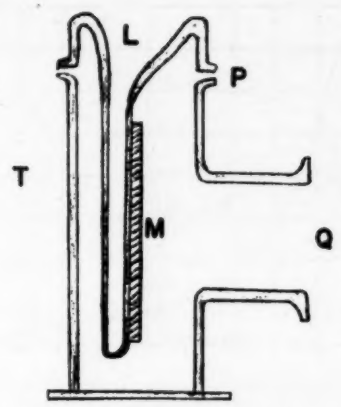

FIG. 2. The cadmium evaporator.

Since three of the metals evaporated are known to react with tungsten and molybdenum at high temperatures, a check was obtained upon the consequences of this fact by taking observations on mirrors evaporated from filaments of both materials. If any effect is present as a result of this, it is either identical for both materials or it is so small that it is masked by the routine irregularities always present between evaporated mirrors. The filaments themselves were in the form of V-shaped troughs. Such filaments were found much more satisfactory from the standpoints of durability and thermal efficiency than the more commonly used spiral filaments.

THE EVAPORATION OF CADMIUM

The evaporation of cadmium presented somewhat of a problem, for previous to this work

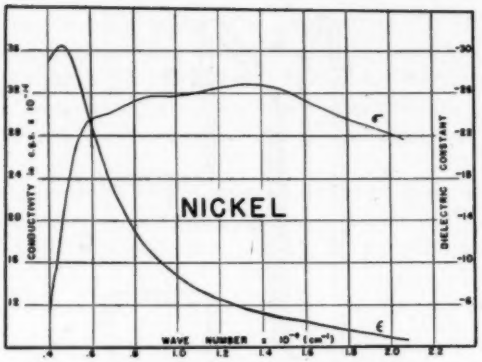

FIG. 3. The dielectric constant (ϵ) and conductivity (σ) of nickel.

efforts to make reasonable size mirrors of this material have been unsuccessful. The device shown in Fig. 2 was devised and used successfully to obtain smooth cadmium mirrors approximately 25 square centimeters in area. It consists essentially of a Corning T (T) mounted on a brass bed plate (not shown). The bed plate was in turn connected to a liquid air trap and the pumping system. Three high current leads entered the T by way of the brass plate. The glass plate to be mirrored with cadmium was mounted on a flat piece of hollow glass tubing which could be filled with liquid air. The seals at P and Q were made using brackets furnished commercially with the T. This system was capable of producing pressures of 10^{-6} mm of mercury.

It became apparent after some preliminary work with this system that the glass surface must be fairly near liquid air temperatures

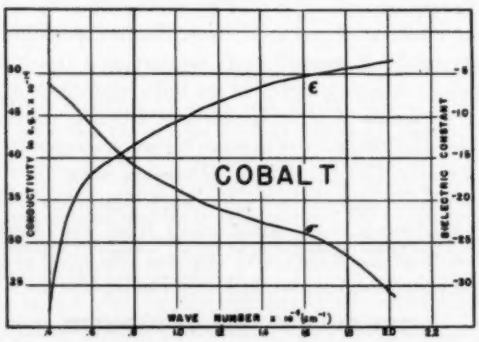

FIG. 4. The dielectric constant (ϵ) and conductivity (σ) of cobalt.

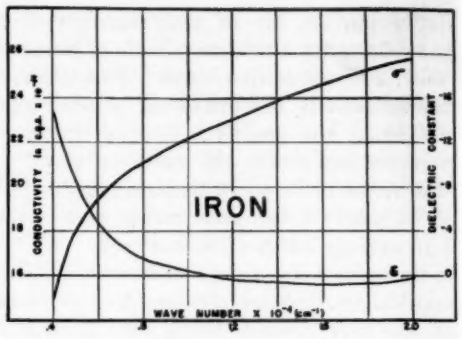

FIG. 5. The dielectric constant (ϵ) and conductivity (σ) of iron.

before the cadmium would deposit smoothly. This fact demands that one provide good thermal contact between the glass plate and the liquid air tube. Therefore, a preliminary metal layer was evaporated upon both the tube and the reverse side of the plate which was to be mirrored in order to obtain better conduction between them. Even with these precautions, the system must be cooled for several hours before the evaporation is to begin.

Because of the fact that one is limited by a mirror to filament distance of about 10 cm in this arrangement and since a spiral filament is demanded by the geometry of the evaporation chamber, the film so obtained is necessarily of non-uniform thickness. Even though such an effect is relatively small (it amounts to a change in the angle of incidence of about 10^{-5} radian in an extreme case), the optical system was stopped down so that only the central portions of the cadmium mirrors were used for measurements. The cadmium mirrors so obtained were repeatable and the three cadmium mirrors meas-

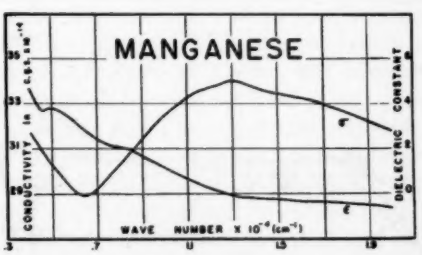

FIG. 6. The dielectric constant (ϵ) and conductivity (σ) of manganese.

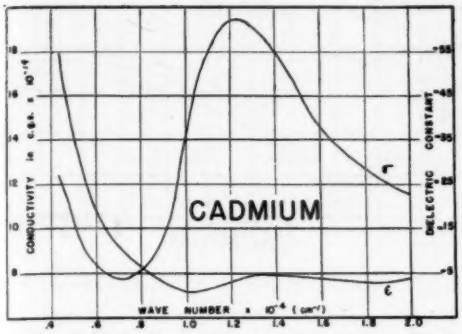

FIG. 7. The dielectric constant (ϵ) and conductivity (σ) of cadmium.

ured showed essentially the same optical properties in the spectral region covered by this investigation.

RESULTS AND DISCUSSION

The results obtained are shown graphically in Figs. 3–12. With respect to the accuracy of these results, it is clear that there are two general types of error which should be mentioned. The first type of error is associated with the repeatability of successive readings on the same mirror and general over-all adjustment of the apparatus. These factors are estimated not to produce errors much in excess of the width of the curves except in the region beyond 2.2 microns where the error is somewhat larger as a result of the low light intensity transmitted by the glass portions of the system. The second, and more serious, source of error is connected with the inability to reproduce exactly the evaporated surface itself. Because of unknown causes, the results sometimes varied rather widely from mirror to mirror of the same metal. This variation became as high as 10 percent in the reflectivities in isolated instances. However, it should be noted that although the reflectivity may vary widely, the conductivity remains fairly constant from mirror to mirror of the same metal. The dielectric constant is more sensitive to the character of the mirror surface. In general, that mirror which showed the highest reflectivity was used for computations.

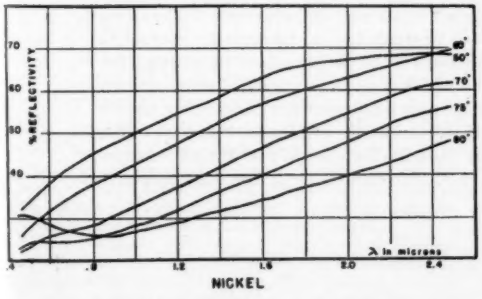

FIG. 8. The reflectivity of nickel.

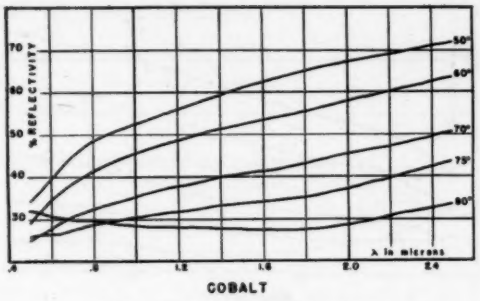

FIG. 9. The reflectivity of cobalt.

Previous work on the metals here studied has been confined chiefly to the visible region. Typical data is that of Minor and Meier[2] for Ni, Co, Mn, and steel. Their values for the conductivity in the small region of overlap are nearly the same as the data here obtained for Ni and Mn while their data for Co and steel are about 20 percent higher than here given for Co and Fe. This latter discrepancy is to be expected since they used polished surfaces which might easily have had an amorphous layer upon them.

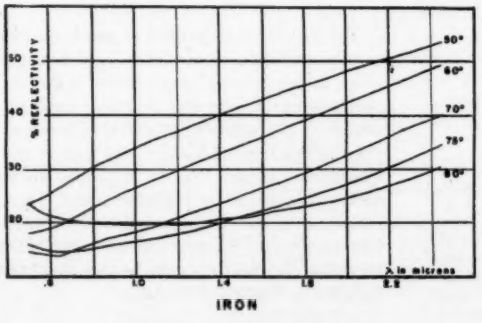

FIG. 10. The reflectivity of iron.

[2] Minor, Ann. d. Physik **10**, 581 (1903); Meier, Ann. d. Physik **31**, 1017 (1910).

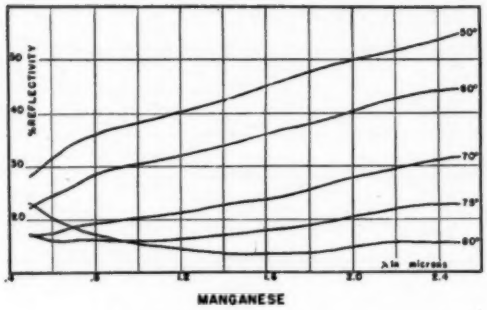

FIG. 11. The reflectivity of manganese.

Such layers have been shown to increase the value of the conductivity in this wave-length region.[3] Bor, Hobson, and Wood[4] have measured nickel out to 1.0 micron. Their results for the conductivity are slightly higher than the values found by this author, the discrepancy being greatest for long wave-lengths. Except for these latter workers' data beyond 0.7 micron, the shapes of the present curves agree well with those obtained by other investigators in that wave-length region where the data overlap.

[3] Lowery, Wilkinson, and Smare, Phil. Mag. **22**, 769 (1936).

[4] Bor, Hobson, and Wood, Proc. Phys. Soc. London **51**, 932 (1939).

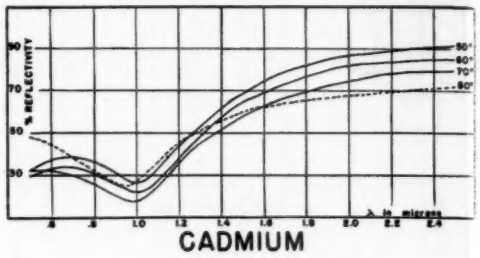

FIG. 12. The reflectivity of cadmium.

It is interesting to notice that the present work has found an absorption maximum for cadmium at a frequency of 3.66×10^{14} sec^{-1}. This is approximately the same frequency at which Bock[5] has found an absorption maximum for zinc. This fact would tend to indicate that the p and s band separation in zinc and cadmium are nearly identical.

ACKNOWLEDGMENT

The author wishes to express his gratitude to Professor D. H. Tomboulian for many thoughtful suggestions during the course of this work. He is also deeply indebted to the late Professor J. R. Collins whose efforts made this work possible.

[5] Robert O. Bock, Phys. Rev. **68**, 210 (1945).

Symposium on Luminescence

The Electronics Division of the Electrochemical Society is making preparations for a symposium on luminescence, to be held during its meeting in Philadelphia, May 5 to 7, 1949. The scope of subjects for presentation is all original and phenomenological material pertaining to fundamental science and technical applications having to do with luminescence. Papers presented at the meeting, together with discussion, will be published in the monthly Journal of the Electrochemical Society, and later in the Transactions. With the consent of the Publication Committee, papers may be published elsewhere, in which case an adequate abstract will be accepted in lieu of the complete paper. Those wishing to present a paper at the meeting should submit title and abstract before December 15, 1948, to Dr. R. M. Burns, Secretary, The Electrochemical Society, 235 West 102 Street, New York 25, New York. Further information regarding the meetings may be obtained from Dr. H. C. Froelich, General Electric Company, Nela Park, Cleveland 12, Ohio.

The Fluorescence of Uranium Trioxide Hydrates [1]

DWAYNE T. VIER,[2] MELVIN L. SCHULTZ,[3] AND JACOB BIGELEISEN[4]
SAM Laboratories, Columbia University, New York, New York

(Received April 1, 1948)

The hydrates of uranium trioxide have been found to be fluorescent when exposed to ultraviolet light. The fluorescence spectra of the different hydrates have been measured. The anhydrous oxides do not fluoresce.

THE hydrates of uranium trioxide exhibit fluorescence at room temperature and below, an observation which has not been reported previously. This paper contains the results of an investigation of this fluorescence at 20°K, 77°K, and, in some cases, at room temperature. Aside from its intrinsic interest, the fluorescence of these hydrates may offer an expedient method for the identification of these hydrates, and also serve as a means for following phase changes in systems containing uranium trioxide in water. However, x-ray diffraction will, in general, offer a superior method of distinguishing the different hydrates.

The main character of the fluorescence of the trioxide hydrates is not unlike that of uranyl ion, but differs from it in the structural detail and insofar as the spectrum falls farther to the red and covers a shorter region. The fluorescence spectra of these hydrates are somewhat similar (though they are easily distinguished), and consist of three or four bands at approximately equal intervals of 810 wave numbers. The spectrum begins at about 5000A and extends through the green portion of the spectrum to about 6000A; the intensity of the bands decreases after the second band at 5300A and fades out almost entirely after the fourth band. The green fluorescence of these hydrates is easily distinguished by the unaided eye from the greenish-yellow fluorescence of uranyl ion.

The absorption responsible for the fluorescence probably involves an excitation of one of the bonding electrons to a 5-*f* orbital in uranium. The structure of the fluorescence is not as yet understood. While much remains to be done toward the understanding of these spectra, the results on the identification and measurement are of sufficient interest to warrant their report at this time.

In addition to the trioxide hydrates other uranium oxides were examined for fluorescence but failed to show any at 77°K. The compounds investigated were:

1. $UO_4 \cdot 2H_2O$.
2. UO_3, anhydrous Mallinckrodt.
3. UO_3, anhydrous, prepared by heating $UO_4 \cdot 2H_2O$ to 350°C in a stream of oxygen.
4. U_3O_8.
5. UO_2.

TABLE I. X-ray classification.

Hydrate	Crystal form	X-ray classification	Starting material	Sample no.	Treatment in water: time hr.	Treatment in water: temp. °C
$UO_3 \cdot 2H_2O$	micro crystalline	I	P	219.123.2	44	77
$UO_3 \cdot 2H_2O$	micro crystalline	IIA	M	235.39.2	192	28
$UO_3 \cdot H_2O$	rhombic hexagonal tablets, 5μ	IIA	P	219.108.1	89	100
$UO_3 \cdot H_2O$	amorphous and some 5μ rhombic hexagons	IIB	M	219.92.3	600	100
$UO_3 \cdot H_2O$	rhombic rods, 5 × 30μ	IIC	P	219.46.2	264	185
$UO_3 \cdot H_2O$	triclinic, 30μ	III	M	235.38	340	185
$UO_3 \cdot \frac{1}{2}H_2O$	monoclinic, 50μ	IV	P	235.26	96	325–350

P = UO_3 from $UO_4 \cdot 2H_2O$. M = Mallinckrodt UO_3.

TABLE II. Appearance of fluorescence spectra of the hydrates.

Hydrate	X-ray classification	Description of fluorescence spectrum 298°K	77°K
$UO_3 \cdot 2H_2O$	I	bands	bands
$UO_3 \cdot 2H_2O$	IIA	continuous	bands
$UO_3 \cdot H_2O$	IIA	no fluorescence	bands
$UO_3 \cdot H_2O$	IIB	no fluorescence	bands
$UO_3 \cdot H_2O$	IIC	no fluorescence	bands
$UO_3 \cdot H_2O$	III	nearly continuous, spectrum displaced toward blue	bands
$UO_3 \cdot \frac{1}{2}H_2O$	IV	weak fluorescence	bands

[1] This document is based on work performed under Contract No. W-7405-eng-50 for the Atomic Energy Project, and the information covered therein will appear in Division VIII, Volume XI-B, of the *National Nuclear Energy Series* (Manhattan Project Technical Section) as part of the contribution of Columbia University.

[2] Present address: Box 1663, Santa Fe, New Mexico.
[3] Present address: Radio Corporation of America, RCA Laboratories Division, Princeton, New Jersey.
[4] Present address: Brookhaven National Laboratory, Upton, N. Y.

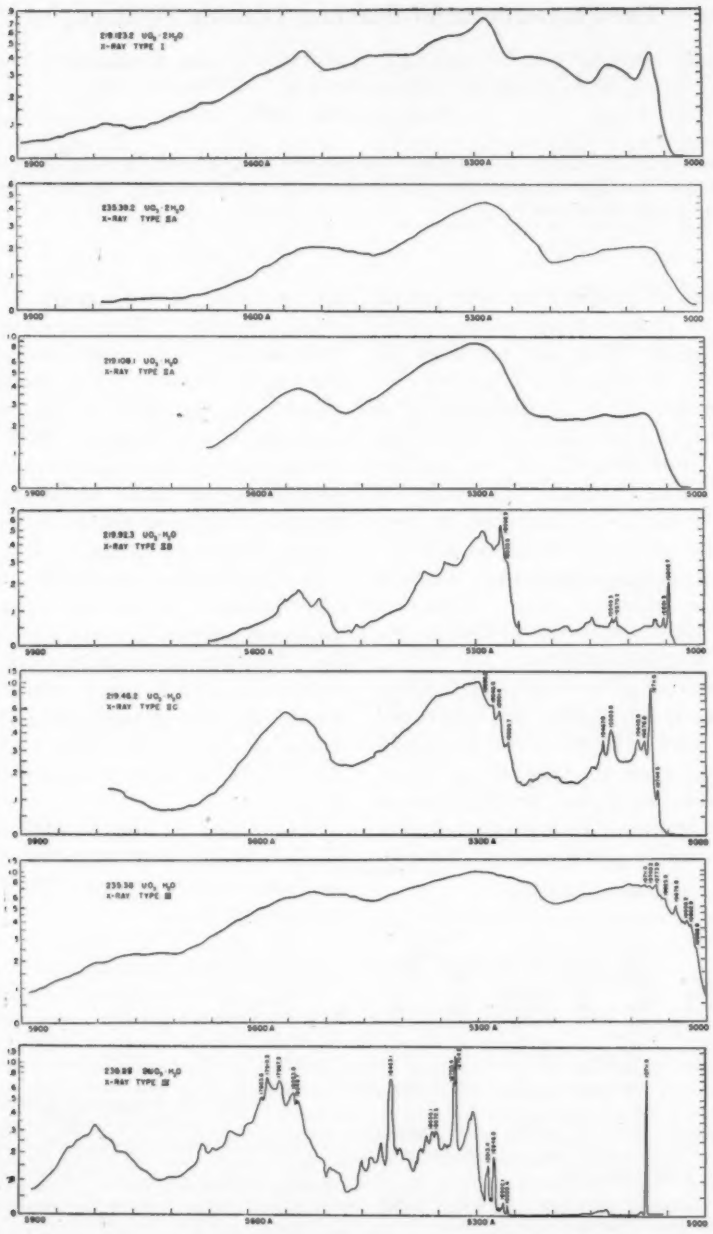

FIG. 1.

The hydrates used in this investigation were prepared from anhydrous UO_3 (either Mallinckrodt UO_3 or UO_3 prepared from $UO_4 \cdot 2H_2O$ by heating in a stream of oxygen at 350°C) and water heated together in sealed tubes in vapor baths. The samples selected represented a choice from a number of similar samples and were selected primarily on the basis of the sharpness

of their x-ray diffraction patterns as compared to similar patterns characteristic of a given hydrate. A description of their preparation and other pertinent data are described elsewhere,[5] a summary of which is shown in Table I. With the exception of the identity of x-ray diffraction patterns type IIA of the dihydrate and type IIA of the monohydrate, the patterns for different crystalline forms of the hydrates and of different hydrates were all distinct.

The x-ray classification designations used in Table I and throughout this paper are the same

TABLE III. Wave number tabulation of the fluorescence spectra of uranium trioxide hydrates.

A: $UO_3 \cdot 2H_2O$, X-ray type I: Sample 219.123.2.

Band	20°K Description of line	20°K $\bar{\nu}$, cm^{-1}	77°K $\bar{\nu}$, cm^{-1}	77°K Description of line
I	Fluorescence begins	19900		
	Strong, broad	19740	19766	Moderate, broad
	Moderate, diffuse	19530	19542	Weak, diffuse
	Moderate, very diffuse	19150	19245	Weak, very diffuse
II	Strong, diffuse	18920	18937	Strong, broad
	Weak, very diffuse	18740	18706	Weak, diffuse
	Weak, very diffuse	18410	18472	Weak, very diffuse
III	Moderate, diffuse	18080	18000	Moderate, broad
IV	Weak, very diffuse	17420	present	Weak, very diffuse
	First band at 19,740 cm^{-1}. Bands repeat every 833±9 cm^{-1}. Secondary lines in bands at 200 cm^{-1} and 550 cm^{-1} from initial line. (Note: the average deviation given after frequency with which bands repeat is probably much less than the actual error in this and all other tables.)			The bands are fairly sharp with structure. Total intensity is low. First band at 19,766 cm^{-1}; bands repeat every 838±9 cm^{-1}. Secondary lines in bands at 230 cm^{-1} and 500 cm^{-1} from initial line.

B: $UO_3 \cdot 2H_2O$, X-ray type IIA; Sample 235.39.2.

I	Fluorescence begins	19900		
	Moderate, very diffuse; shaded to red	19720	19540	Weak, very diffuse
II	Strong, very diffuse	18920	18820	Moderate, very diffuse; shaded to red
III	Moderate, very diffuse	18110	17961	Weak, very diffuse; shaded to red
IV	Extremely weak, very diffuse	present	present	Very weak, very diffuse
	Bands similar to x-ray type I except for absence of secondary structure. First band at 19720 cm^{-1} Bands repeat every 805±5 cm^{-1}.			Bands very diffuse. Total intensity high. First band at 19540 cm^{-1}. Bands repeat every 790±70 cm^{-1}.

C: $UO_3 \cdot H_2O$, X-ray type IIA; Sample 219.108.1.

I	Fluorescence begins	19990		
	Moderate, very diffuse; shaded to red	19730	19549	Weak, very diffuse
II	Strong, very diffuse	18860	18640	Moderate, very diffuse; shaded to red
III	Moderate, very diffuse	18050	17888	Weak, very diffuse; shaded to red
IV			present	
	Spectrum almost identical with that of $UO_3 \cdot 2H_2O$, x-ray type IIA. First band at 19730 cm^{-1}. Bands repeat every 835±25 cm^{-1}.			Spectrum almost identical with that of $UO_3 \cdot 2H_2O$, x-ray type IIA. Bands very diffuse. Total intensity moderate. First band at 19549 cm^{-1}. Bands repeat every 831±79 cm^{-1}.

[5] D. Vier, Columbia Report A-1277, File 2.13, May 26, 1944.

TABLE III.—*Continued.*

D: $UO_3 \cdot H_2O$, X-ray type IIB; Sample 219.92.3.

Band	20°K Description of line	20°K $\bar{\nu}$, cm^{-1}	77°K $\bar{\nu}$, cm^{-1}	77°K Description of line
I	Fluorescence begins	19875		
	Moderate, sharp	19846.7	19866	Moderate
	Weak, narrow	19821.3		
	Weak, narrow (also center of broad band)	19773	19791	Weak
	Weak, narrow	19570.2	19584	Weak, broad
	Weak, narrow	19549.3		
	Moderate, broad	19446	19470	Weak, broad
	Moderate, broad	19420		
	Moderate, broad	19274	19300	Weak, diffuse
	Moderate, broad	19181	present	Very weak
	Weak, narrow	19030.5		
II	Strong, narrow	18998.9	18997	Strong, broad
	Very weak, narrow	18974		
	Strong, diffuse	18909	18919	Strong
	Strong, diffuse	18732	18745	Weak, diffuse
	Strong, diffuse	18631	18605	Weak, diffuse
III	Strong, diffuse	18140	18190	Moderate, broad
	Strong, diffuse	18050	18067	Moderate, broad
	Very weak, very diffuse	17870	17918	Weak, diffuse
	Weak, diffuse	17800	17817	Weak, diffuse
IV	Weak, very diffuse	17330	17349	Weak, very diffuse
	Moderate, very diffuse	17180		
V			present	Extremely weak, very diffuse
	First band at 19846.7 cm^{-1}. Bands repeat every 839±19 cm^{-1}. Secondary lines in bands at 25 cm^{-1}, 90 cm^{-1}, 270 cm^{-1}, and 380 cm^{-1} from initial line.			Bands fairly sharp, with structure. Total intensity moderate. First band at 19866 cm^{-1}. Bands repeat every 839±21 cm^{-1}. Secondary lines in bands at 80 cm^{-1}, 270 cm^{-1}, and 380 cm^{-1} from initial line.

E: $UO_3 \cdot H_2O$, X-ray type IIC; Sample 219.46.2.

I	Fluorescence begins	19797		
	Moderate, sharp	19744.5	19832	Very weak
	Strong, sharp	19711.6		
	Moderate, narrow	19676.8		
	Moderate, narrow	19640.0	19635	Moderate, very diffuse
	Moderate, narrow	19503.8		
	Moderate, sharp	19467.0		
	Moderate	19152	present	Very weak
II	Moderate	19009.7	19004	Weak, broad
	Strong, narrow	18991.6		
	Strong	18946.6		
	Strong, very diffuse	18896.2	18840	Strong, very diffuse
III	Strong, very diffuse	18080	18157	Weak, diffuse
	Strong, very diffuse	17980	17976	Moderate, very diffuse
IV	Moderate, very diffuse	(17240)	17085	Weak, very diffuse
V			present	Very weak, very diffuse
	First band at 19744.5 cm^{-1}. Band structure does not appear to repeat. Bands repeat at 835±20 cm^{-1}.			Bands diffuse. Total intensity high. First band at 19832 cm^{-1}. Bands repeat at 849±15 cm^{-1}.

F: $UO_3 \cdot H_2O$, X-ray type III; Sample 235.38.

I	Fluorescence begins	20030		
	Very weak, narrow	19988.6		
	Weak, narrow	19962.9		
	Weak, narrow	19938.2		
	Moderate, narrow	19876.8		
	Moderate	19825.9		
	Moderate, narrow	19773.0		
	Weak	19740.2		
	Weak	19711.0		
	Strong, very diffuse	19640	19681	Weak, very diffuse
	Moderate, very diffuse	19120	19009	Very weak, very diffuse
II	Strong, very diffuse	18860	18833	Strong, very diffuse
III	Strong, very diffuse	18110	17993	Weak, very diffuse
IV	Moderate, very diffuse	17360	present	Very weak, very diffuse
	First band at 19988.6 cm^{-1}. Bands repeat (but not the structure) every 760±13 cm^{-1}.			Bands diffuse. Total intensity low. First band at 19681 cm^{-1}. Bands repeat every 844±4 cm^{-1}.

TABLE III.—*Continued.*

G: $UO_3 \cdot \frac{1}{2}H_2O$, X-ray type IV; Sample 235.26.

Band	20°K Description of line	$\bar{\nu}$, cm^{-1}	$\bar{\nu}$, cm^{-1}	77°K Description of line
I	Strong, very sharp	19711.9		
	Weak, narrow	19009.4		
	Weak, narrow	18992.1		Absent
	Moderate, sharp	18946.8		
	Moderate, sharp	18913.4		
	Strong	18845		
II	Strong, broad	18764.2	(18780)	Fluorescence begins, very diffuse
	Moderate, sharp	18755.4		
	Moderate, narrow	18672.5		
	Moderate, narrow	18656.1		
	Strong, narrow	18463.1	(18600)	Weak, narrow
III	Moderate, broad	18048.7	(18190)	Weak, narrow
	Moderate, broad	18023.8		
	Strong, narrow	17967.3	(18070)	Weak, narrow
	Strong, narrow	17910.3		
	Weak, broad	17883.8		
	Moderate, broad	17760	(17920)	Very weak, broad
	Moderate, broad	17630	(17820)	Very weak, broad
IV	Moderate, very diffuse	(17180)	(17180)	Very weak, very diffuse

Total intensity high. First band at 19711.9 cm^{-1}. Band structure does not appear to repeat, nor are the intervals between band peaks equal.

Fluorescence, but too weak to measure accurately. Very diffuse bands also present. First band begins at 18780 cm^{-1}. Spectrum very much like x-ray type IIB, but first two strong bands are missing.

as those used in the previous report,[5] and represent an arbitrary system for identifying the different hydrates by their x-ray diffraction photographs. The x-ray diffraction photographs types IIA, IIB, and IIC are quite similar though not all identical, while types I, III, and IV are distinctly different from these and from each other.

It is to be noted that one form of the dihydrate and one form of the monohydrate give identical x-ray patterns (type IIA). The fluorescence spectra of these two hydrates are also identical, as will be seen below. The reason for the apparent identity of these two hydrates has not been investigated, but the circumstance indicates an uncertainty in the existence of this second allotropic form of the dihydrate.

The general appearance of the fluorescence spectra of the hydrates at 77°K and at room temperature, using a Zeiss direct vision spectroscope and a General Electric AH-5 lamp in conjunction with a Corning 586 filter, is shown in Table II. The light source thus consisted primarily of the 3660A mercury line.

The fluorescence spectra of the various hydrates were investigated under higher dispersion at 77°K and at 20°K, using a General Electric AH-5 lamp for excitation and an iron arc for the comparison spectrum. At 77°K a Corning 586 filter was used in front of the light source and the spectra were obtained using a Hilger constant deviation spectrograph. The results at 20°K were obtained from a 21-foot grating, Wadsworth mounting, employing the first order of the spectrum. A Corning 9863 filter was used in front of the light source and a Corning 738 filter before the slit.

The appearance of the spectra at 20°K is shown in Fig. 1, which is a reproduction of microphotometer traces of the fluorescence spectra of the hemi- and of the various allotropic forms of the mono- and dihydrates.

The wave number tables below give the fluorescence lines and bands at 20°K and at 77°K of the different hydrates of uranium trioxide, together with a description of the lines and some remarks on the general nature of the individual spectra. In those cases at 20°K where a listed wave number is not also shown printed on the photographs the values were estimated from the microphotometer traces, so that for bands which contained no measured lines, the error was of the order of ± 50 wave numbers and may possibly have been greater in the fourth band (at the red end of the spectrum). The wave numbers are listed somewhat more precisely than the possible error warrants for the purpose of calculation of differences between lines and bands. All wave numbers at 77°K were measured from the plates with the few exceptions where the numbers are enclosed in parentheses.

The authors are indebted to Dr. Martin Kilpatrick for his interest in this problem and to the kind cooperation of Dr. Gerhart Dieke of the Department of Physics, Johns Hopkins University, in the investigation at 20°K.

Letters to the Editor

On the Inadequacy of the Measurement of Emission Characteristics of Fluorescent Substances without Spectral Resolution

Z. Bodó
Research Laboratory of the United Incandescent Lamp and Electrical Company, Ltd., Ujpest 4, Hungary
June 25, 1948

SOME time ago it was noted in this laboratory that the temperature-dependence curve for total emission of a fluorescent material is not the same for a photo-cell with or without filter, and both again are generally differing from a spectrographic measurement with subsequent integration.

The origin of these discrepancies is to be found in the broadening of the emission spectrum with increasing temperature. Szigeti and Nagy[1] have found that the emission spectra can be approximated with great accuracy with a Gaussian error function, either plotted in energy or photon number *versus* energy in electron volts. For manganese activated zinc silicates the constant $1/(b)^{\frac{1}{2}}$ of the Gaussian $\exp[-b(h\nu-h\nu_0)^2]$ varies from 100°K to 600°K, or from some 0.07 electron volts to 0.18 electron volts.

Denoting with $i(\nu)$ the fluorescent emission and with $E(\nu)$ the spectral response of the photometric instrument, then the integral

$$\int_{-\infty}^{+\infty} i(\nu)E(\nu)d(h\nu)$$

is the only quantity to be measured by these means and the above mentioned broadening is capable of totally destroying the consistency of the results.

A characteristic set of readings is plotted on Fig. 1, where it is assumed for the sake of easier demonstration that the total luminescent emission remains constant, and the increased band-width is compensated by the decrease of the maximum by the same percentage. Curve *A* represents the case of zinc silicate with a maximum at 2.35 ev, curve *B*, a cadmium borate with maximum at 1.95 ev, and curve *C*, a hypothetical phosphor whose maximum coincides with the eye sensitivity maximum. The recording instrument is supposed to be corrected for visibility. The $E(\nu)$ spectral response was replaced for easier calculation by adequate Gaussian functions. The curve *D* of the same figure applies to the extreme case of a monochromatic filter in the emission maximum.

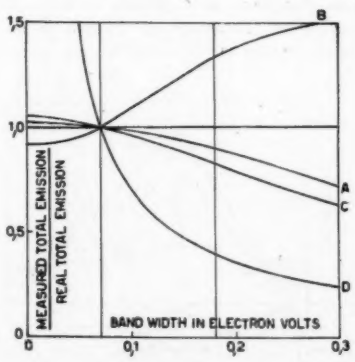

FIG. 1.

It is evident that the results least in error are to be found when the fluorescence maximum is in the neighborhood of the inflexion point of the visibility curve, being the same here for the greatest interval approximately linear. Curve *B* demonstrates the impossibility of measuring red fluorescing substances with yellow-green filters, and the case *C* too is worth noting, namely that the coincidence of the maxima of the sensitivity curves and the emission spectra is far from being a favorable condition; it is really one of the worst. Curves *C* and *D* together rule out the use of devices with too narrow sensitive regions. This state of affairs is still complicated in the case of several materials which show a slight but measurable shift of the maxima with temperature, or with material exhibiting several emission bands of different temperature sensitivity, e.g., zinc beryllium silicate.

It is to be concluded from the above analysis that more careful selection of filters and photo-cells is needed according to the above stated rules, i.e., the sensitivity must be energy-independent in an interval long enough; for measurements claiming physical sense and accuracy the absolute discarding of these devices and replacing them with spectrographic measurements is recommended.

The author wishes to express here his gratitude to Messrs. G. Szigeti and E. Nagy for suggesting this problem and for their helpful advice.

[1] G. Szigeti, E. Nagy, "Luminescence and Dielectric Losses of Zinc Silicate," Publications of the University of Technical Sciences, Budapest, 1, No. 3 (1948).

Standard Response Functions for Protanopic and Deuteranopic Vision

Yves Le Grand
Laboratoire de Physique du Muséum, 57 Rue Cuvier, Paris
June 1, 1948

IN a very interesting paper published under this title,[1] Judd has computed a linear transformation of the *XYZ* colorimetric system:

$$W_p = -0.460X + 1.359Y + 0.101Z,$$
$$W_d = Y, \quad K = Z,$$

such that W_p and K represent average protanopic vision, and W_d and K deuteranopic vision. In order that these

three functions, when taken together, represent the normal observer, it is necessary that the luminous flux retains the same value in both systems. This condition may be written:

$$L_xX+L_yY+L_zZ=L_pW_p+L_dW_d+L_kK,$$

the L being the luminosities of the primary stimuli. As we have:

$$L_x=L_z=0, \quad L_y=1,$$

the identification gives us:

$$L_p=L_k=0, \quad L_d=1.$$

Therefore, as the primary stimulus W_p has no luminosity for the normal observer, it is rather difficult to understand how it may acquire anyone for the protanope.

This difficulty vanishes if we use, instead of W_d, another function which, as Judd points out, agrees more closely to experience:

$$W_d'=0.070X+0.945Y-0.015Z.$$

(Judd's formula (10) is actually 1.12 W_d').
We find now:

$$L_p=0.132, \quad L_d=0.868, \quad \text{and} \quad L_k=0.$$

In conclusion, although calculations are less simple with the W_d' function, it is better to use it, in order to avoid contradictions.

[1] D. B. Judd, J. Opt. Soc. Am. **35**, 199 (1945).

Example of Metamerism: Extreme Example of Color Change with Varying Illuminant

F. C. Dexter and E. I. Stearns
Calco Chemical Division, American Cyanamid Company, Bound Brook, New Jersey
June 4, 1948

A METAMERIC match is a pair of samples which appear to be alike under one illumination but appear to be different when the illumination is changed. This is a well-known phenomenon but, as is the case with any visual effect, it is always well to have an extreme example for illustration. A fairly outstanding example of metamerism was prepared in this laboratory on dyed wool. Anyone wishing to illustrate metamerism may duplicate these samples with the information given below.

Table I. Colorimetric specifications.*

	Trichromatic coefficient		Dominant wavelength	Purity (%)	Luminosity (%)	Munsell notation
	x	y				
Illuminant *A*	0.448	0.408				
Illuminant *C*	0.310	0.316				
Sample A in Illuminant *A*	0.455	0.451	573.0	37	6.2	GY 2.9/4
Sample B in Illuminant *A*	0.515	0.390	600.3	37	6.4	10 R 3.0/2.5
Sample A in Illuminant *C*	0.352	0.383	571.5	29	6.2	1 GY 2.9/2.2
Sample B in Illuminant *C*	0.358	0.376	574.5	29	6.1	7.5 Y 2.9/2.0

* These colorimetric specifications are calculated on the basis of the I.C.I. Standard Observer. A real observer and illuminant to give exactly the same results would have to be similar to the I.C.I. standards. The Munsell notations are renotations for "*C*" illuminant, and the closest book notation for "*A*" illuminant.

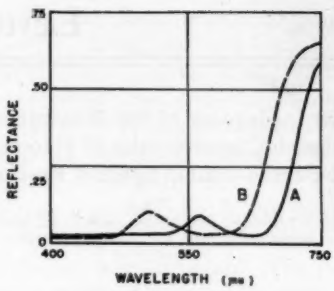

Fig. 1.

The dye formulations of these samples are as follows:

Sample A	
0.25 percent Calcocid blue AX double	(C.I. 714)
0.35 percent Calcocid orange RR	(C.I. 161)
0.60 percent Calcocid fast yellow 2G	(C.I. 639)
Sample B	
0.30 percent Calcocid violet XN	(C.I. 698)
1.50 percent Calcocid fast yellow 3G	(C.I. 636)

The dyes may be applied to the wool in a water bath at the boil for thirty minutes, using 10 percent sodium sulfate and 1 percent sulfuric acid as dyeing assistants.

The spectrophotometric curves of these two samples are shown in Fig. 1.

The colorimetric specifications of these samples are shown in Table I.

Figure 2 shows a portion of the chromaticity diagram with the points plotted. A line drawn from the point representing Illuminant *C* through the point representing Sample *A* viewed in Illuminant *C* (A_c in the diagram) intersects the spectrum locus at 571.5 mu, which means that its dominant wave-length is 571.5 mu and the sample appears green. Similarly, Sample *B* viewed in Illuminant *C* has a dominant wave-length of 574.5 mu which is very close to Sample *A*, and therefore both samples appear green and very nearly alike. When viewed in Illuminant *A* the situation is radically changed. The line drawn from the Illuminant *A* point through the point representing Sample *A* viewed with Illuminant *A* (A_a in the diagram) when extended to the spectrum locus intersects it at 573.0 mu. This indicates that Sample *A* has approximately the same dominant wave-length viewed under either Illuminant *C* or Illuminant *A*. Sample *B*, on the other hand, when viewed under Illuminant *A* has a dominant

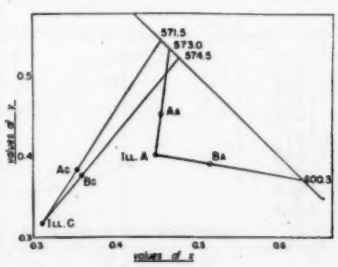

Fig. 2.

wave-length of 600.3 mu. Thus this sample appears to change from a green to a brown when the illumination changes from daylight to tungsten light.

Temperature Dependence of the Emission Bands of Zinc Oxide Phosphors

F. H. NICOLL
RCA Laboratories Division, Radio Corporation of America, Princeton, New Jersey
June 1, 1948

IN two previous notes,[1,2] reference has been made to the electron excited emission of ultraviolet radiation from ZnO phosphors. The presence of such radiation was shown to be dependent on high current density in the electron beam.

Recent experiments with a grating spectrograph have shown marked shift of the UV peak with temperature, while at the same time the peak of the visible light emitted showed no change in position.

The experiments were done on a small cathode-ray tube having an electron spot size about $\frac{1}{10}$ mm in diameter and a current of 100 μa in the beam. Measurements were made with the beam scanning a 525-line television raster, while the end of the tube was maintained at a known temperature by a small furnace.

Figure 1 shows the relative intensities for both visible and UV output on an arbitrary scale. It is apparent that while the UV peak height drops approximately 4× for a 225°C rise, the visible output drops about 23×. Thus the magnitude of the UV output is considerably *less* temperature sensitive than the visible. This is in apparent disagreement with the statements in the first note. The difference is accounted for, however, if the shift of the UV peak with temperature is taken into account. In the earlier results, measurements were made with a Wratten 18A filter and, consequently, at the higher temperatures the UV values were less than they should have been because the filter was then cutting off a larger proportion of the UV.

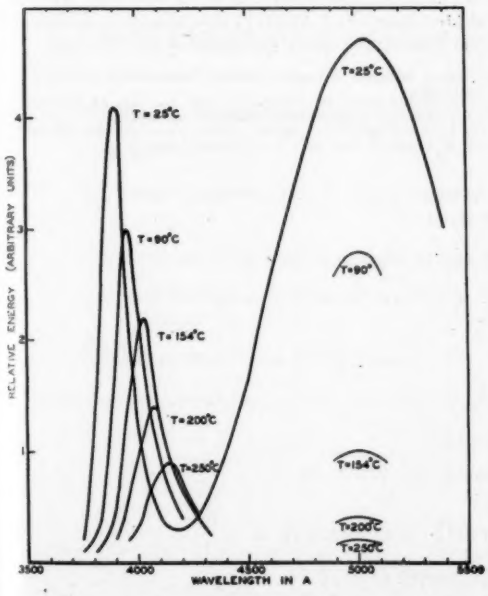

FIG. 1. Relative energy emitted by hex. ZnO:[Zn] phosphor as a function of wave-length for different temperatures. Emission produced by a high current density electron beam, 100 μa focused and scanning a 3″ × 4″ television pattern at 20 kv.

It is of interest to note that the UV peak shift is approximately 1.2A per °C, while the visible shift is zero. This is in agreement with Studer,[3] who reported no shift in wave-length of the UV excited visible emission band of zinc oxide phosphors between liquid nitrogen temperature and room temperature. These results can be compared with those given by Garlick,[4] which would then indicate that the UV shift for ZnO is at least double that found in some other phosphors while the visible shift is negligible. Explanation of this phenomenon by crystal expansion on heating would then appear to be rather unsatisfactory.

Some evidence is available that the UV absorption also moves to longer wave-lengths along with the UV emission. A sample of ZnO phosphor viewed in white light at 25°C appears white (absorption outside the visible), but as the temperature is increased the color becomes markedly yellow as the absorption shifts into the blue.

[1] R. E. Shrader and H. W. Leverenz, "Cathodoluminescence emission spectra of zinc oxide phosphors," J. Opt. Soc. Am. **37**, 939 (1947).
[2] F. H. Nicoll, "Note on ultraviolet absorption of zinc oxide phosphors," J. Opt. Soc. Am. **38**, 417 (1948).
[3] F. J. Studer and L. Gaus, *Preparation and Characteristics of Luminescent Materials* (John Wiley and Sons, Inc., New York, 1948).
[4] G. F. J. Garlick and A. F. Gibson, "Luminescence efficiency changes in zinc sulphide phosphors below room temperatures," Nature **161**, 359 (1948).

Infra-Red Stimulability of $CaSiO_3$:Pb and $CaSiO_3$:(Pb+Mn)

JAMES H. SCHULMAN, ROBERT J. GINTHER, AND LYLE W. EVANS*
Naval Research Laboratory, Washington, D. C.
July 19, 1948

THE preparation and some of the properties of the $CaSiO_3$:Pb, $CaSiO_3$:Mn, and $CaSiO_3$:(Pb+Mn) phosphors have recently been described.[1-3] The purpose of this communication is to call attention to the infra-red stimulability of $CaSiO_3$:Pb and of $CaSiO_3$:(Pb+Mn), a property of these interesting phosphors not mentioned in the foregoing reports.

It has been found that $CaSiO_3$, $CaSiO_3$:Mn, $CaSiO_3$:Pb, and $CaSiO_3$:(Pb+Mn) do not show any infra-red stimulability after excitation by a low pressure mercury lamp, equipped with a Corning 9863 filter (2537A excitation). If the unfiltered radiation of such a lamp is employed, however, a reasonable degree of infra-red stimulability is observed in both $CaSiO_3$:(Pb+Mn) and in $CaSiO_3$:Pb, but

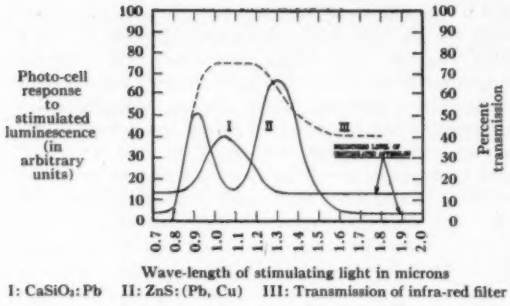

FIG. 1.

neither in $CaSiO_3$:Mn nor in unactivated $CaSiO_3$. The unfiltered radiation from the lamp contains 1849A radiation. Infra-red response is also observable after spark-coil excitation and after excitation by x-rays.

The directly excited visible luminescence of $CaSiO_3$:Pb lies in the blue-violet end of the spectrum, while that of $CaSiO_3$:(Pb+Mn) is in the orange-red region (peak at 6100). The same luminescence colors are observed on stimulation with infra-red.

The stimulation spectra of both phosphors are identical, extending from at least 0.85 micron to 1.3 microns, with a peak stimulability close to 1.0 micron. The accompanying figure shows the photo-cell response to the total stimulated emission of a $CaSiO_3$:Pb phosphor of composition $CaO_1 \cdot SiO_{2.32} \cdot PbF_{2.01}$ (firing temperature = 1200°C, firing time = 1 hour), compared to that of a ZnS:(Pb, Cu) phosphor developed by Fonda.[4] Both phosphors were excited by a spark-coil discharge and allowed to decay for about 30 minutes before the measurements were made. The samples were irradiated with infra-red light, monochromatized by a Beckman Model DU spectrophotometer, using a tungsten lamp source, and viewed by a 1P21 photomultiplier, whose output was amplified and recorded on a Brown recorder. Scanning of the wave-length interval 0.7 to 2.0 microns required about three minutes. A 0.2-mm slit width was used, giving a nominal band width of about 180A at 1 micron. It was necessary to place an infra-red filter between the exit slit of the monochromator and the sample to eliminate scattered visible light from the monochromated beam. The transmission of this filter is shown in Fig. 1. From measurements made using a Wratten No. 88 filter to remove scattered light, it appeared that the stimulation band of the $CaSiO_3$ phosphors may extend as far as 0.7 micron. No attempt was made to keep the incident infra-red light of equal intensity through the wave-length range or to measure its intensity; hence, the curves do not represent true "stimulation spectra."

The ZnS:(Pb, Cu) phosphor used was obtained about a year ago through the courtesy of Dr. C. E. Barnett of the New Jersey Zinc Company, and does not appear to have appreciably deteriorated with time.

It will be noted that the $CaSiO_3$:Pb is inferior to the ZnS:(Pb, Cu) phosphor with respect to contrast; at the infra-red level employed, the ratio of the brightness of the former at the peak of stimulability to its background brightness is about 3:1, while with the Fonda phosphor this ratio is about 16:1 (1.3 micron stimulation peak). The $CaSiO_3$:Pb phosphor is also inferior to the ZnS:(Pb, Cu) phosphor in the matter of stimulated light output, although here the comparison is complicated by the different spectral emission characteristics of the two phosphors.

Further studies of these infra-red stimulable silicates are in progress and will be reported on subsequently.

We wish to express our thanks to Mr. Elias Burstein and Mrs. Margaret J. White of this laboratory for putting at our disposal the optical equipment described above.

* Present address: Sylvania Electric Products, Inc., Emporium, Pennsylvania.

[1] J. B. Merrill and J. H. Schulman, J. Opt. Soc. Am. **38**, 471 (1948).
[2] H. C. Froelich, J. Electrochem. Soc. **93**, 101 (1948).
[3] G. R. Fonda and H. C. Froelich, J. Electrochem. Soc. **93**, 114 (1948).
[4] G. R. Fonda, J. Opt. Soc. Am. **36**, 382 (1946).